Graduate Student Theses, Dissertations, & Professional Papers

Graduate School

2002

Mineralogy petrography and geochemistry of the Picket Pin PGE deposit Stillwater Complex Montana
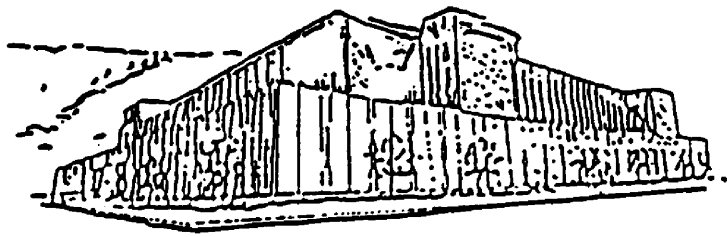
John T. Corkery
The University of Montana

Maureen and Mike
MANSFIELD LIBRARY

The University of **MONTANA**

Permission is granted by the author to reproduce this material in its entirety, provided that this material is used for scholarly purposes and is properly cited in published works and reports.

Please check "Yes" or "No" and provide signature

Yes, I grant permission ✓

No, I do not grant permission _____

Author's Signature _____

Date 5/31/02

Any copying for commercial purposes or financial gain may be undertaken only with the author's explicit consent.

Mineralogy, Petrography, and Geochemistry of the Picket Pin PGE deposit, Stillwater

Complex, Montana

by

John T Corkery

B.A. Lawrence University, Appleton, Wi, 1999

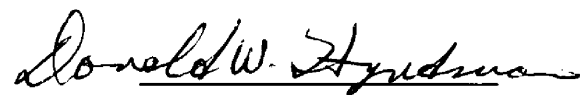persented in partial fulfillment of the requirements
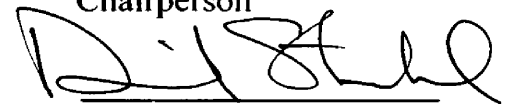
for the degree of

Masters of Science

The University of Montana

May 2002

Approved by:

Chairperson

Dean, Graduate School

6-3-02

Date

Mineralogy, Petrography, and Geochemistry of the Picket Pin PGE deposit, Stillwater Complex, Montana

Director; Don Hyndman *signature*

Abstract

   The processes of transport and deposition of 'reef-type' platinum-group-element (PGE) deposits remain enigmatic although numerous models have been proposed. The Stillwater Complex contains reef-type, PGE-enriched, sulfide-bearing intervals including the J-M Reef and the Picket Pin deposit. The J-M Reef is located approximately 500 m above the upper contact of the Ultramafic Series with the Banded Series. The reef occurs within the Troctolite-Anorthosite Zone I (TAZ I), a complex lithologic unit that contains numerous subdivisions. The Picket Pin deposit, located approximately 3000 m above the J-M Reef, is hosted within the 570-m thick anorthosite (AN II) at the top of the Middle Banded Series. The lack of lithologic complexities within the Picket Pin deposit provides an excellent opportunity to investigate the PGE ore-forming processes.

   Mineralogical and textural evidence suggests four main events for the formation of the Picket Pin PGE deposit. In chronological order these events are: 1) the formation of the large, framework plagioclase grains, 2) crystallization of the intercumulate pyroxenes and plagioclase grains with resorption of the original framework plagioclase grains, 3) infiltration of hydrothermal fluids, and 4) subsequent precipitation of PGE's.

   The evidence presented suggests a strong case for the role of hydrothermal fluids in the transport and deposition of the PGE within the Picket Pin deposit. The above mineralogic evidence suggests that hydrothermal fluids contained (OH), Na, Cl, and Fe^{+++} and were constrained within the pyroxene-poor, coarse-grained zones of AN II. This oxidized hydrothermal fluid may have scavenged and transported PGE's, which were then deposited and concentrated when the fluids encountered the reduced environment of the primary sulfide horizon.

Acknowledgements

TABLE OF CONTENTS

Page

List of Figures

List of Tables

I. Introduction

The processes of transportation and deposition of 'reef-type' platinum-group-elements (PGE) deposits remains enigmatic although numerous models have been proposed (Boudreau, Naldrett, Zientek and others). The goal of this contribution is to test the models using petrographic, textural, and geochemical analyses.

The Stillwater Complex contains reef-type, PGE-enriched, sulfide-bearing intervals which include the J-M Reef and the Picket Pin deposit (Fig.1). The J-M Reef is located approximately 500 m above the contact of the Ultramafic Series and the Banded Series. The JM-reef occurs within the Troctolite-Anorthosite zone I (TAZ I), a complex lithologic unit that contains numerous subdivisions. The Picket Pin deposit, located approximately 3 km above the J-M Reef, is hosted within a thick anorthosite, Anorthosite zone II (AN II) of the Middle Banded series. The lack of lithologic complexities within the Picket Pin deposit provides an excellent opportunity to investigate the PGE-ore formational processes.

Study Area

Access the study area by traveling west from Limestone, Montana on US Forest Service Road 410 (Picket Pin-Iron Mountain road). The road crosses the Picket Pin deposit as the road levels off just south of the Picket Pin cirque. The contact between Anorthosite II (AN II) of the Middle Banded series and the lowermost troctolite of Olivine-Bearing V zone (OB V) of the Upper Banded series (the Picket Pin deposit) trends east down the drainage from this plateau. The study area is down the drainage and approximately 300 m due east from the plateau crest (Fig 2).
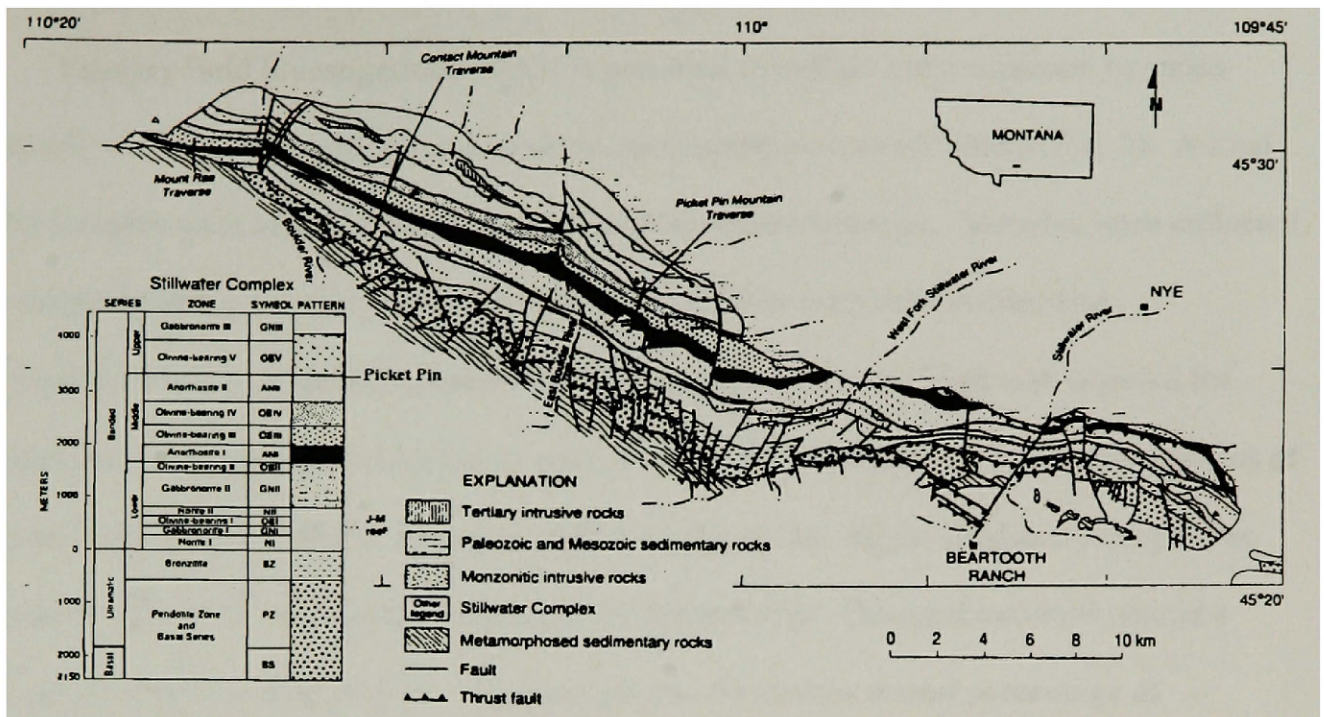
Figure 1. Geologic map of the Stillwater Complex (modified from Zientek, 1985).
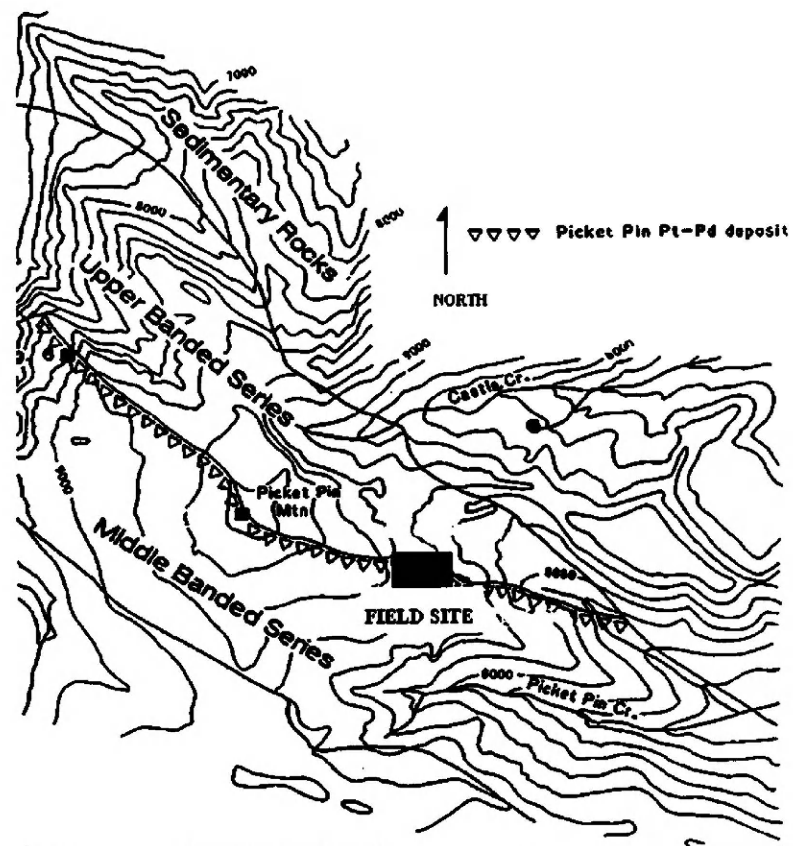
Figure 2. Topographic map of field area (modified from Boudreau, 1986).

Methodology

Primary field investigations of AN II proximal to sulfide mineralization revealed intricately varying compositions on a scale of centimeters to tens of meters (Fig. 3). A total of 150 samples were selected from five highly-mineralized outcrops. Samples were collected on a three-meter square grid to prevent bias and to include both mineralized and unmineralized rock. A single outcrop with dimensions of 15 m by 25 m was selected for detailed petrographic and mineralogical analysis (Fig. 4). Observations and interpretations of this outcrop were later compared to the other 4 sample grids. Initial field and petrographic analyses involved 35 representative samples of this outcrop. The representative samples . were subdivided into four groups. The four groups, divided by modal percentage of intercumulate mafic-minerals (pyroxenes and olivine), are 0-5%, 5-10%, 10-15%, and 15-20% (Fig. 5).

Petrographic microscopy on polished thin sections of each sample were used to determine modal abundance of minerals, textural relationships, and sulfide-oxide relationships. Point counts were preformed on a total of twelve thin sections, three from each pyroxene group. One thousand point counts were preformed on each thin section for a total of 12,000 counts. An additional 4,500 counts were made on select thin sections to determine the olivine/bronzite/augite ratio for each pyroxene group. Point counts were performed on a Leitz/Wetzlar microscope fitted with a James Swift auto-stage and a Hacker Instruments Prior Model G counter set to a 400 micron step interval, and were used to determine modal percentages (Table 1). Preliminary An content was determined using Scanning Electron Microscopy (SEM), Backscattered Electron Imaging (BEI), and Energy Dispersive X-ray Spectroscopy (EDS) was performed at the Image and Chemical Analysis Laboratory (ICAL) at Montana State University, Bozeman. ICAL laboratory facilities
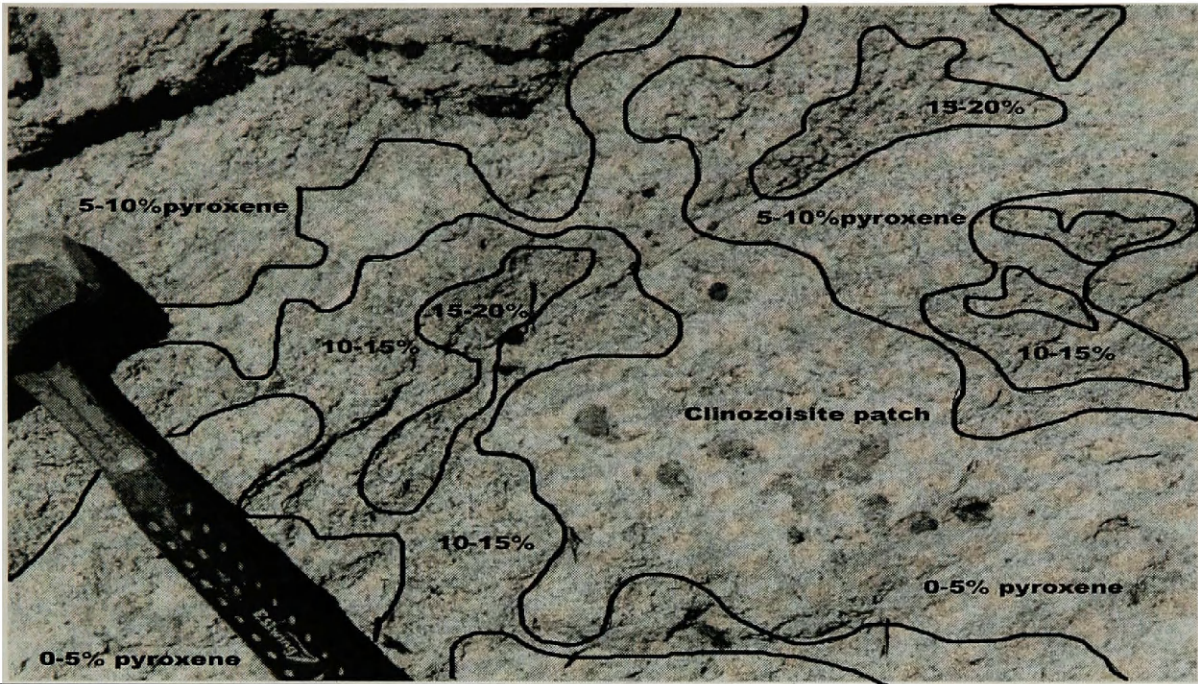
Figure 3. Outcrop photograph depicting varying pyroxene content. Note the clinozoisite patches only occur within the 0-5% pyroxene group.
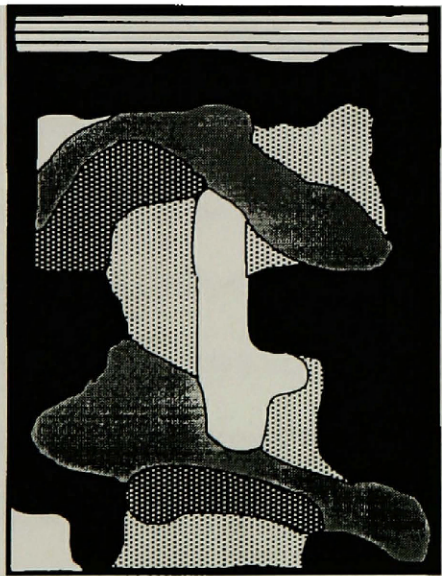
Figure 4a. Compositional map of study area. Width of map is approximately 15 m.

- 0-5% pyroxene
- 5-10% pyroxene
- 10-15% pyroxene
- 15-20% pyroxene
- covered
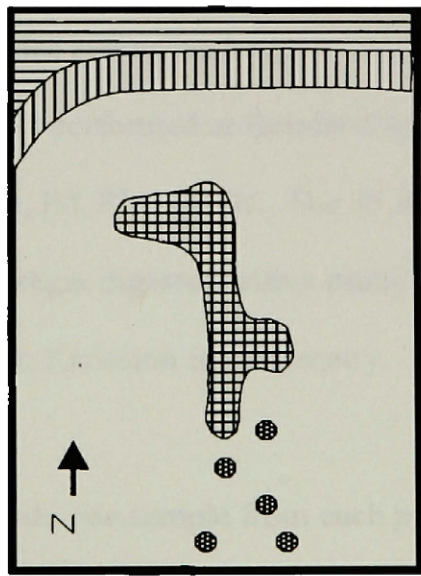
Figure 4b. Plan view of same study area depicting lithologic units and sulfide distribution.

- Troctolite
- Medium-grained anorthosite
- Coarse-grained anorthosite
- Sulfides
- Clinozoisite patches

consist of a Jeol Model 6100/Noran/Oxford microprobe with a LaB_6 source for SEM, X-ray source for EDS, and a Cathode-Luminescence source for BSE. The microprobe used between 15 and 30 kilovolts accelerating voltage, dependant on the element analyzed, 15 nanoamps beam current, and a beam width of 3 microns. Count times were typically 4000 counts per element. Rontgenanalysen-Technik (Rontec) software was used for spectral and elemental analysis, density imaging, and elemental mapping.

Silicate mineral compositions and zoning patterns were determined by microprobe analyses. Microprobe analyses was preformed at Washington State University on a Cameca MBX microprobe with four wavelength dispersive spectrometers, with automation provided by Advanced Microbeam Inc. The microprobe used 12 nanoamps beam current, 20 kilovolts accelerating voltage, with a beam width of 2 microns. Multiple well-constrained standards were used to calibrate the microprobe (see appendix II).

Geochemistry was performed on 32 hand-samples averaging 2 kg per sample. Precious metal assays and whole-rock geochemistry was performed at Bondar-Clegg laboratory, Vancouver, for 35 elements plus Au, Ag, Pt, Pd, Rh, and Os. The 35 major elements were analyzed using plasma analysis of aqua regia digested with a multi acid (HCl-HNO_3., HF-$HClO_4$) technique, detected by ICP- Atomic Emission Spectrometry. The precious metals were analyzed by fire-assay.

Samples selected for fluid inclusion study include one sample from each pyroxene group plus four additional samples from the sulfide-bearing zone for a total of 8 samples. The samples were doubly polished to the standard thickness of 0.03 mm. Analysis was made in the fluid inclusion laboratory at the University of Montana. The laboratory consists of the USGS standard fluid inclusion set up which includes a heated/cooling stage from Fluid Inc., and a Nikon microscope with an 100 power objective.

Representative plagioclase grains of both the large and small groups were chosen for microprobe analyses after petrographic analyses for an average of three grains for the large, and five grains for the small group. An automated linear traverse from opposite grain corners was programmed to take analyses every millimeter for the large grains (roughly 20 analyses), and 0.5 mm for the small grains (roughly 10 analyses). Therefore, each pyroxene group averaged 110 sample points. Analyses were then averaged rim to core between grains and plotted for each plagioclase grain size (large or small), and each pyroxene group.

15-20%   10-15%   5-10%   0-5%

☐ Small, Intercumulate Plagioclase	☐ Olivine ▦ Augite
▥ Large, Framework Plagioclase	■ Bronzite ▨ Altered Pyroxene
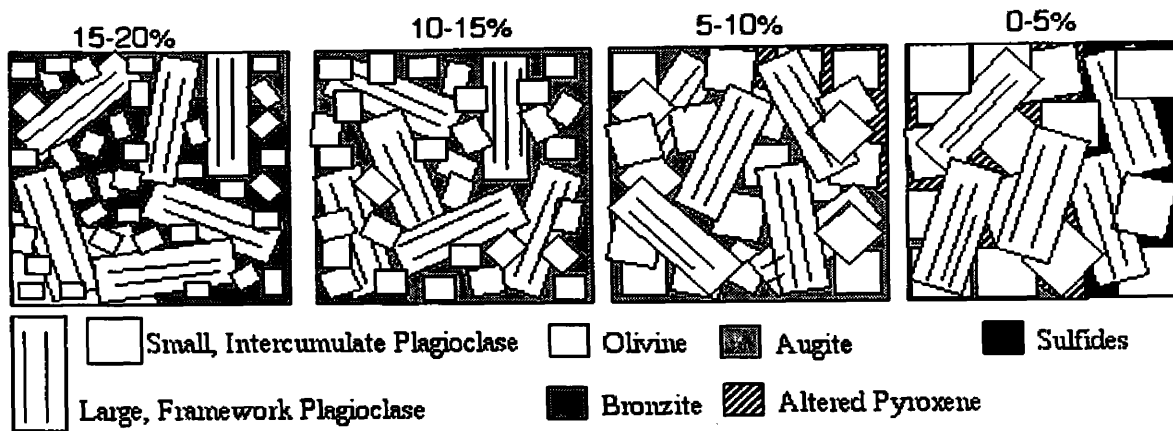
■ Sulfides

Figure 5. Lithologic divisions of study area by modal pyroxene percentage. Note the increase in grain size of the intercumulate plagioclase proximal to sulfide mineralization. All mafic minerals occur as oikocrysts.

Banded series

Upper Banded series — Gabbronorite III zone

Olivine-bearing zone V — Mixed subzone

Troctolite subzone

Middle Banded series — Anorthosite II zone — Medium-grained anorthosite member

Coarse-grained anorthosite

Picket Pin Pt-Pd deposit

10 m
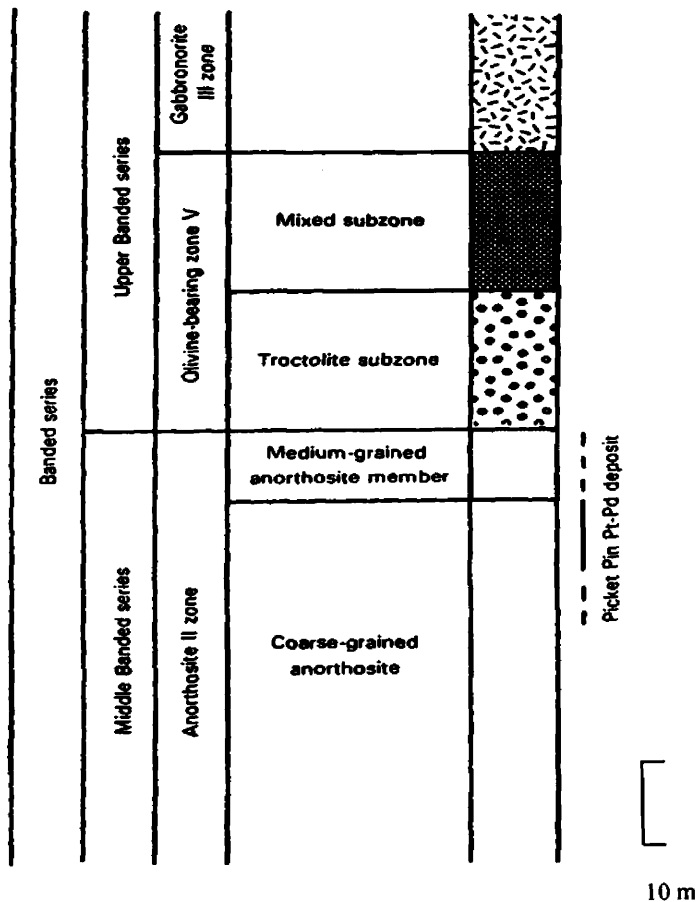
Figure 6. Stratigraphic column of the top of the Middle Banded Series, including the position of the Picket Pin deposit, and Upper Banded Series (after Boudreau, 1986).

7

II. GEOLOGIC SETTING FOR THE STILLWATER COMPLEX

The Stillwater Complex, a 2.7 Ga layered mafic complex, is situated in a fault-bound

block in the northern Beartooth Mountains of south-central Montana (Fig.1). The complex is

exposed along strike (N 60° W) for approximately 48 km (Page, 1985), and attains an

exposed thickness of 6.5 km (Kleinkopf, 1985). The dip of the intrusive layers ranges from

less than 50°N to vertical, and is locally overturned. A 1,555-m continuously cored, vertical

drillhole collared in the Stillwater River canyon indicates 1,990 m of northward

overthrusting during the Laramide orogeny (Geraghty, 1999). The original shape and size of

the complex are unknown but the top part has been removed by erosion. Both geophysical

and gravimetrical data suggest subsurface extension of the complex for several kilometers to

the north and northeast.

The complex intruded into middle Archean gneisses and metasediments. It caused a

wide basal contact aureole up to pyroxene-hornfels grade. This basal contact aureole extends

approximately 8 km perpendicular to strike. Pressure-temperature conditions inferred from

the aureole near the contact are 3 ± 0.5 kbar with a temperature of 850°C (Vaniman et al.,

1980, Labotka et al., 1985, 2001). Evidence from the P-T conditions may suggest that the

complex represents a subvolcanic chamber in which the volcanic carapace has been lost to

erosion (Helz, 1995). Mafic dikes and sills immediately below the complex prompted

attempts to correlate their composition with the Stillwater rocks and possibly determine the

composition of the Stillwater primary magma (Longhi, 1983, Helz, 1985, 1995). Numerous

mafic dikes and granitic bodies of late Archean to Eocene age intrude and cross-cut the

complex. They constrain a relative time of emplacement of the complex.

Isotopic evidence demonstrate one of the following: 1) The Stillwater Complex

crystallized 2,700 Ma from magmas derived from an enriched upper-mantle source, that had

a history of Rb/Sr, Nd/Sm, U/Pb and Hf/Lu enrichment; or 2) the Stillwater Complex

crystallized 2,700 Ma from either a undepleted chondritic source or a depleted source, that

was contaminated with older continental crust that exhibited enrichment in incompatible

elements (Lambert et al., 1985). Isotopic evidence further suggests that numerous

metamorphic events have effected the complex. Since middle Eocene time, the Stillwater

Complex has been subjected to erosion, uplift, glaciation, and minor faulting (Page, 1977).

III. GEOLOGY

Applying the nomenclature of McCallum et al. (1980), the Stillwater Complex has

been divided into three main units: the Basal, Ultramafic, and Banded series (Fig.1). The

Basal Series is laterally continuous, variable in thickness, and locally up to more than 100 m

thick. The unit primarily comprises of orthopyroxenites with subordinate underlying norites.

Massive accumulations of base-metal sulfide minerals, locally PGE-rich, occur throughout

the Basal series. Sulfide occurrence increases downsection toward the basal contact, but is

locally interrupted by reversals and discontinuities (Zientek et al., 1985). The Basal series is

bound above by a sharp contact with the lowermost olivine cumulates of the Ultramafic

series.

The Ultramafic series is divided into two subunits: the lower Peridotite zone and the

overlying Bronzitite zone. The Lower Peridotite Zone consists of cyclic poikilitic (bronzite)

harzburgite (olivine cumulate) with locally PGE-enriched chromite, granular harzburgite

(olivine-bronzite cumulate), that is overlain by bronzitite (bronzite cumulate). The number

of cyclic units varies along strike. Between 8 and 21 cyclic units have been recognized

throughout the Peridotite zone (Zientek et al., 1985). The disappearance of cumulate olivine

marks the sharp contact between the Peridotite and Bronzite zones. The Bronzitite zone

consists of size-graded and laminar-bronzite cumulates. Local cumulus olivine and chromite occur in thin layers within the Bronzitite zone (Raedeke and McCallum, 1984).

The contact between the Ultramafic and Banded series is marked by the lowest occurrence of cumulate plagioclase. The plagioclase-rich cumulates of the Banded series are up to 4.5 km thick, and make up more than three fourths of the exposed Stillwater Complex. The Banded series is divided into the Lower, Middle, and Upper Banded subseries. It is further subdivided into twelve zones by cumulate mineralogy (Fig. 1) (McCallum et al., 1980). The Lower Banded series is approximately 1,590 m thick and contains norites and gabbronorites with minor occurrences of anorthosite, pyroxenite, and troctolite. The An content of the plagioclases decreases up section from An 82 to An 75, which may suggest fractional crystallization from a basaltic magma (Raedeke and McCallum, 1980). The Lower Banded series is host to the laterally continuous, PGE-rich J-M Reef with an average grade of 20-25 ppm Pd+Pt (Leroy, 1985). The upper boundary of the Lower Banded Series is located at the contact of the first thick anorthosite unit (AN I).

The Middle Banded series is approximately 1,750 m thick and contains the two thick anorthosite units, AN-I (350 m thick) and AN-II (570 m thick). AN-II is further divided into a basal coarse-grained anorthosite (~560 m thick) and is overlain by a medium-grained anorthosite (~10 m thick) (Boudreau and McCallum, 1985) (see also Fig. 6). Situated between AN-I and AN-II are two olivine-bearing zones, OB-III (400 m) and OB-IV (430 m thick). Most rock types found within the olivine-bearing units are troctolites, gabbros, and gabbronorites, with the exception of a 90-m anorthosite in OB-IV. Two major petrographic deviations occur within the Middle Banded series; 1) The remainder of the complex is enriched in plagioclase (82 volume percent) which is more than the 60 volume percent expected from fractional crystallization of a noritic magma under the inferred pressures, and

2) The average An content remains consistent throughout the two thick anorthosite units at An $_{76}$, with the exception of the base of AN-I where it is An $_{80}$ (Raedeke and McCallum, 1980). Mineralogy of the two anorthosite units, AN-I and AN-II, consists of approximately 90 volume-percent plagioclase, intercumulate olivine, intercumulate augite and inverted pigeonite, with local intercumulate sulfide minerals and oxides. Intercumulus sulfide and oxide mineralogy consists of magnetite, ilmenite, pyrrhotite, pentlandite, chalcopyrite, minor pyrite, and PGEs. Detailed petrography and mineralogy of AN-II are discussed below. The upper boundary of the Middle Banded series is marked by the reappearance of olivine, and is placed at the upper contact of AN-II with the overlying troctolite of the olivine-bearing zone V (OB-V).

The Upper Banded series is approximately 1,130 m thick and divided into two zones, the lower olivine-bearing zone (OB-V), and upper gabbronorite zone (Gabbronorite III). The lower OB-V (~95 m thick) is characterized by variable sequences of troctolites, anorthosites, norites, and gabbronorites. Gabbronorite III, approximately 1,035 m thick, is a uniform gabbronorite with cotectic proportions of plagioclase, augite, and low-Ca pyroxene. The An contents for the plagioclase in the Upper Banded series are, bottom to the top, An $_{73}$ to An $_{62}$ from the. This is consistent with the fractional crystallization model (Raedeke and McCallum, 1980). An unknown amount of the top of the Upper Banded series has been lost to erosion (Helz, 1995). Paleozoic sedimentary rocks unconformably overlie the upper contact.

CHAPTER TWO: THE PICKET PIN PGE DEPOSIT

I. GEOLOGIC SETTING OF THE PICKET PIN PGE DEPOSIT

The Picket Pin PGE deposit is a zone of disseminated PGE-bearing sulfide approximately located throughout the uppermost 150 m of the coarse-grained and medium-grained anorthosites of AN-II (Fig. 6). The deposit is a vertically intermittent but laterally continuous zone of PGE-bearing sulfide mineralization along the entire 22 km of exposed strike of the deposit. The sulfide distribution typically occurs as recurrent stratabound, podiform, and lenticular concentrations of 1 to 10 percent sulfide minerals occupying intercumulate grain boundaries of plagioclase within the upper portion of AN II (Fig. 7). The sulfide mineralogy consists of pyrrhotite ($Fe_{1-x}S$), chalcopyrite ($CuFeS_2$), pentlandite ($(Fe, Ni)_9S_8$), braggite ($(Pt, Pd)S$), and minor pyrite (FeS), in decreasing order of abundance. Sperrylite ($PtAs$) was identified by SEM. Mineralized pods range in diameter from centimeters to meters; the lenses attain a maximum thickness of approximately 1.5 meters, with a lateral extent of tens of meters (Boudreau and McCallum, 1985). Sulfide mineralization is less abundant in the overlying medium-grained anorthosite and troctolite of OB V. Where it is present, it generally lacks significant PGE content (<5ppb).

II. Previous work and Exploration of the Picket Pin

Howland and Peoples were the first to find PGE-bearing sulfide minerals in the Banded series (Howland et al., 1936). They found two distinct sulfide-bearing horizons in the upper portion of the complex. The uppermost zone of anomalous PGEs, appears to describe the Picket Pin deposit (Boudreau and McCallum, 1985). Jones et al. (1960) noted disseminated sulfide minerals beneath the troctolite at Picket Pin Mountain. Hess (1961)

further noted 3 layers containing 1-2% sulfide minerals 0.25 to 0.5 meters apart near the top

of the anorthosite. He believed that they correlated with the uppermost PGE anomaly of

Howland et al. (1936).

The Manville Corporation (formerly the Johns-Manville Corporation) initiated an

exploration effort in 1967 to discover PGE potential within the Stillwater Complex. Manville

geologists found PGE-bearing mineralization associated with a large lens of bronzitite within

the Banded series, at the contact of the Ultramafic series and the Banded series (currently

considered the Volatile Enriched Zone, VEZ), at the contact between Stillwater Complex

rocks and a young intrusive granite stock south of Picket Pin Mountain, and in the discovery

of the Howland Reef of OB I (more commonly known as the J-M Reef). The Manville

geologists did not include the Picket Pin deposit in their work.

The Picket Pin deposit was staked in 1979 by the Anaconda Minerals Company, and

mapping confirmed the lateral continuity of the deposit. Anaconda evaluated the deposit

with two deep diamond drill holes, 30 shallow "winkie" drill holes, and by numerous grab

samples along 17 km of the deposit from east of the Boulder River to the most-easterly

exposure of the deposit (Fig. 8). Anaconda found anomalous concentrations of PGE

associated with 1 to 2 percent disseminated sulfide in up to six discontinuous layers. The

location of these anomalous PGE sulfide layers is in the anorthosite (An II) just below the

contact with the overlying troctolite of OB V. The highest grades encountered in drill cores

were 1.37 g/tonne (0.04 ounce per tonne, hereafter opt) platinum and 3.09 g/tonne (0.09 opt)

palladium over 1.04 m. Surface grab samples obtained slightly higher grades of 3.77 g/tonne

(0.11 opt) platinum and 4.11 g/tonne (0.12 opt) palladium. Anaconda's exploration program

found the Pt/Pd ratio to be approximately 1:1 (Marshall, 1992).
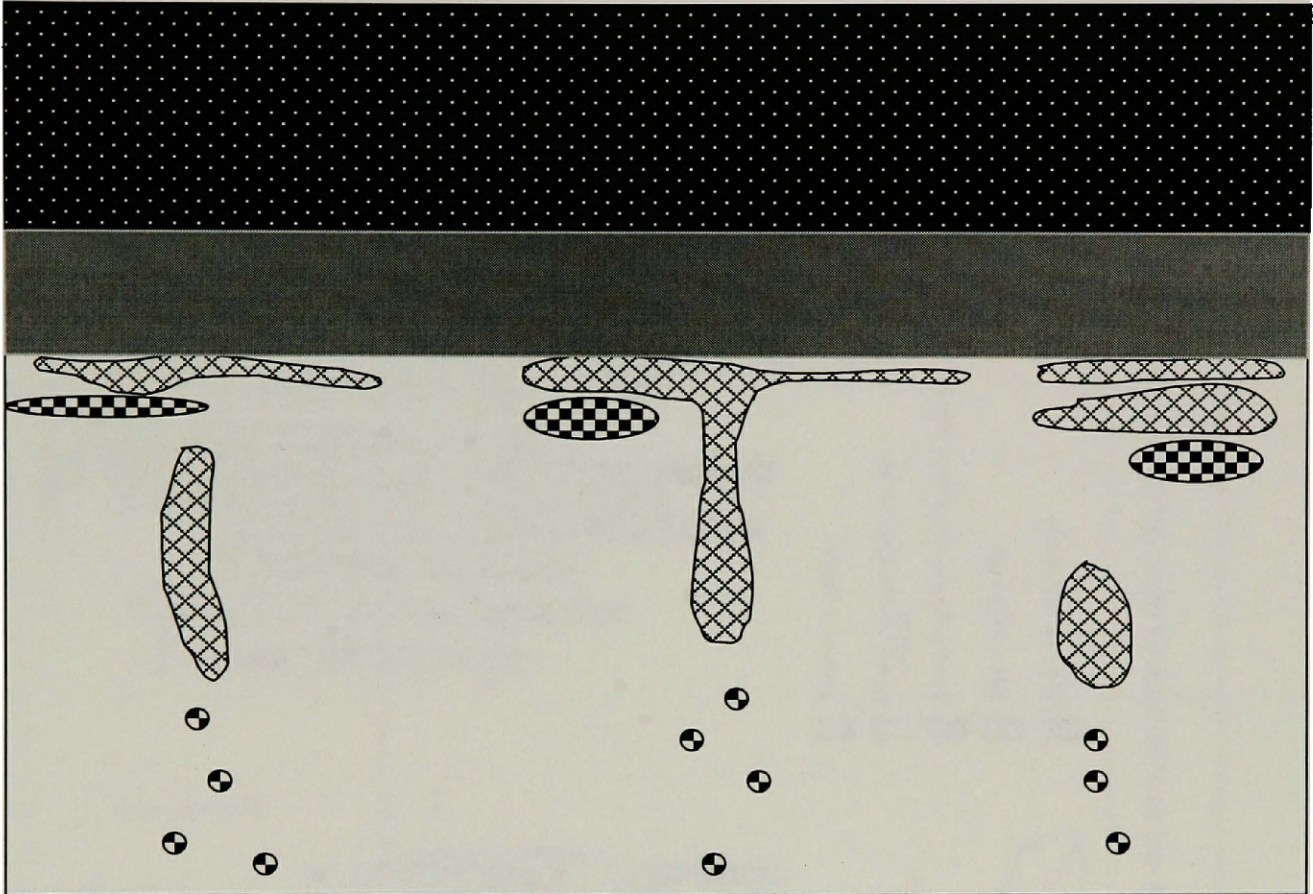
Figure 7. Schematic of sulfide mineral distribution within the Picket Pin PGE deposit.
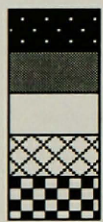
Troctolite
Medium-grained anorthosite
Coarse-grained anorthosite
Sulfide mineralization
Clinozoisite patches

10 m
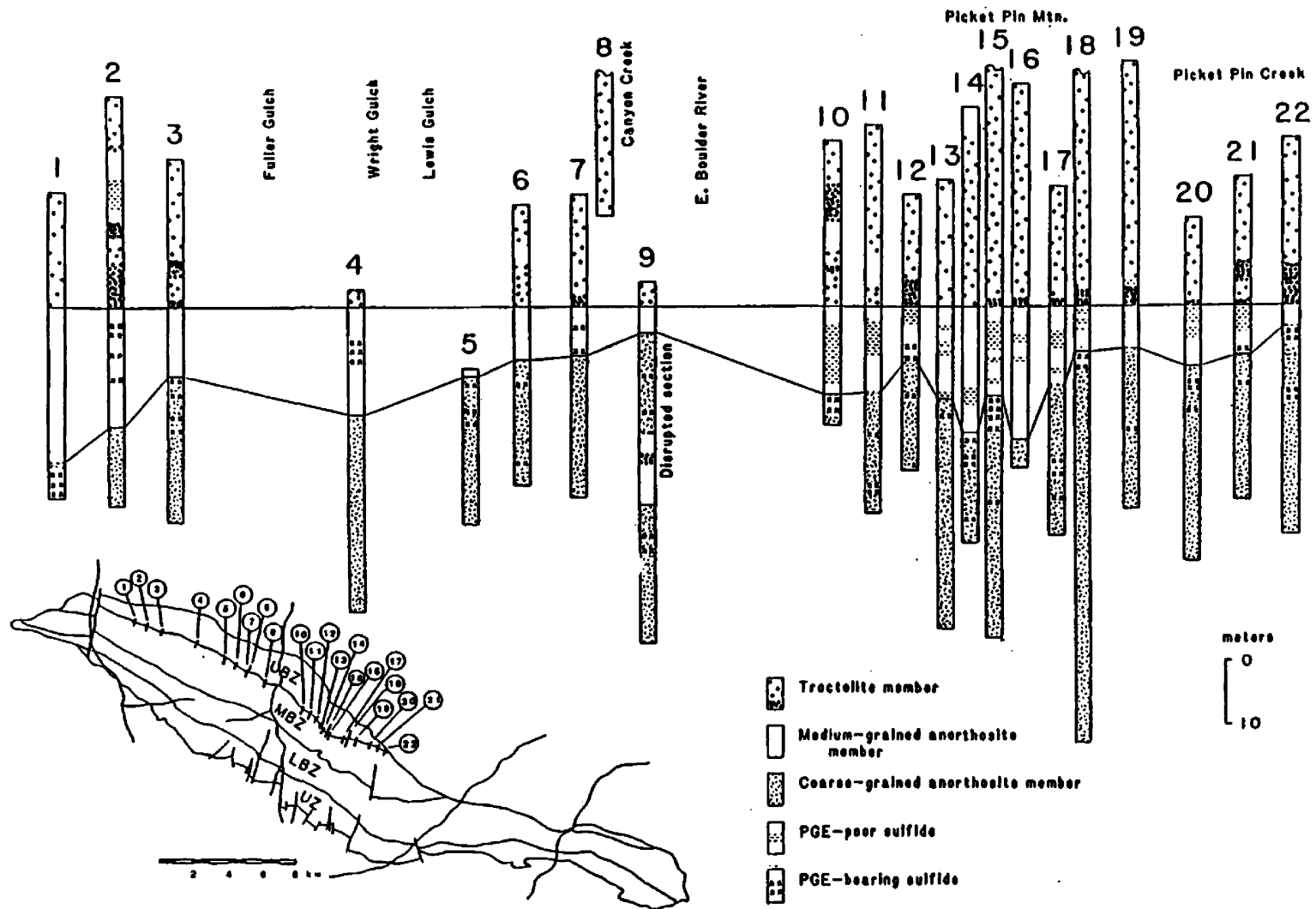
Figure 8. Anaconda drill intercepts of the Picket Pin sulfide mineralization (after Boudreau, 1986).

International Platinum picked up the claims in 1989, and conducted an exploration program on the eastern 10 km of the Picket Pin horizon. The program consisted of mapping, ground geophysics, trenching, and 14 diamond drill holes. Four distinct types of PGE-bearing sulfide zones were encountered in drill core. The four types range from very finely disseminated to coarsely intergranular sulfide mineralization. The intergranular, 1 to 5 percent sulfide zone contained the highest grades of 4.6 g/tonne (0.14 opt) Pt + Pd over 0.61 m. This higher-grade zone was within a larger, 9.9 m-thick zone containing 2.33 g/tonne (0.07 opt) Pt + Pd. The Pt/Pd ratios were approximately 1:1. This mineralized zone is similarly located at the contact of the anorthosite (An II) and overlying troctolite of OB V (Marshall, 1992).

Idaho Consolidated Metals Corporation holds the Picket Pin claims and is currently exploring the deposit. The exploration effort consists of mapping and grab samples; no drilling had commenced as of December, 2001. The highest grades found are 1.955 g/tonne Pt, 2.520 g/tonne Pd, and 0.093 g/tonne Rh for a combined total PGE assay of 4.568 g/tonne (0.143 opt). Although active exploration continues, little has been published on the Picket Pin deposit. Further, there remains a poor understanding of sulfide emplacement, and models are vigorously debated.

III. Origin of Anorthosite II

Any attempt to understand the transport and deposition of ore-body mineralization must include the effects on and the origin of the host rock. The origin of the two thick anorthosites of the Middle Banded zone of the Stillwater Complex, and anorthosites in general, pose a major petrologic problem. Models of the origin of anorthosites can be roughly divided into two groups: 1) An anorthositic magma either from the mantle or from

melting high Ca and Al sediments, and 2) Segregation and concentration of plagioclase by some physical process such as settling or floating of cumulus plagioclase grains. In the case of the Picket Pin deposit, and the Stillwater Complex, critical review of proposed models can lead to plausible inferences. A description of the models leads to a more critical review in the discussion section below.

Hess (1960) suggests that plagioclase was formed near the roof of the intrusion and moved downward by intermittent convection currents. Before the plagioclase could settle, the next density flow of magma would carry the crystals upward. Hess believed that the central part of the intrusion contained enough superheat to resorb the plagioclase, and therefore push the magma composition well into the plagioclase crystallization field. It follows that plagioclase would precipitate for long periods during crystallization of the Middle Banded zone. In opposition, the amount of superheat needed for this process seems unlikely since considerable crystallization in the chamber that had already taken place.

Raedeke (1979), Raedeke and McCallum (1980), and McCallum et al. (1980) expanded on the hypothesis first put forward by Hess (1960). They noted that the plagioclase composition is of near-constant composition throughout the Middle Banded zone, and that the plagioclase grains within the thick anorthosites are on average twice the size of those in the norites, gabbronorites, and troctolites which make up most of the Middle Banded zone. They suggested that plagioclase crystallization was confined to the upper part of the chamber due to suppression of crystallization relative to mafic mineral crystallization at higher pressure. The plagioclase would remain in suspension because of its relative low density compared to the mafic magma and is suggested to have remained in compositional equilibrium. McCallum et al. (1980) suggested a similar mechanism as Irvine (1980) for deposition of the plagioclase as a crystal mush carried in density flows. They suggest that

18

because the ratio of plagioclase to trapped melt was large, the plagioclase remained at a near-constant composition, whereas the mafic-mineral composition was variable due to the variable amounts of trapped melt. On the other hand, the intricate zoning and resorption textures within the plagioclase suggest that the plagioclase is unlikely to have remained in compositional equilibrium with the evolved magma.

Irvine et al. (1983) and Todd et al. (1982) suggest that the anorthosites formed from one of two parental magmas responsible for the Stillwater Complex as a whole. They suggest that the near-consistent composition of the plagioclase may be due to the lateral advance of the crystallization front into a magma column stratified by double-diffusive convection. This process may have been responsible for the deposition of the cumulate plagioclase. However, the observed segregation of pyroxene-rich and pyroxene-poor domains along with the large pyroxene oikocrysts suggest limited mixing of the interstitial fluid. Boudreau (1986) argues that the crystallization sequence of this model has olivine after plagioclase, and therefore should have olivine as a common interstitial mineral. Boudreau (1986) reported intercumulate olivine as a rare occurrence within AN II. The present study has identified large olivine oikocrysts and the intercumulate mafic mineralogy consists of approximately 10% olivine.

The complex zoning patterns of the plagioclase, which include normal, reverse, patchy, and oscillatory zoning, was first considered within the model proposed by Scheidle et al. (1982). This model proposed that the plagioclase intruded as a crystal mush. Scheidle (1983) later suggested that the stratigraphic compositional variations in plagioclase separates represents a mixing of two magmas, the first magma on an olivine-plagioclase cotectic with a second magma on the plagioclase-pyroxene cotectic to produce a hybrid magma within the plagioclase field.

In contrast to Scheidle (1983), Salpas et al. (1983, 1984) found the amount of stratigraphic compositional variation within An II to reflect outcrop-scale heterogeneities. This early study of Salpas et al. (1983, 1984) examined the trace-element distribution within the interstitial mineral assemblage. A true comparison between Scheidle (1983) and Salpas et al. (1983, 1984) may not be appropriate. Scheidle (1983) studied plagioclase separates, whereas Salpas et al. (1983, 1984) studied the interstitial mineralogy, which consist mainly of mafic-mineral phases. Salpas et al. (1983, 1984) concluded that the bulk of the pyroxene has a cumulus chemical signature and formed at the nucleation front of a solidifying magma. They suggested that the quartz and other minor phases such as sulfide minerals crystallized from the minor (<5%) trapped melt. They further suggested that the irregular distribution of the pyroxene oikocrysts suggests substantial interstitial-melt migration. Haskin and Salpas (1992) studied a 10 m X 10 m outcrop of AN II and describe how the two anorthosites may have been constructed from plagioclase crystals and magma. The work was initiated to understand the seemingly random compositional variations observed from traverses across AN I and AN II in the previous work of Salpas et al. (1983). They suggest that an average of 67% cumulus plagioclase formed a stable framework of complexly zoned plagioclase within a melt. The interstitial space within the framework filled in part with plagioclase and pyroxene that crystallized in equilibrium with the bulk melt. The remaining interstitial space filled with pyroxene and plagioclase that crystallized from the trapped melt. Haskin and Salpas (1992) do not attempt to address the origin of the original framework plagioclase.

IV. Stratigraphy and General Geology

Due to the variability in nomenclature from author to author, the U. S. Geological Survey modified the nomenclature used by McCallum et al. (1980) in an attempt to unify the

stratigraphic nomenclature (Zientek, 1985). Further subdivisions of Anorthosite zone II have

been proposed by Boudreau (1986) and are used in this study (Fig. 6). Anorthosite zone II

(AN II) has been divided into the following two members:

Coarse-grained anorthosite member (Fig. 9):   This member comprises most (ca.

600 m) of AN II, and is distinguished from the overlying medium-grained anorthosite

member by a marked change in plagioclase grain size and pyroxene mode. The average

plagioclase grain size of this unit is 2-3 times larger (up to 2.5 cm) than the plagioclase

within the troctolites, norites, and gabbronorites that make up most of the Banded Series

(McCallum et al., 1980; Scheidle, 1983). This unit is massive and unlayered with non-

uniform, variable pyroxene percentage (see also Fig. 3). This unit consists of cumulus

plagioclase with up to 20% interstitial mafic minerals- augite, inverted pigeonite, and olivine,

in decreasing order of abundance. On an outcrop scale the interstitial mafic minerals exhibit

two different textures. In most outcrops the mafic minerals form an extensive

interconnected network, whereas discrete 2 to 10 cm pyroxene oikocrysts are predominant in

others.

The average reported composition of plagioclase is approximately the same for AN I

and AN II (McCallum et al., 1980; Scheidle, 1983; Czamanske and Scheidle, 1985). The An

content for AN I and AN II is between An_{73} and An_{77}, with no apparent change in

composition with stratigraphic height (Loferski and Arculus, 1993). However, Czamanske

and Scheidle (1985) identified numerous complexly zoned plagioclase grains with

compositional variations of as much as 12 mol% An. Plagioclase grains show normal,

reverse, oscillatory, and patchy zoning within single thin sections. From the several thousand

electron-microprobe analyses of the plagioclase grains from both AN I and AN II, four main

points are revealed: 1) it is difficult, if not impossible to recognize adcumulate growth; 2)

associated grains show no evidence of growth in a common equilibrium environment, or uniform response to system wide perturbations; 3) many grains show highly irregular contacts and dissolution along these contacts as revealed by truncated compositional zones; and 4) the zoning patterns may be either regular or more commonly broad, convolute and non-concentric (Czamanske and Scheidle, 1985).

Medium-grained anorthosite member (Fig.10): Although both thick anorthosites (AN I, AN II) are characterized by a variable 1-2 m relatively fine-grained, locally laminated anorthosite at their upper and lower contacts, the top of AN II contains an anomalous 5-15 m relatively fine-grained, locally laminated anorthosite, named the medium-grained anorthosite by Boudreau (1986). This unit shows a marked textural and modal change. The plagioclase grain size, averaging approximately 2 mm, is similar to that of the overlying troctolite and other rocks within the Banded series. Commonly, this anorthosite is monomineralic (Fig. 10), but may contain less than 5% interstitial pyroxene and rare olivine. Where pyroxene is present, it forms skeletal, 2 to 6 cm oikocrysts, and imparts a mottled appearance to the rock in outcrop. The contact between the medium- and coarse-grained anorthosites is generally sharp and planar. Where well-exposed in the field, the contact is less than a centimeter thick. Locally, this contact may be irregular and sinuous on a scale of centimeters. This contact is further complicated by lenses and layers of coarse-grained plagioclase within the medium-grained unit. These coarse-grained layers are generally associated with abundant intercumulus mafic minerals. Layers approximately 1 meter thick that contain intercumulate olivine occur locally (Boudreau, 1986). The medium-grained unit may show modal layering.
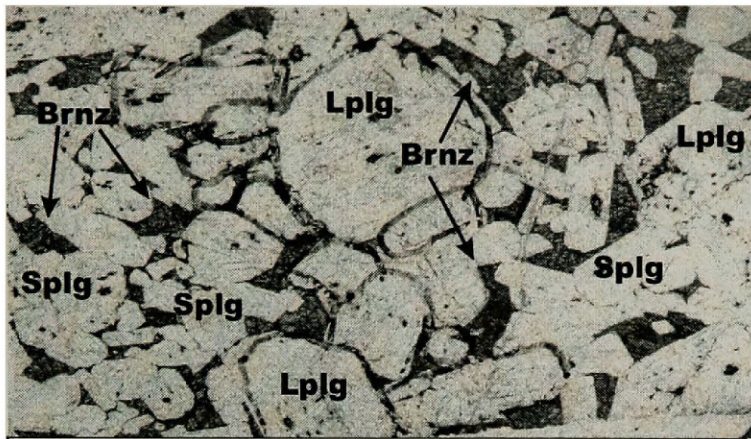
Figure 9. Plain light photograph of the coarse-grained member of AN II. Lplg = large plagioclase, Splg = intercumulate plagioclase, Brnz = bronzite. Width of photo is 35 mm.
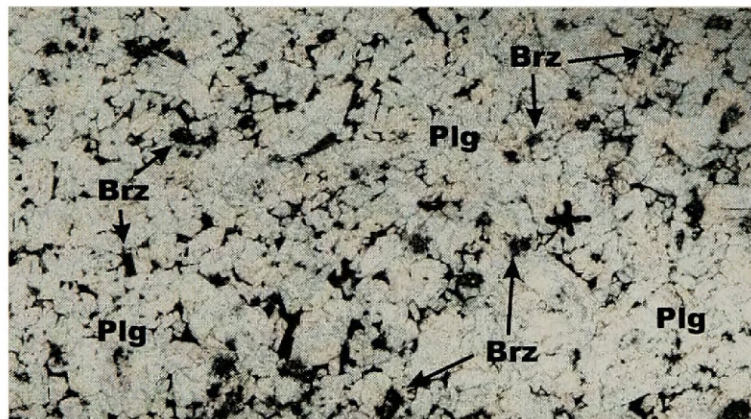
Figure 10. Plain light photograph of medium-grained member of AN II. Plg = plagioclase, Brz = bronzite. Width of photo is 35 mm.
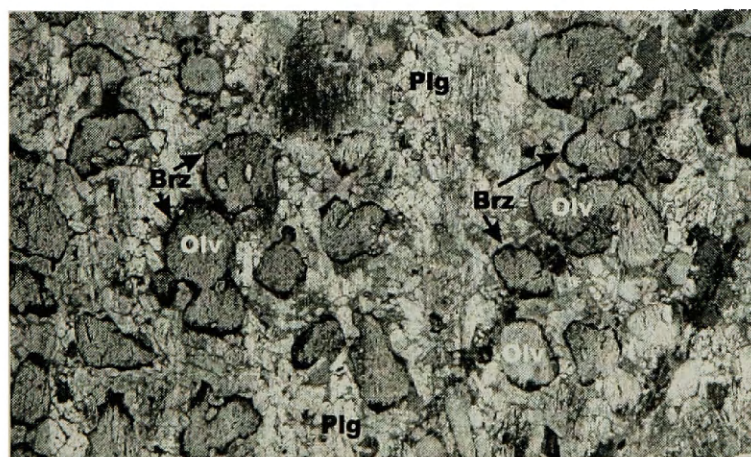
Figure 11. Plain light photograph of troctolite member of the overlying Upper Banded Series. Note small plagioclase (Plg) grain size. Cumulate olivine (Olv) is rimmed by bronzite (Brz). Width of photo is 35 mm.

Locally this unit shows lamination and foliation of the plagioclase. Sulfide minerals are much less common within this medium-grained unit. Where sulfide minerals are present, they are generally devoid of PGE content (Boudreau, 1986).

Troctolite subzone of Olivine-bearing subzone V (OB V)(Fig. 11): The contact between Anorthosite zone II and the overlying troctolites and anorthosites of Olivine-bearing series V mark the beginning of the Upper Banded series. The troctolite subzone is in sharp contact with the overlying medium-grained anorthosite of AN II. This subzone consists mainly of troctolite with subordinate anorthosite. Olivine and plagioclase are the main cumulate minerals within the lower few meters. Pyroxene is absent near the lower contact but increases in modal abundance up section. Bronzite occurs as rims around the olivine and as oikocrysts. Augite occurs as a subordinate interstitial mineral. The troctolite shows both modal and inch-scale layering (Fig. 11). This unit shows crossbedding and cut-and-fill structures which suggest flow banding in a semi-consolidated crystal mush (Boudreau, 1986). These features are exposed at the summit of Picket Pin Mountain.

V. Sulfide distribution

The Anaconda Minerals Corporation completed the most-detailed survey of sulfide mineral occurrence within the Picket Pin PGE deposit. Anaconda drill logs show the variation of mineralization along strike (see also Figs. 7 & 8) (Boudreau, 1986). Most of the sulfide mineralization of the Picket Pin deposit occurs within the uppermost 20 m of AN II. Major accumulations of sulfide minerals are found at and below the contact of the coarse-grained and medium-grained anorthosites of AN II (Boudreau and McCallum, 1985).

Locally, the PGE-bearing sulfide minerals also occur up to the contact with the overlying

troctolite. Minor sulfide minerals within the troctolite unit are typically barren of PGEs.

Mineralization of the Picket Pin deposit on a regional scale is stratabound, but more

accurately it occurs as podiform and lenticular concentrations of 1 to 5% sulfide minerals.

The sulfide minerals fill the intercumulate space between plagioclase grains. Mineralized

pods range in size from centimeters to several meters. The sulfide lenses are approximately

1.5 meters thick and attain a lateral extent of 30 meters. The lateral variation of

mineralization occurs on a scale of tens of meters, where well-mineralized areas are

separated by regions of unmineralized rock. This unmineralized rock locally contains

patches of magnetite and ilmenite.

PGE-bearing podiform and transgressive pipe-like bodies occur to a depth of 150 m

in the coarse-grained anorthosite below the ore zone. The pipe-like bodies locally crosscut

stratigraphy for over 50 m with a width ranging from 1 to 1.5 m, and in some cases lead to

well mineralized lenses and pods. Mineralization within the pipelike bodies is similar to the

stratabound lenses with 1-5% PGE-bearing sulfide minerals. They may have spotty

mineralization for a few meters both above and below. The pipe-like bodies are not related

to growth faults, fractures, or intrusive bodies that occur within AN II (Boudreau, 1986).

CHAPTER THREE: PETROGRAPHY

Coarse-grained anorthosite member:

Plagioclase is the principal component making up from 80 to 87% of the anorthosite; the grains form a interconnected network (see also Fig. 9). Grains range from lath-shaped to equant and from anhedral to subhedral. Haskin and Salpas (1992) divided the plagioclase grains into two groups: Large (>0.5 cm) framework plagioclase, and small (<0.5 cm) plagioclase. The large framework grains are interpreted to be original cumulate minerals and make up from 43 to 50% of the anorthosite. The small plagioclase grains occupy the space between the large grains, and are interpreted to be intercumulate plagioclase (Haskin and Salpas, 1992). Where the large, framework plagioclase grains appear to be consistent in size, the small, intercumulate plagioclase grains are not. The ratio of large to small plagioclase grains increases towards mineralization, and is highest in the mineralized samples. Thus, mineralization is concentrated within the coarser-grained intercumulate plagioclase rocks. The significance of this is that there is a minimum of okocrystic mafic minerals, which may act as a cement and restrict hydrothermal fluid flow.

Unusual erosional textures are apparent within the large plagioclase grains. These erosional textures appear to be either more abundant or more prominent away from mineralization. Numerous grains show a ragged, dissolution texture, whereas others have smooth grain boundaries. The large plagioclase grains are partly altered to sericite, epidote, and clinozoisite along grain boundaries. Many of the plagioclase grains are complexly zoned with a compositional variation of up to 12 mol% An. The zoning patterns may be either regular or more commonly broad, convolute, and non-concentric (Czamanske and Scheidle, 1985). Zoning patterns are difficult to identify microscopically, but appear to be either

oscillatory or reverse. This zoning appears to be randomly distributed from sample to sample. An interesting feature of these large plagioclase grains is the apparent lack of adcumulate growth. It has been reported that the composition of the plagioclase throughout Anorthosite zone I and Anorthosite zone II is consistent and do not change with stratigraphic height (McCallum et al., 1980; Scheidle, 1983; Czamanske and Scheidle, 1985).

Intercumulus pyroxenes typically make up 10 to 15 percent of individual samples, but range from trace to 20 percent (see also Fig. 5). Approximately 75% of the intercumulate pyroxene is clinopyroxene (augite), 15% is orthopyroxene (inverted pigeonite); the remaining 10% is olivine. The orthopyroxene contains blebs and lamellae of clinopyroxene and the clinopyroxene contains exsolution lamellae of orthopyroxene. The pyroxenes appear to be zoned by mineralogy. Bronzite is more abundant, making up 70% of the intercumulate mafic minerals, within the pyroxene-rich domains, and clinopyroxene is dominant (85%) within the pyroxene-poor domains. This may reflect a compositional change within the melt. The pyroxene alteration products include serpentine, amphibole, albite, and chlorite.

Intercumulate olivine has been identified in approximately 10% of the total samples in this study. The olivine may be optically continuous poikilocrysts that enclose one half of a thin section. The olivine occurs most predominantly within the 15-20% group (pyroxene plus olivine) and locally within the 10-15% group. It does not occur in any sample containing less than 10% intercumulate mafic-minerals. Alteration of olivine grades from iddingsite-magnetite, serpentinized with veins of magnetite, to only slightly altered, with a rim of serpentine. Most olivine falls into this last group.

The intercumulate mafic-mineral mode is not uniform within the coarse-grained anorthosite, and has been divided into ranges that fell within 0-5% pyroxene, 5-10%, 10-15%, and 15-20% pyroxene (Haskin and Salpas, 1992). The subdivisions into modal

pyroxene groups are important in delineating the sulfide-bearing horizons, which occur in the 0-5% range, the most altered pyroxenes. The modal divisions are also important in understanding the formational dynamics of AN II. Point counts on a Leitz/Wetzlar microscope fitted with a James Swift auto-stage and a Hacker Instruments Prior Model G counter were used to determine percentages (Table 1). Three thin sections from each pyroxene group was sampled with 1,000 counts, for a total of 12,000 counts. The variation between orthopyroxene and clinopyroxene was sampled with 4500 total counts. Below are the petrographic analyses of these divisions within the study area.

0-5%   pyroxene:

The major modal abundances of this group are: plagioclase (87%), sulfide minerals (10%), and relict clinopyroxene (2%). This division consists of a framework of large (0.5-2 cm), lath-shaped plagioclase grains. These large plagioclase grains are sericitized, highly altered to clinozoisite, and make up 46% of this rock type. Resorption textures occur on approximately 60% of the large plagioclase grains. Small (<0.5 cm), blocky plagioclase grains, also altered, make up 40% of this group (Fig. 12). The large to small plagioclase grain ratio is approximately 1:2, suggesting that the small plagioclase grains are one half the size of the large plagioclase grains. Clinozoisite and epidote (14%) occurs as a replacement within the plagioclase and as an alteration zone surrounding the sulfide minerals (Fig. 13). The sulfide minerals (up to 11%) fill the intercumulate spaces. Individual sulfide grains are also rimmed by quartz and albite. The relict pyroxene is altered to chlorite, albite, sulfide minerals, and epidote (Figs. 14 & 15).
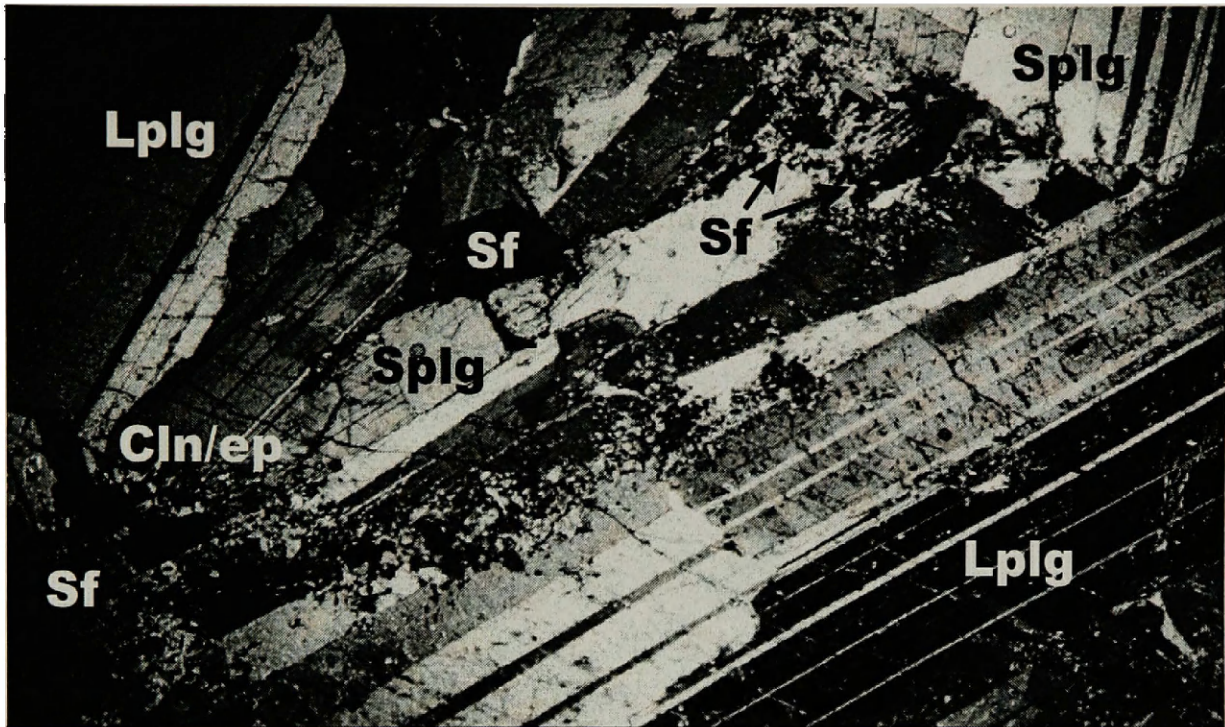
Figure 12. Crossed-polarized photomicrograph of the 0-5% pyroxene group. Clinozoisite/epidote (Cln/ep) forms extensive alteration along plagioclase grain boundaries. Note coarse grain size of the small plagioclase (Splg).
Lplg = large plagioclase, Splg = small intercumulate plagioclase, Cln/ep = clinozoisite/epidote alteration, Sf = sulfide grain (black). Width of photo is 25 mm.
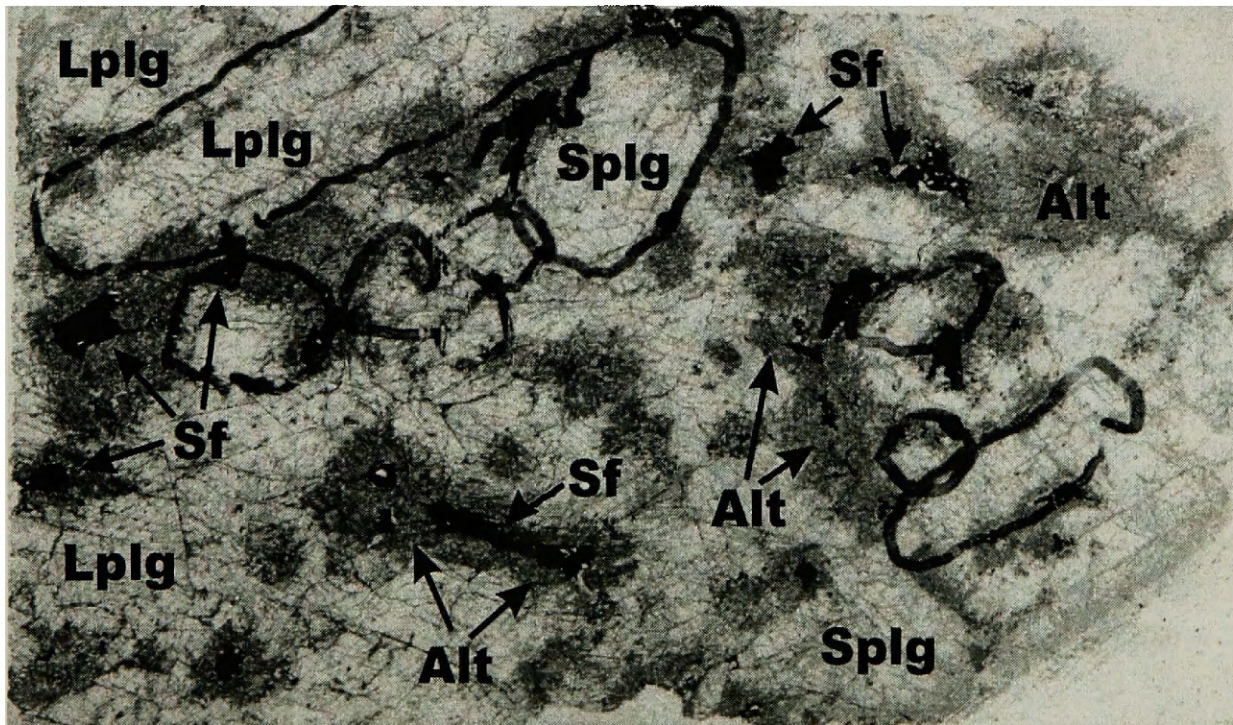
Figure 13. Plain-light microphotograph of the 0-5% pyroxene group. The clinozoisite/epidote alteration halo (alt) is obvious in this photo. Lplg = large plagioclase, Splg = small intercumulate plagioclase, sf = sulfide grains, alt = alteration halo. Length of photo is 35 mm.
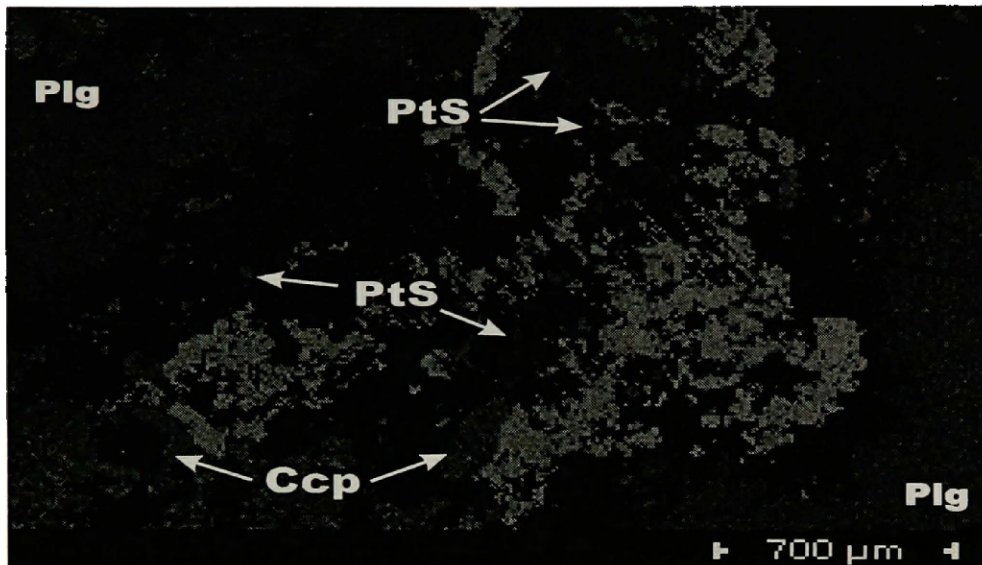
Figure 14a. Energy Dispersive Spectrometry photomicrograph of a relict clinopyroxene grain. The PGE-bearing sulfide (blue-green) is unevenly distributed and follows the pyroxene lamellae. This distribution may suggest infiltration and subsequent deposition of PGE-bearing sulfides from a hydrothermal fluid. Ca = red, S = yellow, Pt = blue.
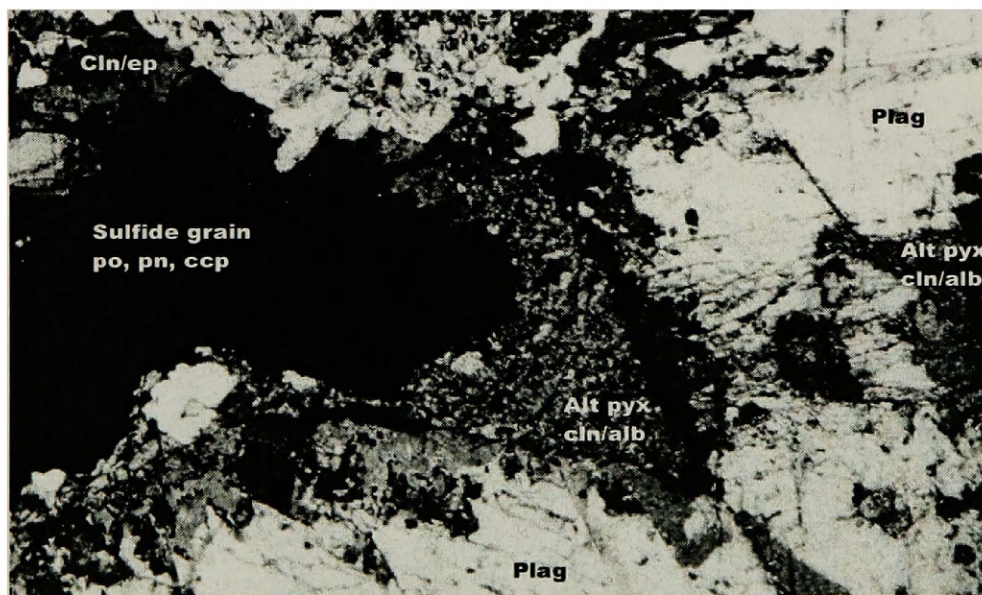
Figure 14b. Altered pyroxene (alt pyx) replaced by sulfide grain. Note comb texture of the clinozoisite/epidote into sulfide grain. This texture suggests that the emplacement of the sulfide grain is either contemporaneous or after crystallization of the clinozoisite. plag = plagioclase, cln = clinozoisite, ep = epidote, alb = albite, po = pyrrhotite, pn = pentlandite, ccp = chalcopyrite. Length of photo approximately 5 mm.
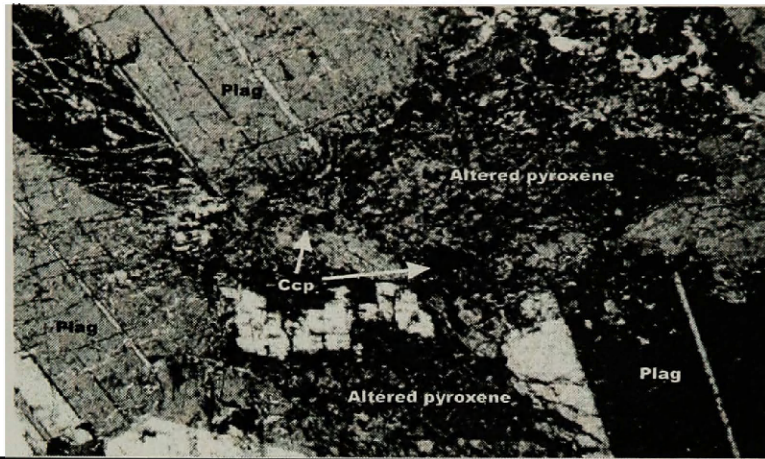
Figure 15. Pyroxene grains from the 0-5% group altered to clinozoisite and chlorite. Length of photo is 10 mm.
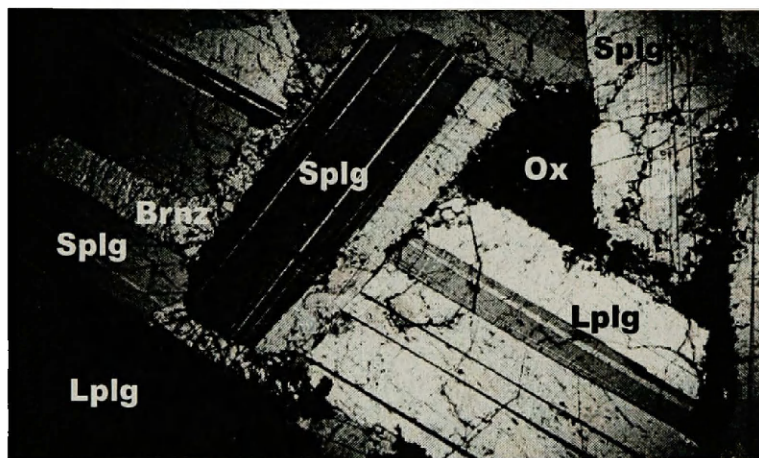
Figure 16. Crossed-polarized photomicrograph of the 5-10% proxene group. Lplg = large plagioclase, Splg = small intercumulate plagioclase, Brnz = bronzite, Alt = alteration. Length of photo is 25 mm.

Figure 17. Relict pyroxene (0-5% group) altered to albite (light areas) and chlorite (dark area). Alteration follows the original lamellae of the clinopyroxene. This sample was taken 50 m down section and may suggest movement of fluids.

5-10% pyroxene:

The major modal (by volume) abundances of this group are: plagioclase (87%), clinopyroxene (8%), sulfide minerals/oxides (3%), and bronzite (2%) (Fig. 16). The large plagioclase grains (0.5-2 cm) are slightly altered, and make up 43% of this rock type. Resorption textures occur on 77% of the large plagioclase grains. The small plagioclase grains (<0.5 cm) form 44% of this group. When the total number of individual grains are counted, the large to small plagioclase grain ratio is approximately 1:4. The increase of the grain-to-grain ratio, when compaired to the 0-5% group, implies that the small, intercumulate plagioclase grains are reducing in size. The pyroxene (5-10%) is highly altered and shows very little of its original composition (Fig. 17). The pyroxene is completely replaced by amphibole, chlorite, clinozoisite, and albite. Clinozoisite (4%) replaces the plagioclase and forms at grain contacts. Minimal sulfide minerals are found within this group.

10-15% pyroxene:

The major modal (by volume) abundances of this group are: plagioclase (83%), clinopyroxene (12%), bronzite (3%), oxides (2%), ± olivine (Fig. 18). The large plagioclase grains (52%) within this group are fresh with minor local alteration. Approximately 94% of the large plagioclase grains within this group show resorption textures. The small plagioclase grains (35%) are also fresh with minor local alteration. When the total number of individual grains are counted, the large to small plagioclase grain ratio is 1: 5.4, further implying the reduction in the small plagioclase grain size. The pyroxene (inverted pigeonite and augite) is locally altered to amphibole. Clinozoisite is a minor constituent (<4%); it locally replaces the plagioclase at grain boundaries. No sulfide minerals are present within
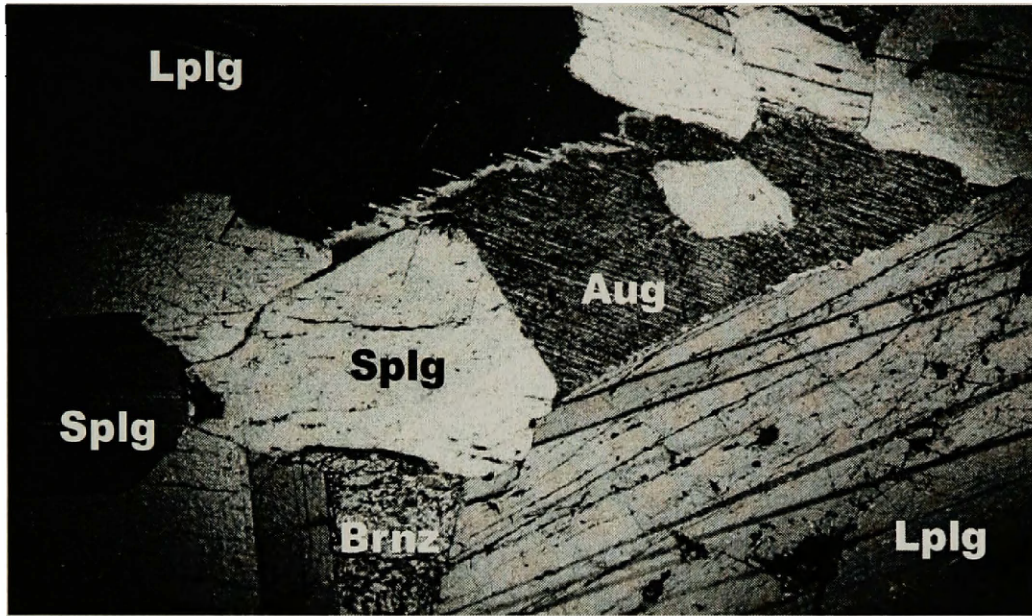
Figure 18. Crossed-polarized photomicrograph of the 10-15% pyroxene group. Lplg = large plagioclase, Splg = small intercumulate plagioclase, Aug = augite, Brnz = bronzite. Length of photo is 15 mm.
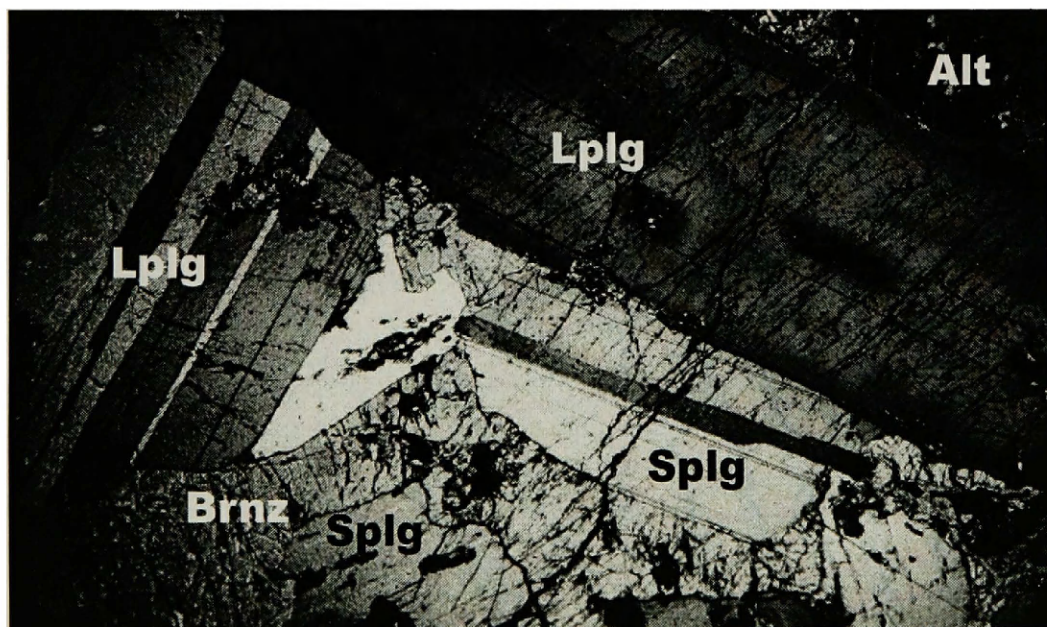
Figure 19. Crossed-polarized photomicrograph of the 15-20% pyroxene group. Lplg = large plagioclase, Splg = small intercumulate plagioclase, Brnz = bronzite. Length of photo is 15 mm.

this group. Interstitial oxides, magnetite and ilmenite, locally comprise up to 2%. Epidote is the common alteration mineral surrounding the oxides. The compositional change in the alteration assemblage from clinozoisite to epidote suggests a local change in equilibration of the hydrothermal fluid.

15-20% pyroxene:

The major modal abundances of this group are: plagioclase (80%), bronzite (13%), clinopyroxene (5%), oxides (2%), ± olivine (Fig. 19). The large (50%) and small (30%) plagioclases are fresh and unaltered. Numerous grains show complex, diffuse zonation. Resorption textures (Figs. 19, 20) occur on 95% of the large plagioclase grains. When the total number of individual grains are counted, the ratio of large to small plagioclase grains is 1:6.3, suggesting that the smallest intercumulate plagioclase grain size are within the highest modal pyroxene group. Pyroxenes in this group include orthopyroxene (inverted pigeonite) and clinopyroxene (augite). The pyroxenes are only locally altered to amphibole. Intercumulate olivine is locally present. No clinozoisite or sulfide mineralization is visible in thin section. Magnetite and ilmenite are present in trace amounts (>2%).

Table 1. Point count data.

0-5% pyroxen e	Sample Number	Lrg. Plag percent	count	Sm. Plag percent	count	Pyroxene percent	count	Sulfide/Oxide percent	count	Clinozoisite percent	count	Other percent	count	Total percent	count
	808101a	19.4	97	43.4	217	0	0	9.2	46	12.4	62	15.6	78		500
	808101b	22.4	112	34.8	174	0	0	11.6	58	15	75	16.2	81		500
sample average		20.9		39.1		0		10.4		13.7		15.9		100	
	808201a	11.2	56	35.4	177	0	0	14.8	74	19.8	99	18.8	94		500
	808201b	20.6	103	44.4	222	0	0	12.6	63	14.8	74	7.6	38		500
sample average		15.9		39.9		0		13.7		17.3		13.2		100	
	811106a	26	130	41.2	206	5.4	27	8.6	43	8.8	44	10	50		500
	811106b	14	70	45.4	227	4.2	21	10.6	53	14.8	74	11	55		500
sample average		20		43.3		4.8		9.6		11.8		10.5		100	
	Total average	19		41		2		11		14		13			3000

5-10% pyroxene	Sample Number	Lrg. Plag percent	count	Sm. Plag percent	count	Pyroxene percent	count	Sulfide/Oxide percent	count	Clinozoisite percent	count	Other percent	count	Total percent	count
	808002a	32.2	161	47.6	238	7.6	38	3	15	2.2	11	7.4	37		500
	808002b	34.6	173	43	215	8.8	44	3.6	18	4	20	6	30		500
sample average		33.4		45.3		8.2		3.3		3.1		6.7		100	
	811101a	19	95	58.8	294	10.4	52	2.8	14	3.4	17	5.6	28		500
	811101b	27.6	138	45.8	229	8.6	43	4.4	22	5.4	27	8.2	41		500
sample average		23.3		52.3		9.5		3.6		4.4		6.9		100	
	808006a	41.6	208	30.6	153	10	50	2.8	14	6.4	32	8.6	43		500
	808006b	32.8	164	40.4	202	10.8	54	3	15	3.2	16	9.8	49		500
sample average		37.2		35.5		10.4		2.9		4.8		9.2		100	
	Total Average	31		44		9		3		4		8			3000

10-15% pyroxene	Sample Number	Lrg. Plag percent	count	Sm. Plag percent	count	Pyroxene percent	count	Sulfide/Oxide percent	count	Clinozoisite percent	count	Other percent	count	Total percent	count
	808102a	55.2	276	26.2	131	14.4	72	1.4	7	1.2	6	1.6	8		500
	808102b	42.8	214	37	185	16.8	84	0.6	3	1.8	9	1	5		500
sample average		49		31.6		15.6		1		1.5		1.3		100	
	811007a	35	175	43.8	219	12.8	64	0.6	3	3.8	19	4	20		500
	811007b	45	225	34	170	14.8	74	0.4	2	3.3	16	2.6	13		500
sample average		40		38.9		13.8		0.5		3.55		3.3		100	
	808007a	54	270	22.4	112	13.6	68	1.2	6	4	20	4.8	24		500
	808007b	43.4	217	25.6	128	20.6	103	2.2	11	4	20	4.2	21		500
sample average		48.7		24		17.1		1.7		4		4.5		100	
	Total Average	46		32		16		1		3		3			3000

15-20% pyroxene	Sample Number	Lrg. Plag percent	count	Sm. Plag percent	count	Pyroxene percent	count	Sulfide/Oxide percent	count	Clinozoisite percent	count	Other percent	count	Total percent	count
	808004a	41.2	206	32.6	163	24.6	123	0.6	3	0.2	1	0.8	4		500
	808004b	47	235	31.2	156	18.8	94	0.6	3	0.8	4	1.6	8		500
sample average		44.1		31.9		21.7		0.6		0.5		1.2		100	
	808003a	55.2	276	19	95	12.6	63	5	25	5	25	3.2	16		500
	808003b	58.6	293	16.4	82	14.4	72	3.4	17	4.6	23	2.6	13		500
sample average		56.9		17.7		13.5		4.2		4.8		2.9		100	
	811011a*	38.6	193	40.6	203	19.2	96	0.4	2	0.2	1	1	5		500
	811011b*	44	220	33	165	18.4	92	0.2	1	1.8	9	2.6	13		500
sample average		41.3		36.8		18.8		0.3		1		1.8		100	
	Total Average	47		29		18		2		2		2			3000

35
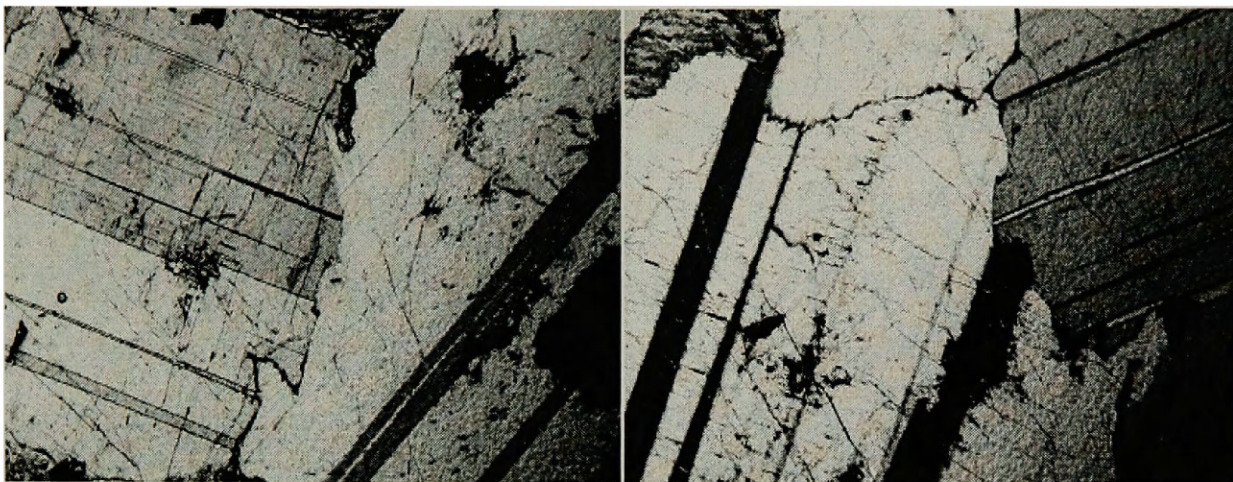
Figure 20. Crossed-polarized micrograph of resorption textures within the large, 'framework' plagioclase grains. Width of photograph approximately 5 mm.
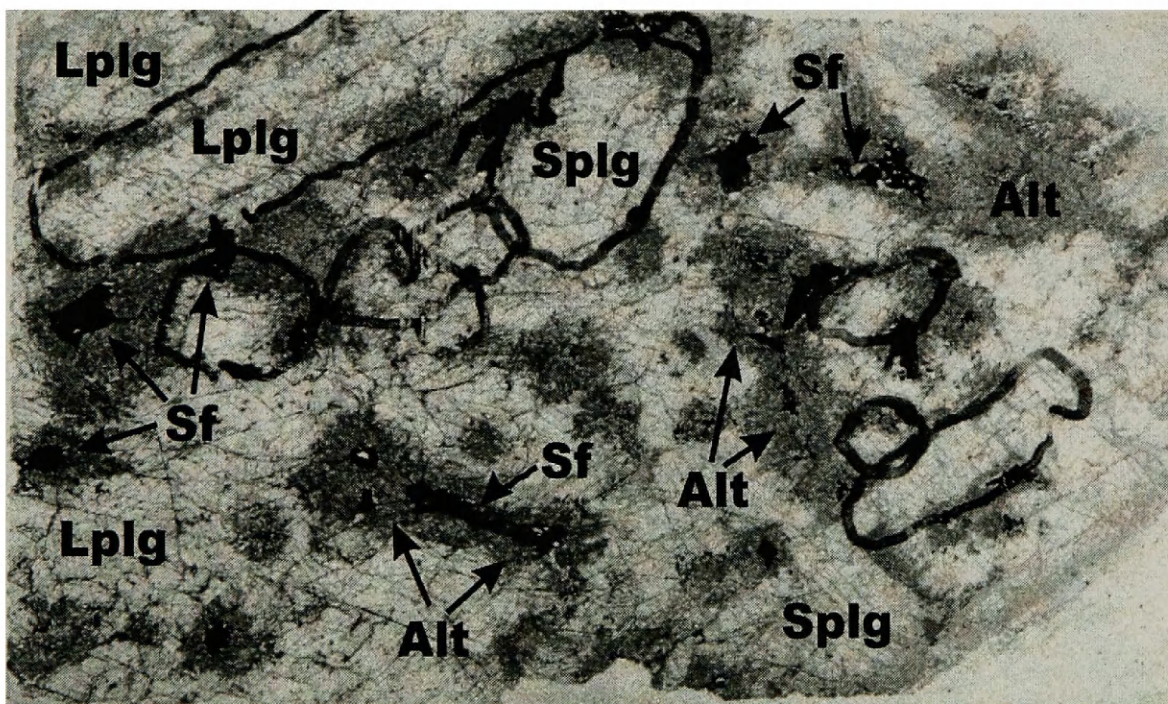
Figure 21. Plain light photomicrograph of the alteration halo enveloping the sulfide grains. Lplg = large plagioclase, Splg = small plagioclase, Sf = sulfide grains, Alt = alteration halo. Width of photo is 35 mm.

II. Sulfide Mineralogy

The sulfide minerals can be divided into two groups: Large (millimeter scale), blocky grains occupy most of the intercumulate space; and patches of numerous small (micron scale) grains occur within the alteration assemblage of clinozoisite/epidote-quartz that envelopes the large sulfide grains (Fig. 21). Albite is common at the contact of the large sulfide grains and the plagioclase grains which may suggest exsolution of albite from the plagioclase grains in contact with hydrothermal solutions. Analysis with SEM and EDS reveals a sulfide compositional zoning pattern between pyrrhotite, pentlandite, chalcopyrite, and the PGE-bearing sulfide minerals. The sulfide grains are roughly concentrically zoned with pyrrhotite, pentlandite in the center enveloped by chalcopyrite and PGE, which is further enveloped by distal oxides. The large sulfide grains are mainly pyrrhotite with exsolution and zoning of pentlandite (Fig. 22). Pentlandite occurs as blade-like inclusions within the pyrrhotite, or is concentrated to the rim of the pyrrhotite. The patches of small sulfide grains are commonly chalcopyrite and braggite. Chalcopyrite is commonly present as small (<0.25 mm) isolated grains and is concentrated to the rims of both pyrrhotite and pentlandite within the clinozoisite/epidote-quartz halo (Fig. 23). Discrete PGE-bearing sulfide minerals occur as isolated 25-micron grains (Fig. 24) that also occur within the alteration halo. There is a negative correlation between the sulfide grains and the PGEs (Fig. 25). The PGEs mainly occur along the Fe-sulfide grains boundaries. Trace PGE occur within the large pyrrhotite grains, which suggest that PGEs either occur in fluid inclusions, ionic replacement of Fe, Ni, or S, or the PGE are trapped within the crystal lattice of the pyrrhotite. Plotting the apparent sulfide zoning pattern on an Eh/pH diagram shows a trend from reduced to neutral with the PGEs occurring at near-neutral conditions (Fig. 26).
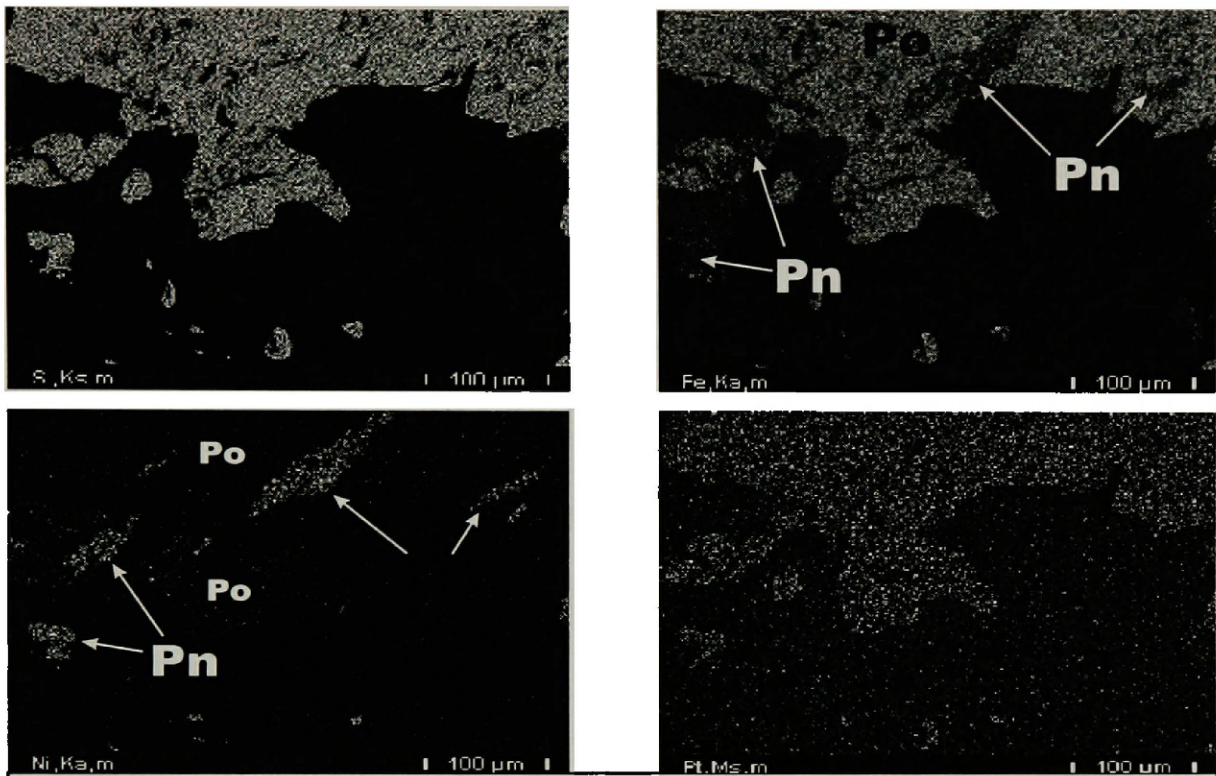
FIGURE 22. Elemental photomicrographs of a typical large sulfide grain. The lower left photograph shows blade-like inclusions of pentlandite within pyrrhotite suggestive of original exsolution textures. Note trace amounts of Pt within the sulfide grain.
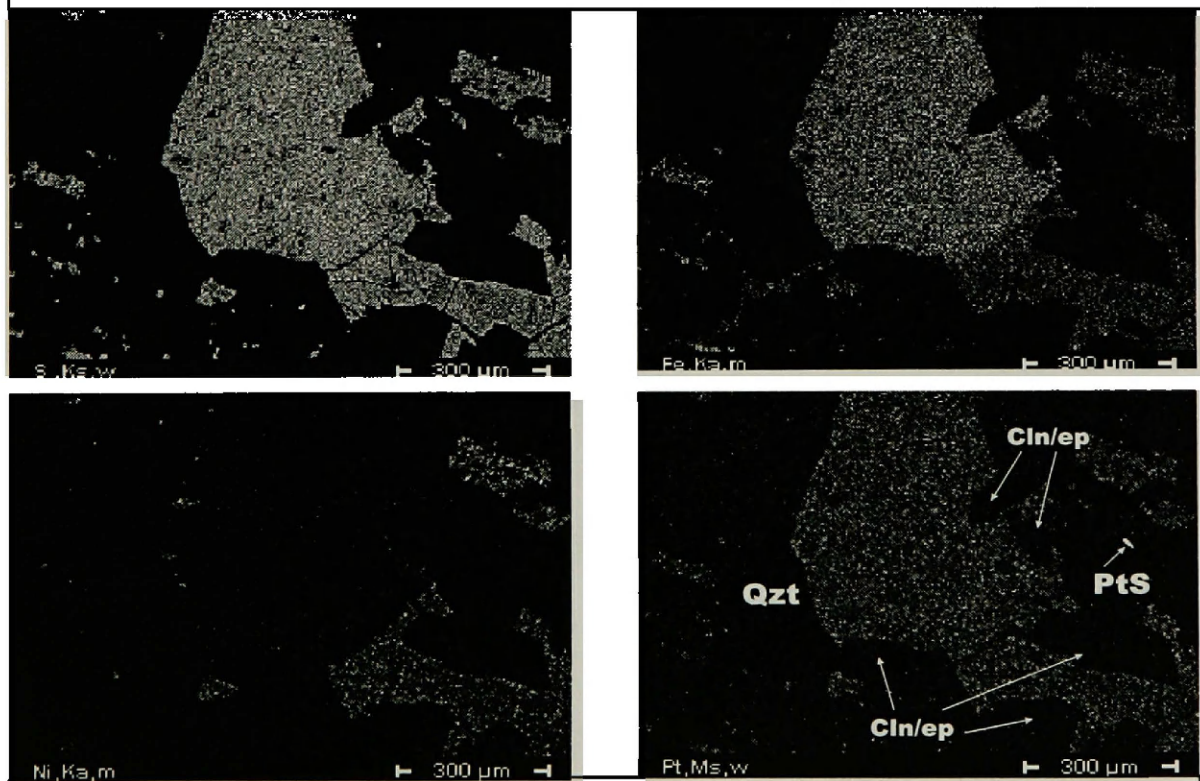
FIGURE 23. Elemental photomicrographs of a typical large sulfide grain showing compositional zoning of pyrrhotite (Fe$_{1-x}$S) and pentlandite ((Fe, Ni)$_9$S$_8$). Chalcopyrite occurs as isolated grains in the upper right and lower left of the large Fe-sulfide grain. Note the isolated Pt grain (right side center) on the lower right photograph. This Pt grain is typical of the Picket Pin deposit. The surrounding material is mostly clinozoisite with minor epidote.

38
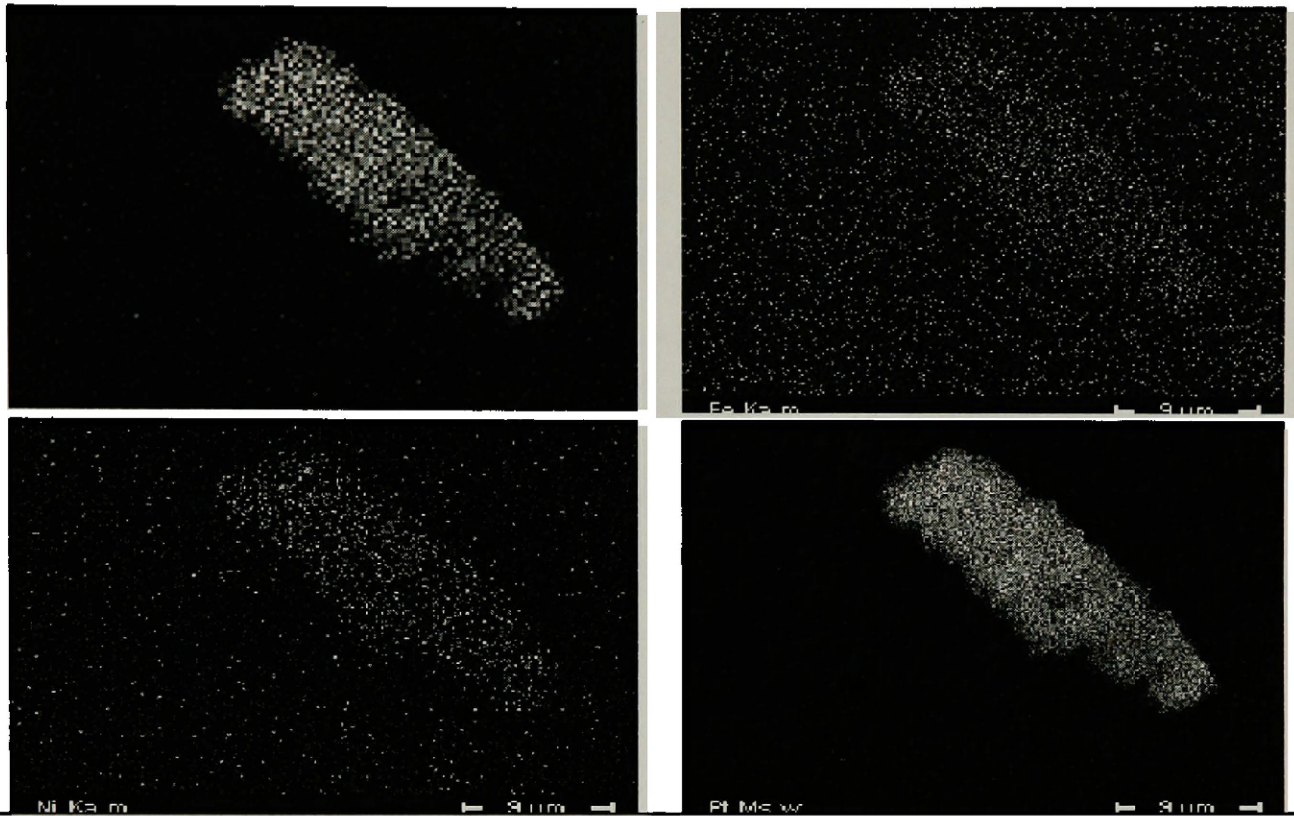
FIGURE 24. Elemental photomicrographs of an isolated bragite ((Pt, Pd)S) grain typical of the Picket Pin deposit. The surrounding material is mostly clinozoisite with minor quartz.
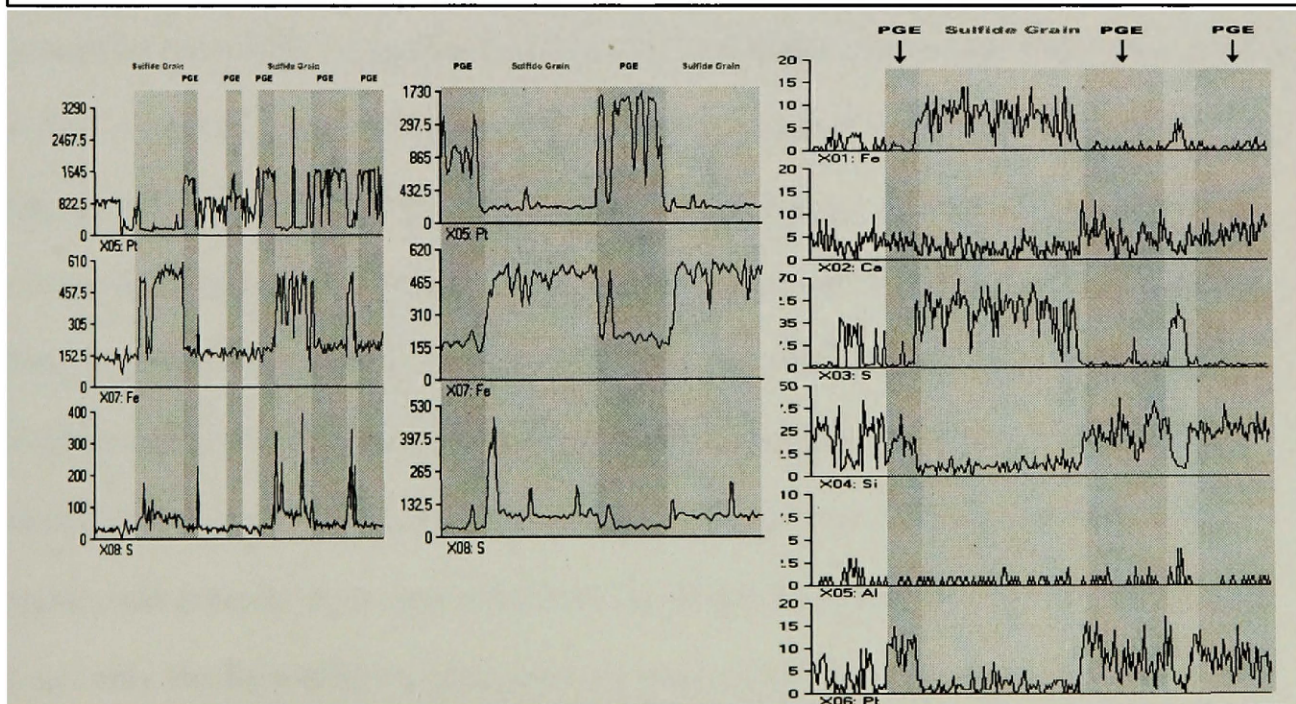
Figure 25. Linear EDS traverses across a portion of a thin section. Note the negative correlation between the Fe-sulfide grains and the PGE-enriched areas. Blue = PGE; Red = Fe-sulfides. Scale is in counts per second.

<u>Oxides</u>

Intercumulate ilmenite and magnetite occur away from sulfide mineralization, within the 5-10% pyroxene zones of AN II. The ilmenite may contain manganese and vanadium. Quartz and apatite are more abundant close to the oxides. Epidote with trace clinozoisite encloses all oxide grains. The close relationship between epidote and the oxides clearly suggests a higher oxidation state of the melt or fluid that precipitated these phases. A linear trend is apparent when the oxides are plotted on the above Eh/pH diagram which may suggest evolution of the ore-bearing fluids. No PGE-bearing sulfide minerals are present near the oxides.

<u>III. Alteration Mineralogy</u>

Clinozoisite, epidote , albite , quartz, and apatite, in decreasing order of abundance, accompany the sulfide mineralization (Fig. 26). Abundant clinozoisite with minor epidote enclose all sulfide grains. This apparent alteration halo erodes the plagioclase grain boundaries and locally cross-cuts the large pyrrhotite grains. Where the plagioclase grain boundaries are preserved, and in contact with the large sulfide grains, they are altered to albite (Fig. 28). Minor amounts of this alteration may locally occur away from sulfide mineralization (10-15% group), but only at plagioclase grain boundaries. The highest amount of alteration is associated with sulfide mineralization (0-5% pyroxene group). Alteration drastically decreases away from the sulfide mineralization (5-10% group), and occurs only locally within the pyroxene-rich rocks (10-15% and 15-20% groups). This alteration pattern suggests the hydrothermal fluid selectively migrated in the rocks with low-pyroxene content, and may suggest a physical constraint (low pyroxene content and coarser-grain plagioclase) for the migration of the hydrothermal fluid.

In the field, clinozoisite and epidote form 0.5 to 5 cm circular patches that lead upward in the section to more abundant sulfide mineralization (Fig. 29). Microscopic investigation of one such patch reveals a 1 mm central oxide (magnetite) grain surrounded by 0.5 mm envelope of epidote, which is further enclosed by 1 cm of clinozoisite, an outward decrease in iron. This outward decrease in iron is opposite of the outward increase in iron proximal to the sulfide horizons where magnetite and epidote is outward of clinozoisite and the sulfide minerals. Discrete PGE and apatite grains occur between the alteration boundary and the unaltered rock (Fig. 30). The clinozoisite patches have obliterated both plagioclase and pyroxene grains. Only near the margin of the clinozoisite patch can relict plagioclase be inferred. The clinozoisite patches appear to be a good field indicator of high-grade sulfide mineralization. Multiple random samples of clinozoisite patches totaling 5 kg were analyzed (Table 2) to test the relationship between the clinozoisite patches and sulfide mineralization. The clinozoisite samples were collected throughout the eastern section of An II and away from visible sulfide mineralization. Anomalous PGE and Au within the samples may support an intimate connection between the ore-bearing fluid and the clinozoisite.

Interstitial quartz and minor apatite occur locally and may form a halo surrounding the sulfide minerals. Quartz and apatite may also be found as discrete anhedral secondary grains within the clinozoisite envelope. Quartz and apatite appears to be more abundant near the oxides.
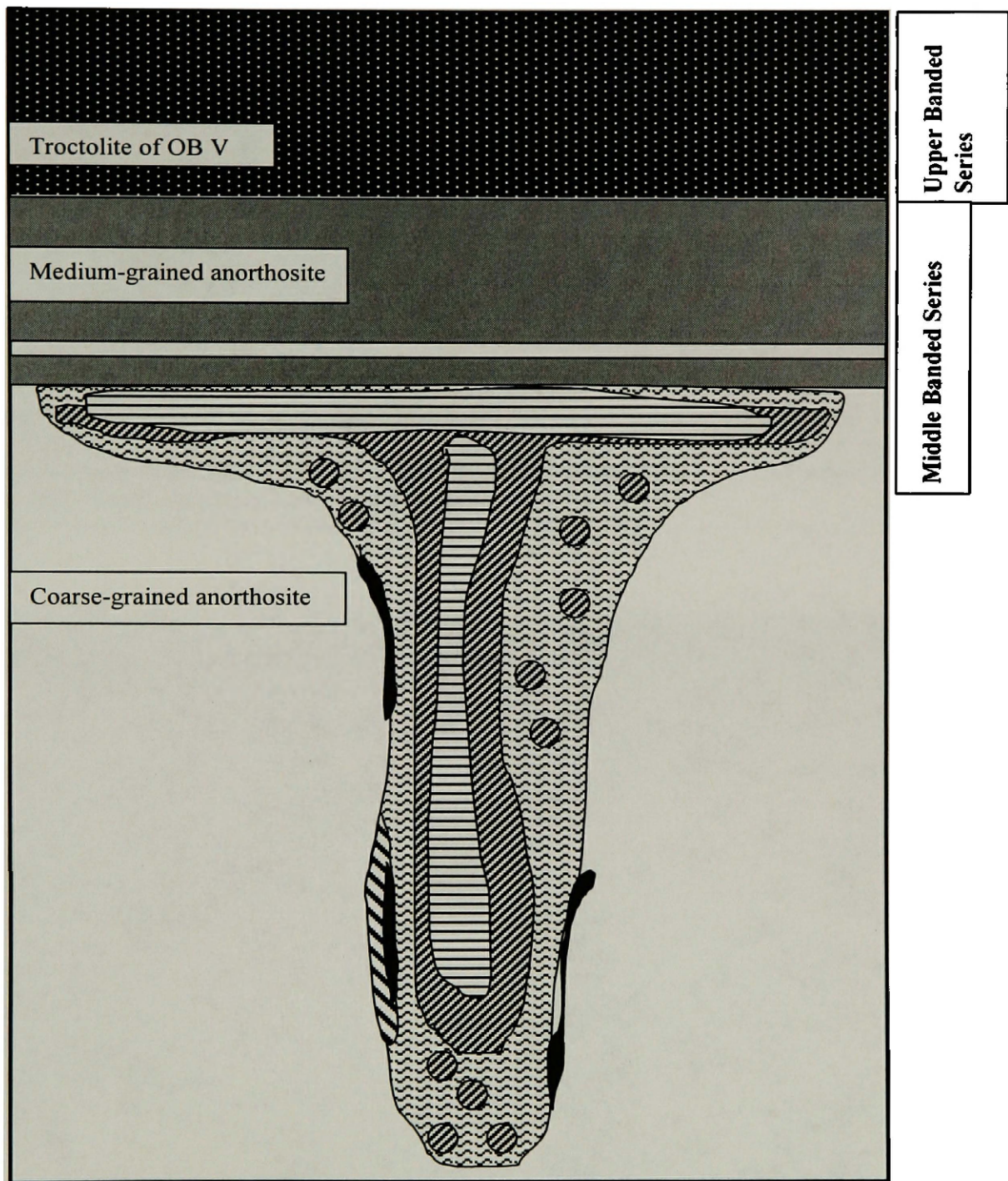
Figure 26. Schematic of alteration halo enclosing the sulfides.

Legend:

- Troctolite
- Medium-grained anorthosite
- Coarse-grained anorthosite
- Sulfide minerals
- Clinozoisite halo
- Epidote
- Magnetite/ilmenite
- Chloritic-albitic alteration

Upper Banded Series

Middle Banded Series

Troctolite of OB V

Medium-grained anorthosite

Coarse-grained anorthosite
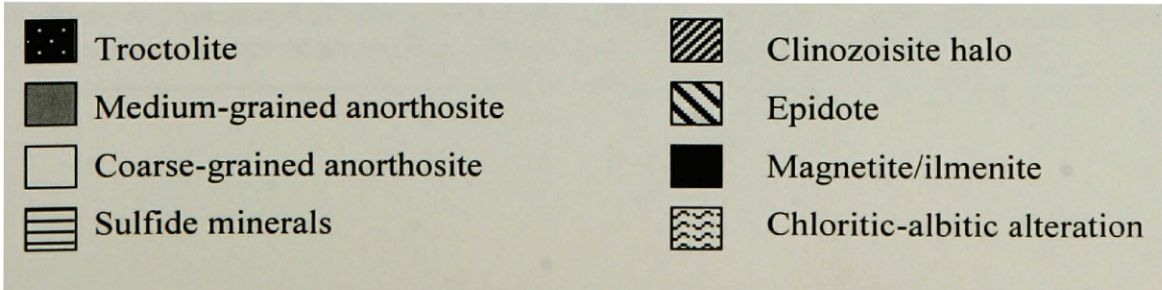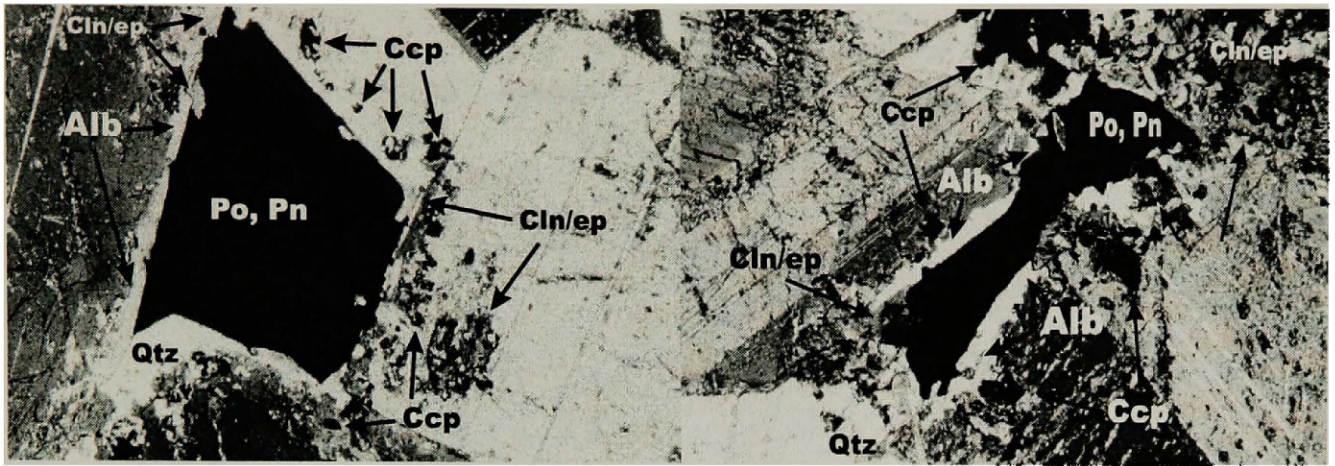
Figure 27. Polarize photomicrographs of two sulfide grains. The surrounding material on the grain on the right is less altered than the grain on the left. However, both grains are rimmed by albite and contain intergrowths of clinozoisite. Po = pyrrhotite, Pn = pentlandite, Ccp = chalcopyrite, Alb = albite, Qtz = quartz, Cln/ep = clinozoisite/epidote.
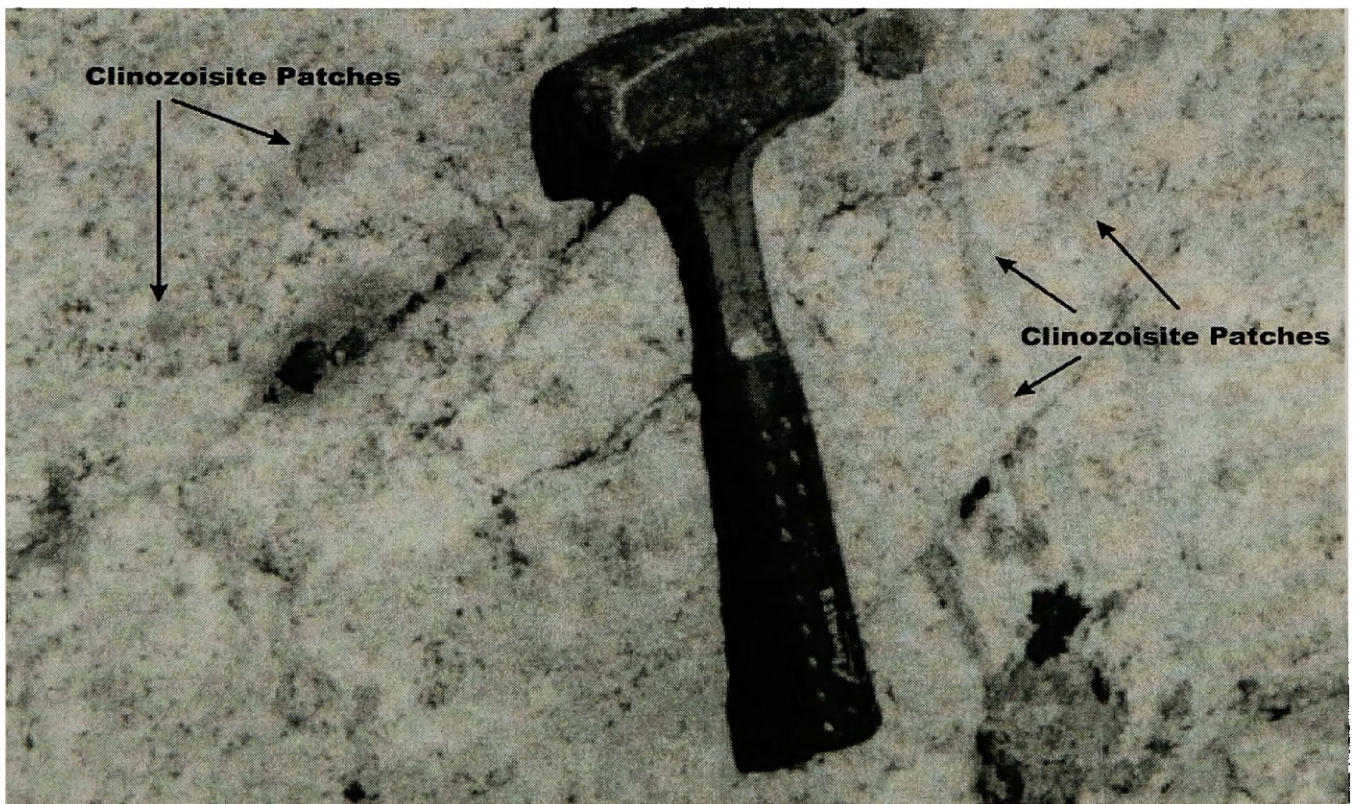
Figure 28. Outcrop photograph of clinozoisite patches. Significant sulfide mineralization is less than 1 m below the right-hand corner of photograph. Up-section is towards lower right-hand corner.
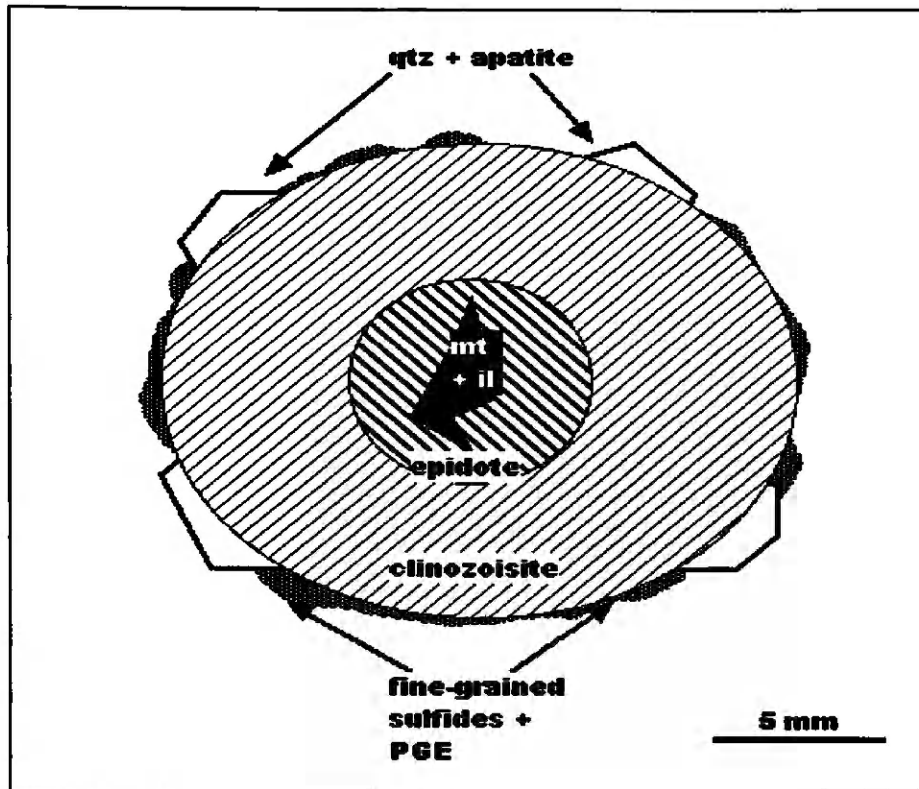
Figure 29. Idealized cross-section of a clinozoisite patch. Note the trend from the central oxidized zone outward to the reduced, PGE-bearing sulfides.

Table 2. Clinozoisite analysis.

	TiO2	Al2O3	Fe2O3	MnO	MgO	CaO	Na2O	K2O
Clinozoisite 1	0.2	7.68	1.84	0.2	0.46	3.2	0.67	0.09
Clinozoisite 2	0.1	12.2	1.55	0.2	0.52	4.86	1.34	0.212
Average (%)	**0.15**	**9.94**	**1.7**	**0.2**	**0.5**	**4.0**	**1.0**	**0.15**
	Cu	Ni	Cr	Co	Sr	Ba	La	
Clinozoisite 1	490	237	44	8	32	10	10	
Clinozoisite 2	427	304	39	12	51	20	10	
Average (ppm)	**459**	**271**	**42**	**10**	**42**	**15**	**10**	
	Pt	Pd	Au	Ag				
Clinozoisite 1	320	320	41	200				
Clinozoisite 2	241.5	220	18	200				
Average (ppb)	**281**	**270**	**30**	**200**				

CHAPTER FOUR: GEOCHEMISTRY

I. Review of recent literature

Comparison between recent literature and the data presented below is difficult. Excluding the work done by Haskin and Salpas (1992), the analyses involved in recent literature do not divide the lithologies into pyroxene-content groups. The divisions made in previous research are between sulfide-rich/pyroxene-poor and sulfide-poor/pyroxene-rich zones which roughly correlate to the 0-5% and 15-20% groups respectively, applied to this contribution. Broad correlations, however, can be made for major and trace-element trends.

Salpas et al. (1983) have shown that the sulfide-rich/pyroxene-poor rocks are preferentially enriched in incompatible trace elements. Haskin and Salpas (1992) show that SiO_2, TiO_2, Al_2O_3, Na_2O, and K_2O correlate negatively with MgO. They also found negative correlations between MgO and the rare-earth elements, Zr, Hf, Ta, Th, U, Rb, Cs, Sr, Ba, and Br. Research by Boudreau (1986) displays a negative correlation between Sc and Ni, suggesting that the sulfide minerals are replacing the pyroxene as the intercumulate phase. A strong positive Eu anomaly within the overlying troctolite and medium-grained anorthosite members as well as the sulfide-poor zones in AN II suggest the plagioclase grains accumulated from a melt that had not yet crystallized substantial amounts of plagioclase. A slight negative Eu anomaly, suggestive of removal of plagioclase, within the sulfide-rich zones is interpreted to suggest these plagioclase grains were derived from a trapped melt (Boudreau, 1986). This melt was not in communication with the main melt chamber of the complex which would be replenished with Eu with each new pulse of magma into the chamber. Boudreau further suggests that the sulfide

minerals replacing the pyroxene do not account for the enrichment of incompatible trace elements within the sulfide-rich rocks. More recent research (Meurer et al., 1999) provides a cautionary note on the interpretation of the of whole-rock trace-element trends since the trace-element concentrations may have been strongly modified by migrating fluids without changing the major-element compositions.

Enrichment of the incompatible trace and major elements within the sulfide-bearing zone suggests that the sulfide-bearing zones formed either from an evolved melt, or were enriched by a later hydrothermal event. This argument is used in favor of the hydrothermal origin for the sulfide-bearing zones. The magmatic origin model for the sulfide minerals (see below), however, hypothesizes that a mix of a primitive and more-evolved melt resulted in sulfide saturation and hence, sulfide precipitation. Since both arguments may be valid, therefore, incompatible element trends should be used with caution when deriving a genetic model for the origin of sulfide precipitation.

II. Whole-rock Analyses

In the present study the rocks of An II have been divided by modal pyroxene percentage. Therefore the whole-rock analyses (see appendix I) confirm the obvious (that MgO is higher in rocks with higher pyroxene content). The apparent lack of stratigraphic variation in the plagioclase composition within the two anorthosites (AN I and AN II) (McCallum and others) may reflect mixing and mingling of two compositionally distinct melts to form An II. However, there are revealing trends from this data that must be

considered for models of the formation and precipitation of the PGE-bearing sulfide minerals (Fig. 30).

The whole-rock geochemical trends of Mg, Fe, Na, and K versus pyroxene mode confirm the above interpretations that the sulfide-bearing samples are enriched in Na, K, and incompatible trace elements and depleted in Mg (Boudreau, 1986; Salpas et al., 1983). This trend may suggest that the intercumulate melt fractionated outward from the high-pyroxene zones toward the low-pyroxene and sulfide-bearing zones. These data in conjunction with the microprobe data (see below) for the plagioclase grains suggest that the sulfide-bearing zones were the last to crystallize and were enriched in volatiles. Alternatively, a hydrothermal fluid influx would enrich the sulfide-bearing zones with Na, K, incompatible trace elements, and volatiles. Microprobe data on the intercumulate plagioclase grains (An >74) within the sulfide-bearing zones supports that at least some of the incompatible-element enrichment may have been derived from the melt as opposed to complete enrichment by a hydrothermal fluid.

As suggested above, both Na and K show enrichment towards the low-pyroxene, sulfide-bearing group. This enrichment may overstate the obvious that Na and K do not go into the pyroxene lattice and are therefore enriched in the pyroxene-poor areas. This trend does support differentiation outward from the more-mafic regions. Both Na and K deviate from this trend within the 5-10% pyroxene group. The pyroxenes within this group are highly altered to chlorite and albite, and this deviation may be due to the hydrothermal alteration. This may suggest that the intercumulate melt fractionated, concentrating the incompatible elements in the sulfide-bearing zones and a later hydrothermal event further enriched the zone.

The relationship between Fe and modal percent pyroxene displays obvious Fe enrichment as the result of sulfide and oxide concentrations in the low-pyroxene groups (0-5% and 5-10% groups). Upon closer examination (Fig. 31) the relative Fe enrichment within the sulfide/oxide zones can be approximated. The importance of this approximation is to examine whether the sulfide/oxide assemblages could be formed directly from the alteration of pyroxene, which textural evidence suggests, or if the hydrothermal fluid contained Fe. This Fe enrichment is discussed in detail below.

The relationship between Pt, Pd and pyroxene mode confirms the exclusivity of the PGEs to occur within the pyroxene-poor regions of AN II. Therefore, the PGEs are also associated with the incompatible major and trace elements. As mentioned above, this evidence argues against the magmatic model which would place the sulfide minerals and PGEs in a zone of more primitive composition. In contrast, this relationship between the sulfide minerals, PGEs and incompatible elements supports the late-stage fluid or hydrothermal hypothesis. Alternatively, the PGEs and immiscible sulfide melt may have migrated into these zones before precipitation of the sulfide minerals.

Figure 30. Relationships between whole-rock major elements and pyroxene modal percent.
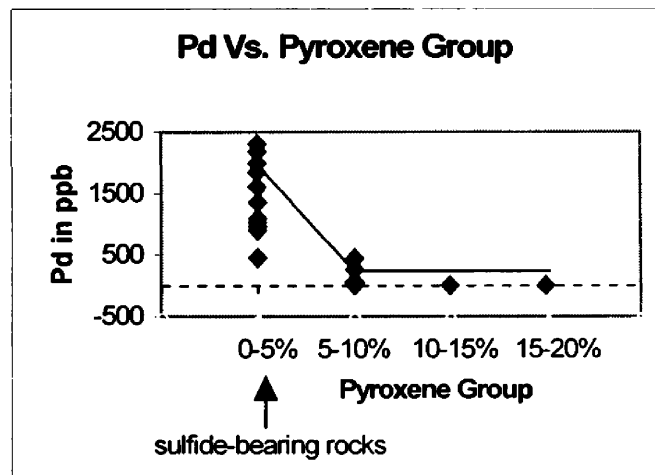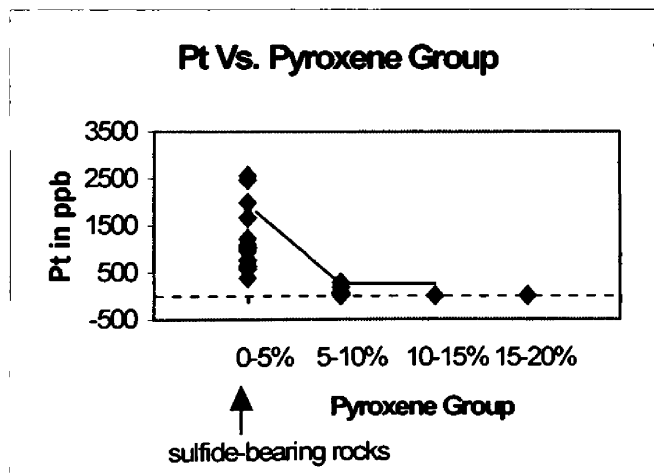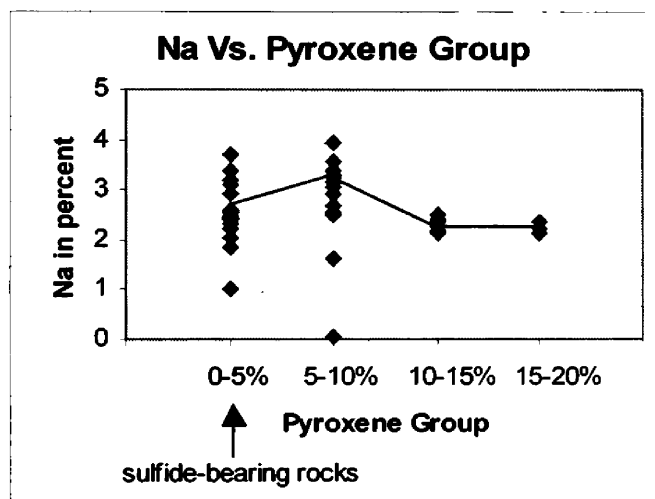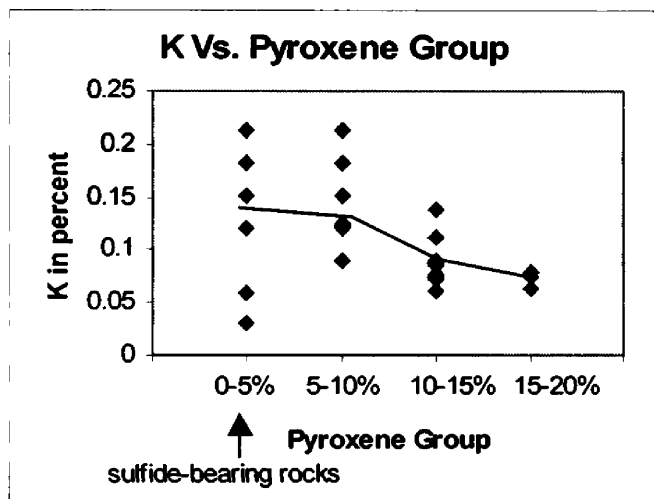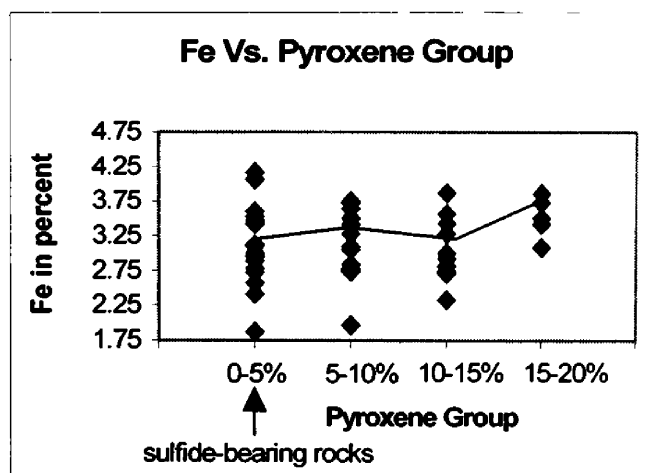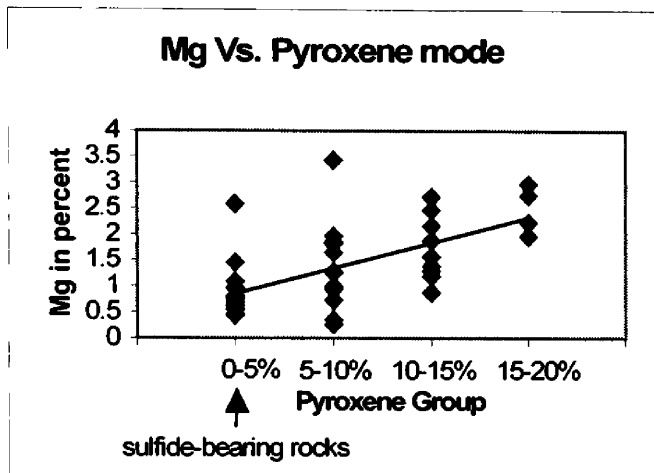
Figure 31. Fe enrichment per pyroxene group. The lower curve were derived from microprobe data of the pyroxenes.

Fe Enrichment per Pyroxene Group

whole-rock Fe

Fe enrichment

Fe percent of pyroxene grains

Fe in percent

3.75
3.25
2.75
2.25
1.75
1.25
0.75

0-5%   5-10%   10-15%   15-20%

sulfide-bearing rocks   **Pyroxene Group**
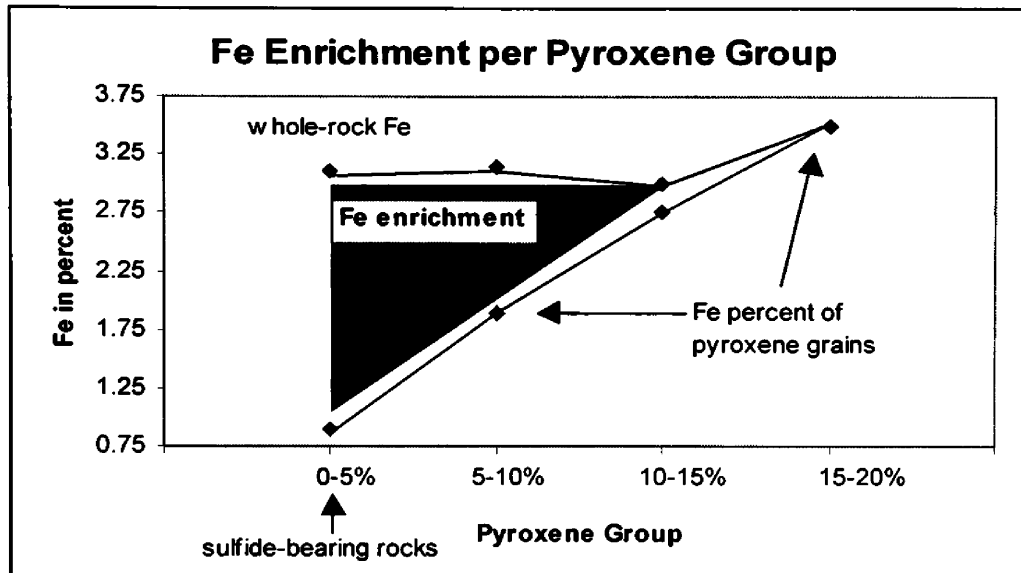
Figure 32. Cr abundance in pyroxene modal groups, medium-grained anorthosite, and clinozoisite patches. Note that the amount of Cr in the clinozoisite patches is equivalent to that of the medium-grained anorthosite unit. Cln patch = clinozoisite patches, Med. An = Medium-grained anorthosite unit.

Cr Vs. Pyroxene Group, Clinozoisite Patches, and Medium-Grained Anorthosite

Cr in ppm

70
60
50
40
30
20
10
0

Cln patch   Med. An   0-5%   5-10%   10-15%   15-20%

Group

sulfide-bearing rocks
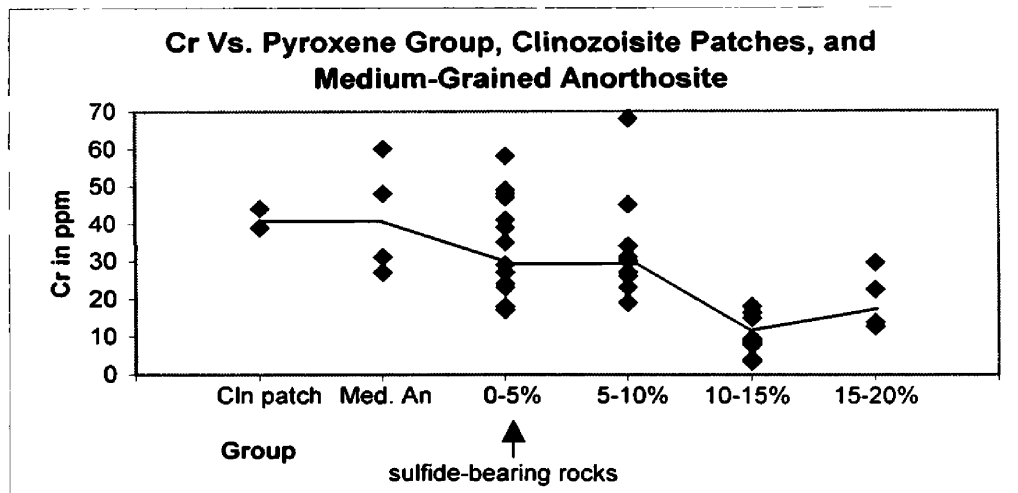
The Cr content in relationship to the modal percentage pyroxene groups, the clinozoisite patches, and the medium-grained anorthosite unit (Fig. 32) shows that the average Cr content is higher in the hydrothermally altered zones in comparison to the olivine-bearing zones. The increase of Cr within the hydrothermal fluids suggests that Cr is mobile under low-temperature (500-600°C), oxidized conditions. The comparably high Cr value in the medium-grained anorthosite unit suggests that the medium-grained unit may have been effected by late-stage fluids, or infiltraited by hydrothermal fluids. Boudreau (1986) suggests that the high level of Cr may be due to metasomatism that would have effected this unit by up-welling late-stage magmatic fluids because Cr does not enter the plagioclase crystal structure.

In Figure 33 the PGEs are compared to S, P, and the chalcophile elements. No good relationship is observed which suggests the PGE's have precipitated in phases other than the sulfide minerals and may have been adsorbed on silicate grain boundaries. Boudreau (1986) noted that the PGEs show a good regression with As and Sb. He then suggests that these discrete phases of PGE and arsenic and antimony exsolved from a high-temperature monosulfide solution but presents no data to support the suggestion. Both As and Sb migrate freely in hydrothermal fluids. The lack of a good correlation between the PGEs and the sulfide phases supports the hypothesis that the PGEs have migrated in a hydrothermal event. This may suggest that deposition of the sulfide minerals and the PGEs involved two different events or a gradual change in alteration-fluid composition. If the elements responsible for the sulfide phases migrated with the PGEs, then better

Figure 33. PGE relationship with sulfur, phosphorus and chalcophile elements.

52
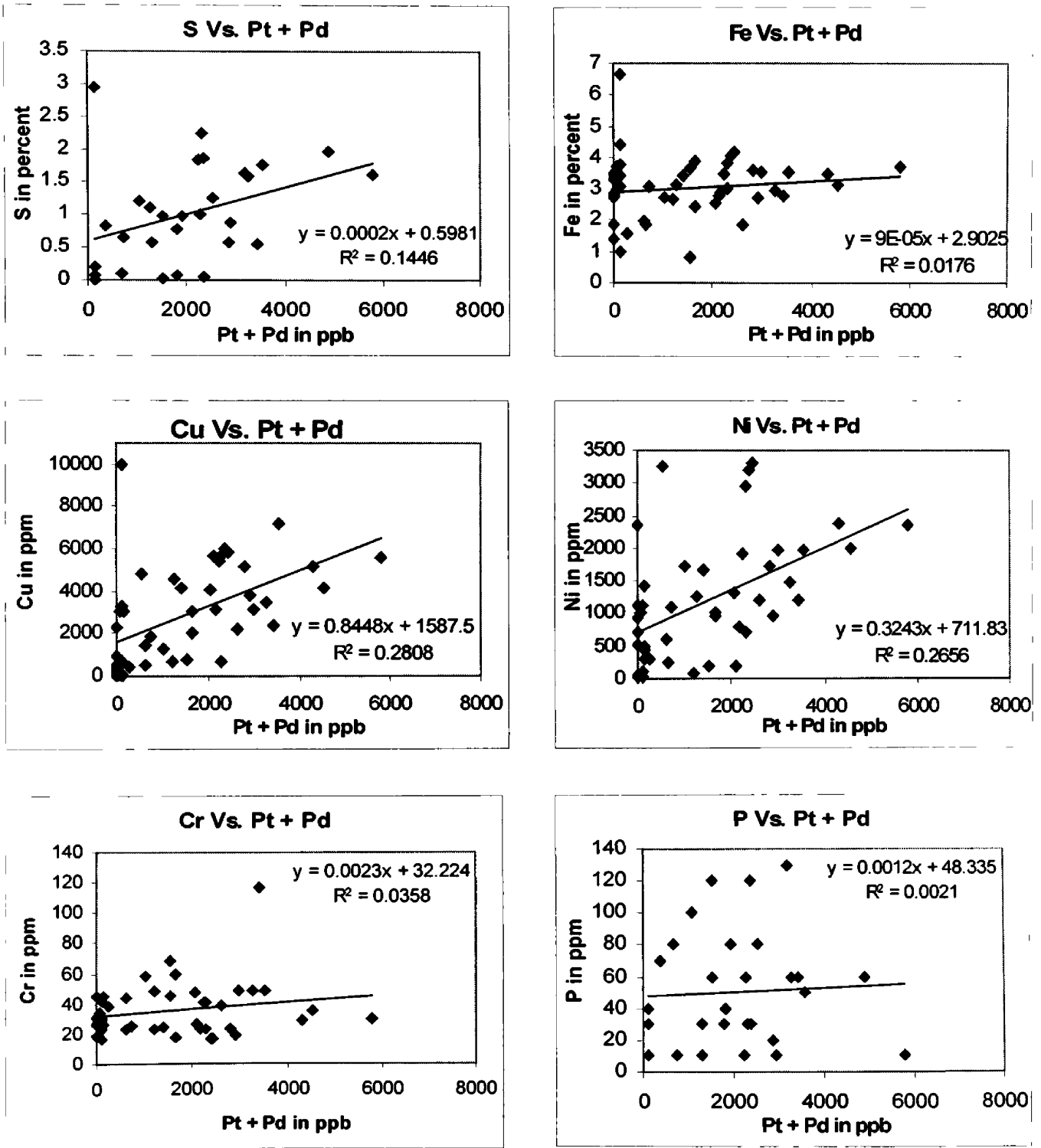
correlations between these elements might be expected. This lack of correlations also affects

the magmatic emplacement hypothesis that proposes that the PGEs were

scavenged by sulfide droplets migrating through the melt. Again, if the sulfide melt model

were valid, then better correlations would be expected. It has been suggested by many

authors that the abundance of the phosphate mineral chlorapatite implies that the PGEs

migrated in a Cl-rich fluid. Numerous apatite grains were identified proximal to sulfide

grains. The slightly positive correlation between P and the PGEs which may support the

hypotheses that the PGEs migrated in a Cl-rich fluid although background values of P

prohibit any definite relationship. The random occurrence of chlorapatite throughout AN II

(see below) does suggest that AN II formed from an unusually volatile-rich melt, or that the

volatiles were concentrated at this level of the Stillwater Complex. This weak correlation and

the abundant albitic alteration may imply that a sodium-rich fluid was responsible for PGE

mineralization. Figure 31 may suggest a relationship between sodium and PGE

mineralization. Potassium and the PGEs also show a weak correlation. This may suggest

that the hydrothermal event responsible for PGE mineralization also may have been

responsible for the enrichment in incompatible elements.

III. Microprobe Analyses

Representative samples from each of the four pyroxene groups, the medium-grained

anorthosite member, and the troctolite member of Olivine-bearing V (OB V), a total of 6

polished sections, were prepared for microprobe analyses. Silicate mineral compositions and

zoning patterns were determined by microprobe analyse at Washington State University on a

Cameca MBX microprobe with four wavelength dispersive spectrometers, with automation

provided by Advanced Microbeam Inc. The microprobe used 12 nanoamps beam current, 20

kilovolts accelerating voltage, with a beam width of 2 microns. Multiple well-constrained standards were used to calibrate the microprobe (see appendix II).

Microprobe analyses established major-element compositions, chemical zonation on a grain scale, and determination of variations in silicate chemistry within each of the pyroxene groups. The two main research questions proposed were: 1.) Is there evidence of mingling and mixing of two compositionally distinct melts? 2.) What is the compositional trend between the unmineralized groups (15-20%, 10-15% and 5-10% modal pyroxene) and the mineralized group (0-5% modal pyroxene)?, and 3) If there was evidence of mingling between two melts, what is the compositional trend of this melt?

Plagioclase Analyses

In the present study the plagioclase was divided by grain size into two groups: Large grains of 'framework' (cumulate) plagioclase (>0.5 cm), and small, intercumulate plagioclase (<0.5 cm). The division was arbitrarily chosen after petrographic thin section analyses, and further inspired from the previous work by Czamanske and Scheilde (1985). Czamanske and Scheilde (1985) found the large plagioclase to be reversely zoned with a variation in An content up to 12% within a single grain. In contrast, the intercumulate plagioclase grains were more calcic and exhibited less compositional zoning.

Two different compositional trends are apparent in Figure 34: 1) a dissimilar average An content of the large and small plagioclase grains within the 0-5% pryoxene group, and 2) a noticeable decline in An content in both plagioclase groups from the high to low-pyroxene modal division. They are most sodic near sulfide mineralization. The decline in An content in the large plagioclase group (5%) may be close to the margin of error, whereas the small plagioclase group is significant (10%). This may support the hypothesis that the

intercumulate melt was trapped and fractionated outwards from the high-pyroxene (15-20%) group to the low-pyroxene group (0-5%) and may explain the enrichment in Na, K, and the incompatible elements within the 0-5% group. Alternatively, this enrichment and plagioclase compositional trend may be the result of the migration of late-stage melt concentrating in the low-pyroxene group as proposed by Boudreau (1986) and Czamanske and Loforski (1996). Conversely, Sheidel (1983) suggests that the depletion in An content resulted from albitization, which the present study found to be significant in the 0-5% pyroxene group.

The variation between An content and distance from the core of each grain was plotted for both large and small plagioclase grains from each pyroxene group (Fig. 35). The small plagioclase grains show normal zoning and show no oscillations suggesting that they formed from a melt without perturbations or mingling of a compositionally different melt. This may further support that melt 2, the intercumulate melt, was trapped and did not have communication with the remainder of the main melt in the chamber. The large plagioclase grains are reversely zoned and show wild oscillations of up to 12% molar Ca near the rims. Further inspection suggests that the large plagioclase grains are zoned normal from the core outward for some distance then began to oscillate and ultimately end up reversely zoned. Thus, the normal-zoned core may be the original cumulate grain whereas the oscillations and high-Ca rims are adcumulate and perhaps derived from the intercumulate melt (Fig. 35a-b). To verify this, the An content of the rims of the large plagioclase grains were plotted with the cores of the small plagioclase grains per pyroxene group (Fig. 36). The An content of the rims match the An content of the cores well within the margin of error. Detailed petrographic analyses of the large plagioclase grains to identify the adcumulate growth. The results of the petrographic analyses were marginal. Very few grains displayed a 'dusty'

outline of the original grain. Numerous grains displayed a significant increase in inclusions within the reversely zoned margin of the plagioclase grains. More detailed petrographic analyses are needed to discern the possible adcumulate growth of the large plagioclase grains.

Figure 34. Relationship between the average An content of the large and small plagioclase grains and pyroxene group.

An Content: Average Large Vs. Small Plagioclase
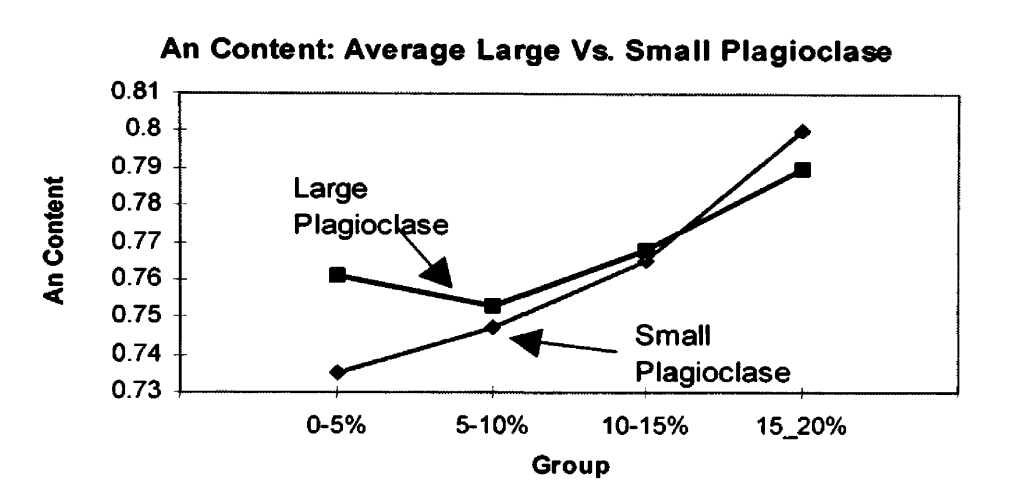
Figure 35a. Compositional zoning of large plagioclase grains for each pyroxene group.

(15-20%) Large Plagioclase An Vs. Distance

(10-15%) Large Plagioclase AN Vs. Distance

(5-10%) Large Plagioclase An Vs. Distance

(0-5%) Large Plagioclase An Vs. Distance

57
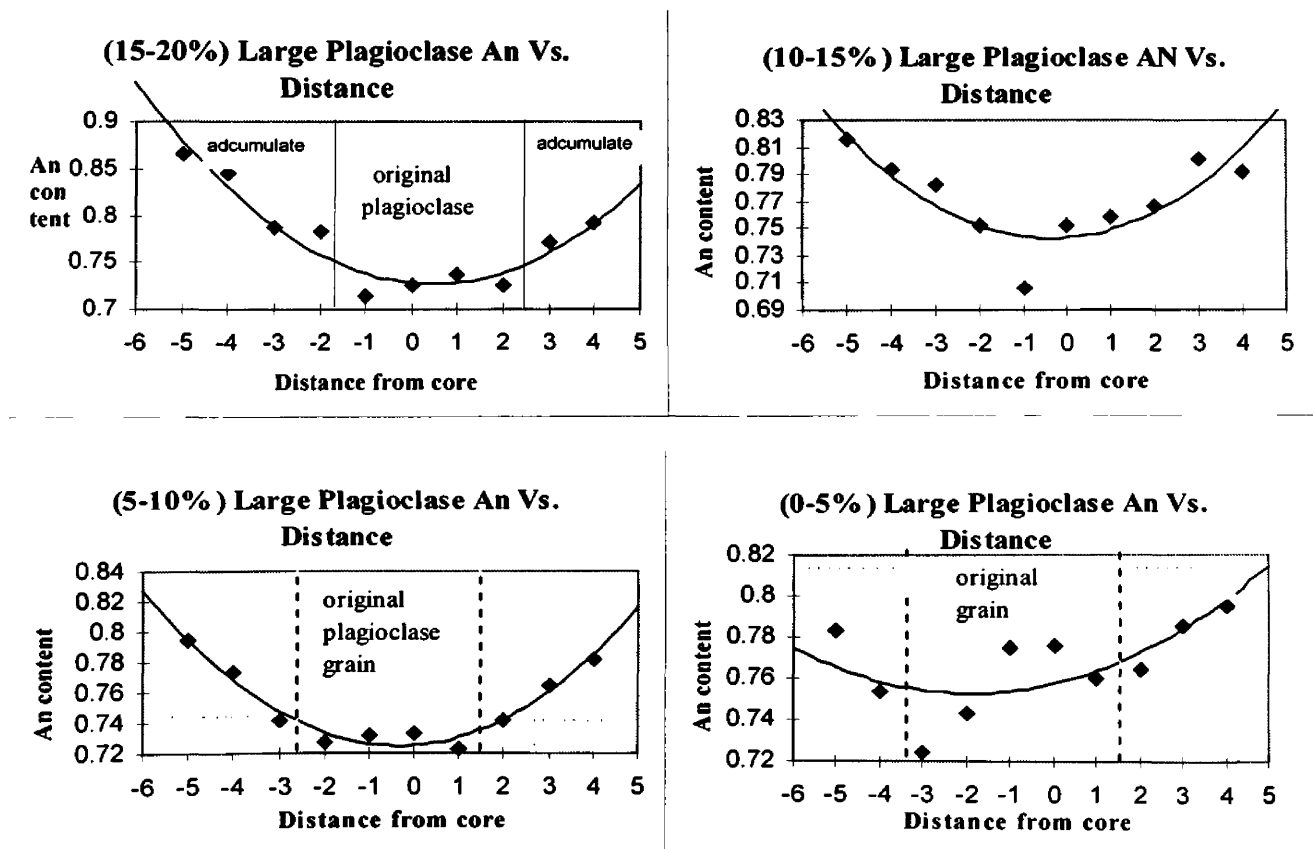
Figure 35b. Compositional zoning of small plagioclase grains for each pyroxene group.

(15-20%) Small Plagioclase An Vs. Distance

(10-15%) Small Plagioclase An Vs. Distance

(5-10%) Small Plagioclase An Vs. Distance

(0-5%) Small Plagioclase An Vs. Distance
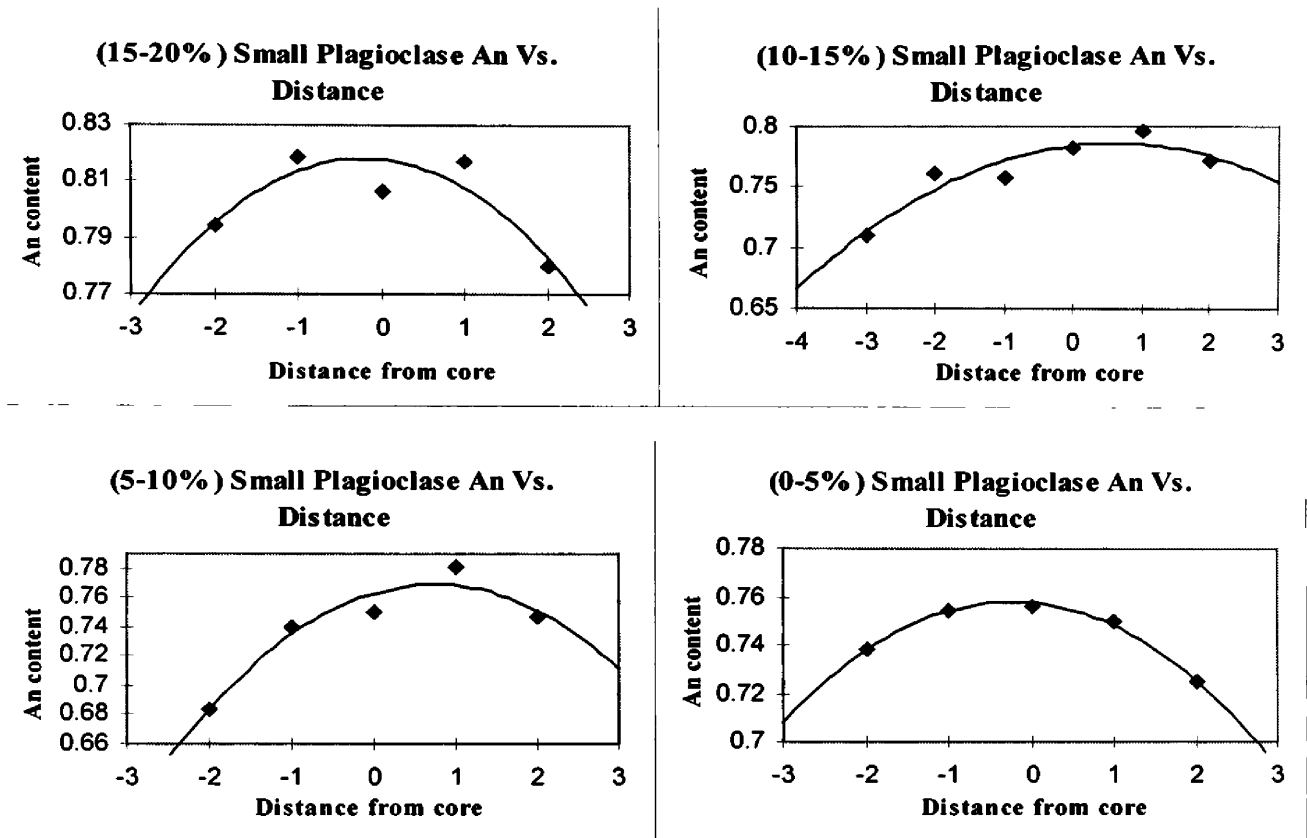
Figure 36. Relationship between the large plagioclase grain rims and the small plagioclase grain cores.

An Content: Large Rim Vs. Small Plagioclase core
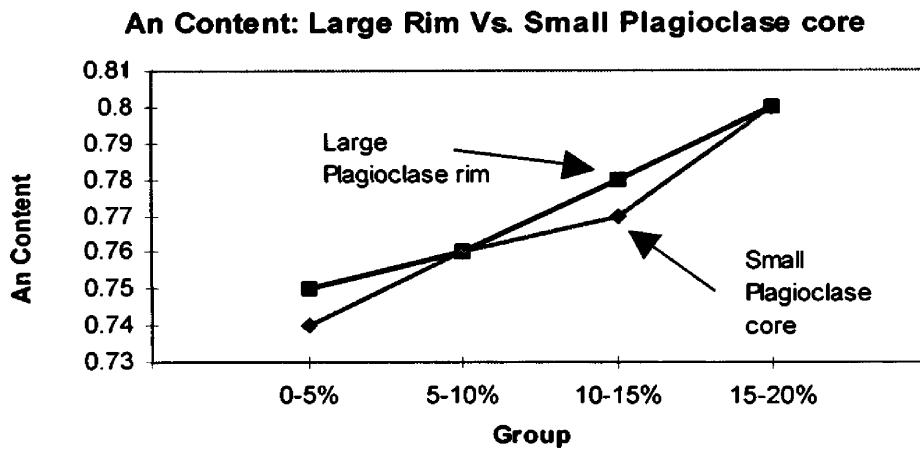
Pyroxene

The plagioclase analyses suggest that the small (intercumulate) plagioclase grains were derived from a more primitive melt than the large (cumulate) plagioclase grains. The data also suggest that this intercumulate melt fractionated and became more sodic from the high-pyroxene (15-20% group) zones to the low-pyroxene (0-5% group) zones. To test this hypothesis, the intercumulate pyroxenes and olivines were analyzed with the microprobe. If the intercumulate melt was indeed trapped and fractionated, then the Mg number (Mg/(Mg + Fe)) of the mafic minerals should show Fe enrichment in the more-fractionated, pyroxene-poor (0-5% group) zones. Due to the oikocrystic nature of the intercumulate mafic minerals, grain orientation, i.e., compositional zoning patterns, is difficult to control. Therefore, a microprobe traverse perpendicular to mineral zoning patterns is similarly difficult, or impossible. Pyroxenes also exhibit considerable subsolidus diffusion in their exsolution lamellae; therefore the pyroxene compositional trends may not reflect the compositional trends of the original melt. Also the much smaller Mg and Fe^{++} can diffuse more easily than the Si and Al of plagioclase that are locked into the tetrahedral lattice structure.

In the 15-20% pyroxene group the orthopyroxenes and olivines are homogeneous and contain 70 mol % Mg end-member. The compositional zoning fluctuations are insignificant and below the margin of error at 1 mol % Mg end-member. The Mg-number, which does not support a primitive melt, and the lack of compositional zoning may suggest a compositionally stable environment for crystallization of the mafic minerals within the 15-20% pyroxene group.

In contrast, the pyroxenes of the 10-15% group typically display modest Mg enrichment (75 mol % Mg end-member) and considerable compositional variation (up to 12 mol % Mg) within a single grain. The Mg-number varies slightly across the clinopyroxene

lamellae within the orthopyroxene grain (±1 molar % Mg), but is below the margin of error and therefore is considered insignificant. This variation and enrichment may reflect a mixing and mingling of a more-primitive Mg-rich melt. Alternatively, this Mg enrichment may be the result of subsolidus diffusion, as mentioned above.

Within the 5-10% group, the pyroxenes are mostly altered to chlorite. Microprobe analysis of the unaltered parts of pyroxene grains show a drastic decrease in Mg for an average Mg-number of ~20 mol % Mg end-member. Direct comparison between chlorite and the clinopyroxene it replaced may not be valid, but does warrant interpretation. Chlorite is similarly Fe-enriched with an average Mg-number of ~20 mol % Mg end-member. If the chlorite does reflect the Mg-number of the original pyroxene, then that pyroxene is extremely enriched in Fe. This may reflect a compositional change within the melt. If this were strictly due to compositional change in the melt, then this would support the hypothesis that the melt was trapped within the plagioclase framework and did not communicate with the melt within the Stillwater Complex chamber. Alternatively, this Fe enrichment may be caused by Fe-rich hydrothermal fluids that altered the clinopyroxenes. Further support of this hypothesis is the high Fe content within the clinozoisite patches (up to 2 mol % Fe), which are hydroxide minerals of unquestionably hydrothermal origin. The above microprobe and whole-rock geochemistry data have strong implications for the origin of the sulfide-bearing horizons and may support either a model of remobilization of the sulfide minerals or that the sulfide minerals are of strictly hydrothermal origin.

Within the 0-5% group all pyroxenes are altered to albite, chlorite, zoisite, clinozoisite, and quartz, or are replaced by sulfide minerals. Microprobe data of these altered pyroxenes show a similar enrichment in Fe (<20 mol % Mg end-member) in the above 5-10% group and may suggest the fluid responsible for alteration was enriched in Fe.

Minerals Enclosing the Sulfide Grains

Microprobe analyses were made along the sulfide-silicate boundary within the 0-5% group. These data confirmed the presence of albitic rims enclosing all the sulfide grains. These data also show the compositional trend for the clinozoisite/epidote grains that accompany the sulfide/oxide minerals. Clinozoisite, a monoclinic hydrous calcium-aluminum-iron silicate, changes structure to orthorhombic zoisite where less than 7% of the octahedral sites are occupied by Fe^{3+}. Conversely, clinozoisite and epidote form a continuous solid-solution series with the substitution of Fe^{3+} for Al^{3+} in the octahedral sites. Clinozoisite with greater than 15% Fe^{3+} in the Al^{3+} site changes optic sign to become epidote. Therefore, zoisite, clinozoisite and epidote are useful indicators of the iron content and oxidation state of the hydrothermal fluid that they are derived from.

Microprobe analyses revealed a compositional trend between zoisite, clinozoisite, and epidote. From immediately adjacent to the sulfide grains outward to the iron oxide minerals, the compositional trend is zoisite, clinozoisite, and epidote. This may appear obvious in that the sulfide minerals are reduced and the oxides are oxidized, but this trend can also be used to interpret the change in the composition of the hydrothermal fluid. If an oxidized hydrothermal fluid was transporting Fe amongst other metals and began to precipitate the oxides ilmenite and magnetite, the fluid would become more reduced. Further, if the hydrothermal fluid, now reduced, became saturated in Fe, it would be more able to precipitate Fe-sulfide minerals. Alternatively, the oxidized hydrothermal fluid may have been flushed out by an invading reduced and sulfide-bearing fluid, or the oxidized hydrothermal fluid came in contact with a magmatic sulfide horizon, reacted and deposited

the metals. The latter would support the remobilization or hydrothermal hypothesis for the origin of the sulfide horizons.

IV. Fluid Inclusions

Within the two thick anorthosites (AN I, AN II) and other rocks of the Middle Banded series, multiphase inclusions of pyroxene + ilmenite + apatite have been found in the cumulus plagioclase grains (Loferski and Arculus, 1993). Most inclusions are 50-150 microns across, although some inclusions are up to several hundred microns. Most inclusions occur within the interior of plagioclase grains and along twin planes; they are not related to fractures within the grains of plagioclase. Most inclusions are clinopyroxene with a variety of shapes: many are rounded, whereas others are elongate with a length to width ratio of 4:1. Textures and consistant mineralogy suggest that these inclusions have been incorporated in the plagioclase as liquid droplets rather than solid aggregates. The clinopyroxene inclusions enclose single or multiple grains of ilmenite and apatite. The larger inclusions consist of all three phases and the clinopyroxene may have 120° triple junctions between grains. Distinctively manganiferous ilmenite and the presence of baddeleyite (ZrO_2) suggest the inclusions formed from a liquid of unusual composition. Apatite within the inclusions has a high percentage of the halides F and Cl. Microprobe analyses of apatite, from AN II with interstitial olivine, had up to 3.2 wt.% F, whereas samples from AN II without olivine contained up to 2.7 wt.% Cl (Loferski and Arculus, 1993). The presence of these halides may be significant and is considered crucial for the transport of the PGEs (Boudreau and McCallum, 1989).

From the multiphase inclusion data Loferski and Arculus (1993) suggest a model of origin for the two thick anorthosites (AN I and AN II) and other rocks within the Middle

Banded series. They hypothesized that the inclusions formed from droplets of immiscible liquid that exsolved from the main liquid responsible for the crystallization of the anorthosites. This is supported by the overlap of compositions of interstitial and inclusion pyroxene and ilmenite. However, the timing of crystallization of both the inclusions and the interstitial fluid is not known. Secondly, if the inclusions exsolved from the initial melt and therefore separated from the melt, then the final compositions of the two should not be the same. The composition of the interstitial melt is assumed to not change over time, because any change would only affect the open system of the interstitial melt, and obviously not the composition of the inclusions. Loferski and Arculus (1993) suggest a two-melt system for the origin of the anorthosites: one was highly polymerized aluminosilicate melt (analogous to Haskin and Salpas, (1992) 'framework' plagioclase) and the other, depolymerized. They suggest that highly polymerized, low-density melt separated from lower in the magma chamber and moved upward as diapirs to form large zones (AN I and AN II), suggesting both a compositionally and density-stratified magma chamber. They further suggest that crystallization of the anorthosites from a mixing of a polymerized melt with a non-polymerized melt may account for distinctive features such as the coarse grain size and complex plagioclase zoning.

Prior to this study fluid inclusions of the Picket Pin deposit have only been studied by Boudreau (1986). Boudreau found fluid inclusions in the interstitial quartz of both mineralized and unmineralized coarse-grained anorthosite. Most of the inclusions are only a few microns in diameter, secondary, and difine trails and planes. Many contain a vapor bubble, a cubic daughter crystal (NaCl?), dark rod-shaped crystals (rutile?), and/or highly birefringent crystals (carbonate?). A wide range of homogenization temperatures may reflect

the variety of compositions within the inclusions. Boudreau found the range of temperatures (200-500°C) to be consistent with greenschist facies alteration.

In contrast to the inclusion data of Loferski and Arculus (1993), the primary fluid inclusions within this study area range from < 2 μm up to 20 μm in diameter. Geometries of the inclusions are: circular to roughly circular single phase, circular with vapor bubble, rod-shaped single phase, rod-shaped with vapor bubble, and circular three-phase with vapor bubble and cubic crystals (NaCl?), in descending order of abundance. The rod-shaped inclusions may contain opaque minerals (rutile?, sulfide minerals?) next to sulfide grains. Many fluid inclusions proximal (< 1 cm) to sulfide grains appear to enclose a sulfide phase. Numerous, small (<5 μm) apatite grains were identified within the zoisite and clinozoisite that surrounds sulfide grains.

Analyses of the fluid inclusions was problematic. The temperature of homogenization for the inclusions away from sulfide mineralization was above the maximum temperature (>700°C) of the analytical methods used. Within the sulfide-bearing samples the iron oxides derived from weathering and the murky nature of the clinozoisite/epidote made analyses difficult to obtain, and in most cases, impossible. The small size of most inclusions further inhibited analyses. In view of the difficulties, only the most reliable 45 analyses are plotted below (Fig. 37). Due to the difficulties, caution is recommended for interpretation from the data.

The identification of several fluid inclusions which include cubic crystals (NaCl?) is indicative of a highly saline fluid that contained 26 wt % NaCl, $CaCl_2$, or KCl. This, along with the albitic rims surrounding the sulfide grains and the alteration of the pyroxenes support the presence of a Na-rich hydrothermal fluid. The large number and small (<5 μm) size of the inclusions is generally interpreted as the result of rapid cooling. Rapid cooling is,

however, in conflict with the obvious slow cooling history of the Stillwater Complex. This interpretation is either erroneous or the inclusions formed from a post-magmatic hydrothermal fluid emplaced after the complex cooled significantly. The temperature of homogenization data concentrates into five groups with average temperatures of: 348, 435, 470, 570, and >700°C. Interestingly, the temperature of homogenization increases away from the sulfide grains (Fig. 37). From this data, it appears that the hydrothermal fluid near the sulfide grains cooled last. Caution should be used in any interpretation due to the extreme difficulty in obtaining the data.

.

Figure 37. Fluid inclusion temperature of homogenization

Temperature of Homogenization Vs Distance
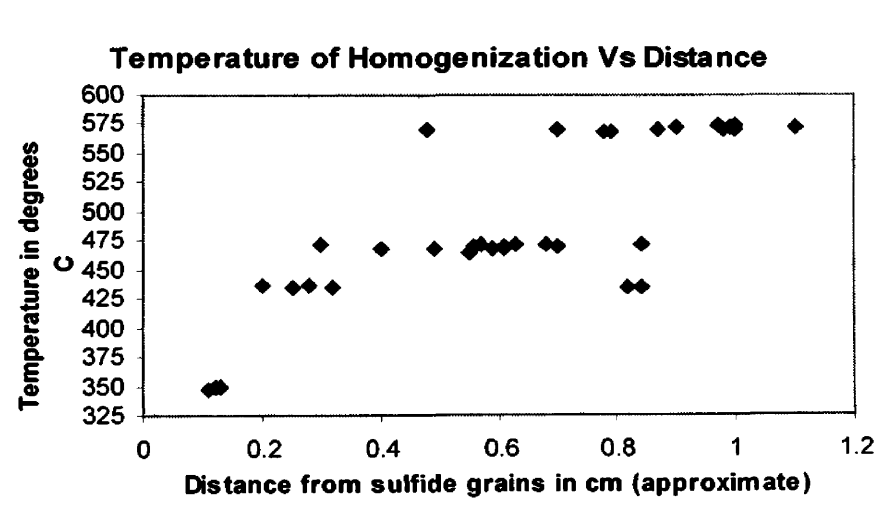
CHAPTER FIVE: PLATINUM GROUP ELEMENT DISTRIBUTION

I. PGE Distribution in the Stillwater Complex

The Picket Pin deposit is typical of the other PGE-bearing zones within the Stillwater Complex with a thickness that varies from centimeters to a meter. The PGEs occur in discordant sulfide pods and lenses that lead up-section to the strata-bound horizon ("reef"). Pyrrhotite, pentlandite, chalcopyrite, and millerite are the main sulfide minerals within the deposit. Up to 20 different platinum group minerals have been identified; most important are moncheite, braggite, vysotskite, cooperite, sperrylite, and ferroplatinum (Stumpfl, 1985) (Fig. 38). The maximum values of total PGE in the J-M reef are in excess of 15 oz/ton (Barnes and Naldrett, 1985). Exploration and assay values to date suggest that the Picket Pin deposit averages a low-grade (0.15 oz/ton) PGE deposit (Corkery, 2001).

Figure 38. STILLWATER ORE MINERALOGY

Braggite	$(Pt, Pd, Ni) S$
Cooperite	$(Pt, Pd, Ni) S$
Isoferroplatinum	$Pt Fe_3$
Moncheite	$(Pt, Pd) (Te, Bi)_2$
Sperrylite	$PtAs_2$
Vysotskite	$(Pd, Ni, Pt) S$

* Approximately 80% of Pd in the JM Reef is hosted as solid-solution or submicroscopic inclusions in:

Pentlandite	$(Fe, Ni)_9 S_8$

The sulfide minerals occupy intercumulus spaces, on grain boundaries, and in complex intergrowths with hydrous silicate minerals (Cabri, 1981). Sulfide minerals also crosscut olivine grains within a rim of serpentine which suggest a deposition, or redeposition temperature of 500° C. Boudreau and McCallum (1985) found that the PGEs occur in

pyroxene-poor, quartz-rich zones, whereas the PGE-barren zones are marked by pyroxene-

rich zones that contain magnetite. This zonation pattern may suggest a redox interface

between the oxidized, magnetite-bearing rocks and the reduced, sulfide-bearing rocks. There

is a strong positive correlation between the distribution of sulfide minerals and the amount of

the hydrous silicates amphibole, micas, talc, and serpentine (Barnes and Naldrett, 1985).

Some authors have suggested that both the sulfide and hydrous minerals precipitated from a

fluid phase (Boudreau and McCallum, 1985, Barnes and Naldrett, 1985). Upward migration

of Cl-rich fluids is supported by evidence presented by Boudreau and McCallum (1985).

They describe transgressive sulfide pipes with silicate assemblages enriched in incompatible

elements and in hydrous minerals below the Picket Pin deposit supporting upward migration

of volatiles. Secondly, they describe pegmatitic rocks with 60% olivine, chlorapatite,

graphite, and Cl-rich biotite that occur below the JM Reef.

II. PGE Distribution in other deposits

High concentrations of PGE's have been found in both marine and non-marine

sedimentary deposits. The Kupferschiefer-type deposits have recently described to contain

high concentrations of PGEs, with a maximum value of 200 ppm Pt. Kucha (1981) was the

first to survey the mineralogy of PGEs within the Polish Kupferschiefer. Above-average

concentrations of PGE, Au, and Ag have been mapped with a stratigraphic thickness of 1

meter, and a lateral extent of 1500 meters. The discrete PGEs occur in the contact zone

between a white sandstone (oxidizing), and a black shale (reducing). The Kupferschiefer

mineralization is considered to be entirely a hydrogeological process acting at redox

interfaces, with the organic material acting as a catalyst. The organic material within the

shale may supply an excess of carbon, therefore keeping the migrating fluids under a

reducing condition. When the fluids reach the white (oxidized) sandstone, the fluids oxidize and the PGEs precipitate out (Kucha, 1981). Conversely, the fluids may have migrated within the oxidized sandstone and precipitated when in contact with the reduced shale. This evidence further supports the intimacy between a redox reaction and PGE transport and deposition.

The distribution of PGEs in marine sediments has only recently been investigated (Stumpfl, 1985). The concentration of PGEs in ferromanganese nodules and crusts have average values of 293 ppb Pt, and 0.68 ppb Pd (Hodge et al., 1985). The relative enrichment of platinum over palladium can be ascribed to more intensive complexing with chlorine and bromine (Boudreau and McCallum, 1985). In seawater, platinum and palladium are present as doubly negative tetrachloro anions (Hodge et al., 1985), and iridium as iridium hexafluoride (Zoller et al., 1983) which are then incorporated into the hydrous minerals of manganese nodules (Hodge et al., 1985).

The New Rambler Pt-Cu-Au deposit, Wyoming, has been interpreted as an intermediate-temperature (200-700° C) deposit with remobilization of PGEs by hydrothermal fluids (McCallum et al., 1976, Nyman et al., 1990). Evidence that suggests a hydrothermal origin includes: 1) ore textures that suggest replacement by a hydrothermal process, 2) association of PGEs with hydrothermal alteration assemblages (chlorite + epidote + clinozoisite + albite + magnetite), 3) higher concentrations of soluble PGEs (Pt and Pd) relative to the less soluble PGE's (Ru, Rh, Os, and Ir), 4) enrichment of other elements (Bi, Cu, Au, and Ag) in the altered host-rock (Nyman et al., 1990). Fluid inclusions from this deposit have homogenization temperatures that range from 335 and 365°C, which further support a hydrothermal origin (Nyman et al., 1990). The composition of the fluid inclusions in the New Rambler are similar to inclusions found in the Bushveld Complex. The gross

compositional similarities are; 1) pure condensed gaseous inclusions (CO_2 and N_2) and 2) aqueous brines composed of NaCl, $CaCl_2$ and $\pm$ $MgCl_2$ (Nyman et al. 1990). These similarities may suggest a common origin between PGE deposits. The Picket Pin deposit parallels these similarities.

Although the above environments are very different (Bushveld, New Rambler, Kupferschiefer), they share common traits and associations. In the above examples, the PGEs are transported, or at least affiliated with the halides. In the Picket Pin, the PGEs are accompanied by the halide minerals chlorapatite and clinoamphibole (fluorine). Similar halides are found in all the above examples of different PGE deposits. Furthermore, PGE deposition in both the Picket Pin and the Kupferschiefer is associated with redox interfaces. The Kupferschiefer PGE deposition occurs between a reduced black shale and an oxidized white sandstone. The Picket Pin deposit PGE deposition occurs between sulfide-rich (reduced) zones and magnetite-rich (oxidized) zones.

The above evidence suggests that it is possible to view transport, formation and mineralization of the strata-bound, reef type, PGE deposits of layered mafic complexes as a result of complex evolution of melt-fluid systems (Ballhaus et al., 1985). The progression of melt-fluid evolution leading to the formation of reef type PGE deposits may be as follows: 1) Mantle melting +/- contamination of C and S, 2) Differentiation of silicate melt, 3) Melt/fluid segregation, formation of pegmatites, strongly reducing conditions with the formation of graphite, sulfide minerals, and PGEs, 4) Injection of a new pulse of magma, 5) Mingling of the reduced fluids and oxidizing new magma, 6) Precipitation of sulfide minerals and PGEs at redox interface, 7) Low temperature ($500°C$) alteration, local remobilization and deposition of PGEs (Ballhaus et al., 1985).

III. Experimental PGE Fractionation and Solubility

Experimental and theoretical PGE fractionation and solubility should be compared to the alteration mineral assemblage within natural systems. The alteration assemblage should yield important information on the fluids involved in the transport and deposition of the PGE-bearing minerals. The alteration assemblage in this study has been divided into high-grade and low-grade. High-grade (>3 ppm PGE) alteration assemblages are clinozoisite>>quartz>albite>epidote with numerous inclusions of apatite within the clinozoisite. Low-grade (<3 ppm PGE) alteration assemblages are quartz>albite>> clinozoisite>epidote. From the evidence above, the fluid responsible for the alteration assemblage can be inferred to contain: (OH), Na, Cl, Fe^{+++}, and SiO_2. Metallic elements in the oxide/sulfide phases that may have been transported in the hydrothermal fluid are: Ti, Fe^{+++}, Fe^{++}, Cu, Ni, PGE, S, O, and As.

There remains a lack of published experimental data on the hydrothermal solubilities of the PGEs. Most solubility data has been extrapolated from experiments that range in temperatures from 25 to 300°C (Mountain and Wood, 1988; Wood, 1987; Gammons and Bloom, 1992; Gammons et al., 1992; Fleet et al., 1999). Experimental and theoretical (thermodynamic) data strongly disagree as to which model of PGE transport each author favors. The natural systems alteration assemblages which co-exist with the PGE-bearing minerals were not considered by the authors in interpreting their experimental data. There exists one example of a natural system (McKibben et al., 1990), and one comparison between theoretical data and a natural system (Mathez, 1989). The evedence from natural systems is discounted by numerous 'experimental' authors, and the experimental work is not addressed by Mathez.

McKibben et al. (1990) studied the solubility and transport of PGEs and Au in a geothermal well in the Salton Sea geothermal field. They found the Salton Sea brines could transport up to 1 ppb of PGEs and Au at temperatures near 300°C at a near-neutral pH (5.4), and with an oxidation state near aqueous SO_4-H_2S equilibrium. They suggest the lack of PGE enrichment in downhole scale deposits is consistent with transport of these elements mainly as chloride complexes. McKibben et al. (1990) found a four to six orders of magnitude increase in PGE concentrations compared with predicted by published experimental models. They conclude that a saline, relatively oxidized hydrothermal fluids can transport much greater amounts of PGEs than is currently believed. Mineralogic and geochemical evidence from the current study support this conclusion where PGE enrichment co-exists with saline (albite), oxidized (epidote), hydrothermal fluids (zoisite, clinozoisite, chlorite).

Mathez (1989) compares oxygen fugacity to temperature for drill cores from the Makaopuhi lava lake, MORB, QFM, and Fe-Ti oxides from a drill core of MORB (Fig. 39). The data from Makaopuhi lava lake displays a rapid increase in oxygen fugacity as the magma cooled from between 750 to 700°C. The increase in oxygen fugacity remains high until approximately 570°C then reduces to a level near the QFM buffer below 500°C. Although the author makes a significant conclusion, that the increase in oxidation is due to the influx of meteoric waters, he ignores this process in the transport of the PGEs. It appears that the experimental and theoretical research on the solubility and transport of the PGEs is biased towards high-temperature transport of the PGE's to the point of ignoring data from natural systems.

Theoretical work by Sassani and Shock (1990) acknowledges the constraints of the co-existing mineral assemblages. They suggest that the data from mineralogy, mineral
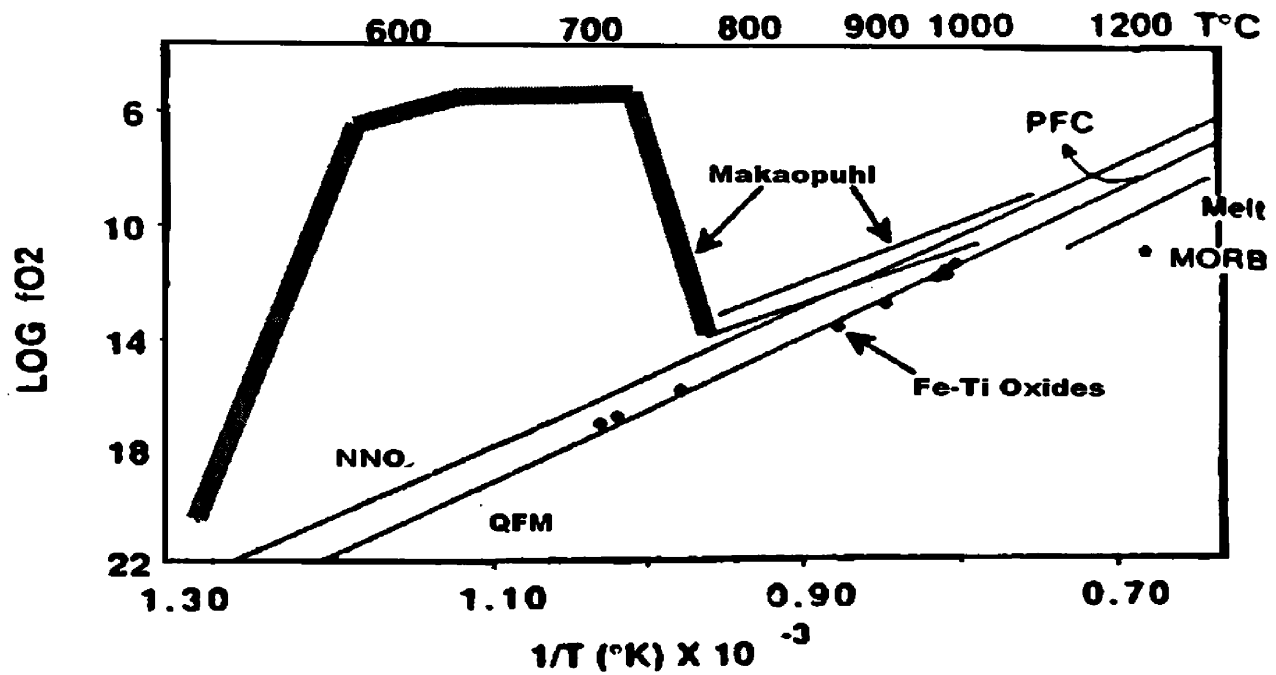
Figure 39. T-fO$_2$ paths for some mafic systems. All but the data from Makaopuhl Lava Lake is theoretical. The data highlighted (red) is an oxidized zone due to the influx of meteoric waters in the Makaopuhl Lava Lake (after Mathez, 1989). This data suggests that an influx of meteoric waters can greatly increase the oxidation state of a melt. The PGEs migrate most effectively in a saline, oxidized fluid at temperatures between 400 and 600°C.

chemistry, and fluid inclusions correspond to temperatures of 500-800C, oxidation value of the QFM buffer, pH in the range of 4-6, and total chloride concentrations of up to 10 m. Under these conditions their calculations indicate that Pd solubility could reach 0.1 ppm and would be sensitive to changes in pH and oxidation. Their calculations further suggest that even at modest NaCl concentrations, chloride complexes are the predominate Pd^{++} species.

These data fit well with the observed mineralogic, geochemical, and temperature estimates of the current study. This evidence suggests that the PGEs were transported in an oxidized hydrothermal fluid at a near-neutral pH between 500 and 550°C. A rapid change in

oxidation state to a more reduced condition; the PGEs were no longer soluble and precipitated. This rapid change in oxidation state may be the result of the hydrothermal fluid encountering a sulfide horizon.

CHAPTER SIX: DISCUSSION

I. Magmatic Origin of PGE's

The following is a review of modern concepts and experimental results for a magmatic-sulfide melt as presented by Naldrett (1989). The main hypothesis of the formation of magmatic sulfide minerals is that the sulfide melt segregates from the silicate melt to form an immiscible sulfide/oxide melt that becomes concentrated in a particular location. This sulfide melt is thought to settle gravitationaly since sulfide liquid specific gravity is >4 and the silicate magma <3. Partitioning of transition group VII metals Fe, Co, Ni, Pd, Pt, Rh, Ru, Ir, and Os with Cu, and Au into the sulfide/oxide melt may occur. Sulfide droplets that segregate should be in equilibrium with the melt where the sulfide droplet composition is controlled by the magma composition. If at equilibrium, the silicate and sulfide melt should have the same Fe_2/Fe_3 ratio. Natural magmas have limited range of FeO content and oxidation state. If the sulfide melt is at equilibrium it should exhibit the same restricted range of FeO content and oxidation state. Fudali (1965) suggests that the fO_2 of mantle sources for magmatic sulfide melts are in the FMQ buffer (10^{-8} fO_2 at 1200°C), then magnetite should precipitate first. In contrast, Cermer (1987) notes that the oxygen content depends on the Fe/Ni+Cu ratio. The presence of Ni+Cu may lower the oxygen so that it falls in the pyrrhotite field instead of the magnetite field.

For the Fe-S-O system, the eutectic temperature of sulfide melt is assumed to depend on Fe/S ratio where the Fe-rich eutectic is 988° C, and the sulfur-rich eutectic is 1083° C. Therefore the sulfide melt should start to crystallize between 1160 and 1120° C based on thermodynamic data. The model suggests that this crystal/melt mixture would be able to migrate, and therefore this temperature is considered a minimum temperature for mobilization in a partly liquid state. This model is based on a 60.5 wt. % Fe system, which is

predicted to have a solidus temperature of between 1010 and 1050 °C. Experimental work suggests that the addition of up to 20% Ni has no measurable effect on the solidus temperature. However, the addition of 2 wt % Cu lowers the solidus by 20° C. The addition of more than 2 wt % Cu would have a greater effect and would distinctly lower the solidus temperature. The amount of sulfur within a natural melt is problematic and therefore crustal sulfur is extremely important in the magmatic sulfide model. However, isotopic research has shown that all the worlds major Ni-Cu deposits, the Bushveld, and possibly the Stillwater Complex exhibit a variety of crustal contamination of sulfur (Naldrett, 1989).

With the volatiles, incompatible elements and excess SiO_2 would also segregate from a mafic silicate melt and perhaps mix with the sulfide/oxide melt. No research has attempted to measure the distribution or amounts of these volatiles and elements or their effects on the sulfide/oxide melt. The volatile content of a mafic melt is considered too low to have any significant effect on the system as a whole. It seems most likely that these elements would have an effect on the oxidation state, solidus temperature, and composition of the sulfide/oxide melt. Further, the effect of buoyancy on the sulfide melt due to volatile content has never been addressed. Perhaps these volatiles and elements act as a catalyst to partition and scavenge the transition metals and cause the melt to reach sulfur-saturation, which may result in the establishment of an immiscible sulfide/oxide melt.

The magmatic sulfide theory as it pertains to the Stillwater Complex has been proposed by many authors. Barnes and Naldrett (1986) suggest that a mixing of two different melts occurred to form the JM Reef, the presently exploited PGE-bearing sulfide interval. The first magma, A-type, is on the plagioclase solidus and near sulfide saturation, is mixed turbulently with the second more-primitive melt on the olivine + chromite solidus (Fig. 40). The sulfide droplets would be mixed turbulently and ultimately achieve the high
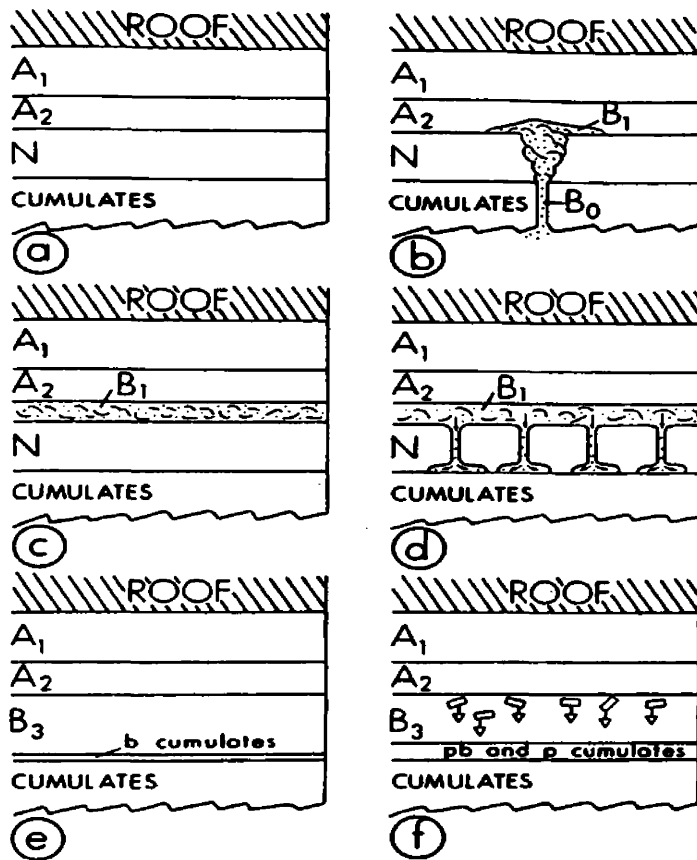
Figure 40. Magmatic sulfide model as proposed by Naldrett (1989). A primitive melt (B0/B1) is injected between a norite (N) and anorthosite (A1-2) layer, mixes turbulently (C) scavenging PGEs, downspouts (d) to a neutral buoyancy to form a layer ('reef') of PGE-enriched sulfides. From Naldrett (1989).

PGE content by scavenging the PGE during this turbulent mixing. The evidence for this mixing is: the resorbed, reverse zoned plagioclase of the probable A-type melt; the ameboidal olivine suggested to have formed by rapid growth from the primitive trapped melt; and the resorbed olivine jacketed with bronzite from further impulses of primitive melt. Sulfide saturation was achieved from the most persistent pulse of primitive melt that formed the JM Reef. In order to accommodate the large quantity of sulfide in this pulse, they suggest that any sulfide associated with other pulses was resorbed into the melt until sulfur saturation (Naldrett, 1989). However, there are numerous, albeit minor, strata-bound sulfide occurrences below the JM Reef (Corkery, 2001, 2002). The sulfide occurrences within the Stillwater Complex are located a meter above, below or straddling a major change in modal

abundance of mafic minerals. This may suggest a reaction involving a partially solidified melt on the plagioclase solidus, influx of a primitive mafic melt, a release of volatiles, and subsequent precipitation of sulfide minerals.

The first part of the Naldrett (1989) model is applicable to the Picket Pin deposit. AN II displays resorption textures and reverse zoning in the plagioclase grains. The high Mg-number and high An content of the intercumulate mafic minerals and plagioclase grains suggests mingling of a more primitive melt with a more-fractionated melt. Grains of apatite and baddeleyite (ZrO_2), and the oikocrystic nature of the intercumulate mafic minerals may suggest that volatiles including H_2O were a significant part of sulfide formation. Further, the sulfide minerals occur in the most fractionated area of the melt, i.e., both K and Na increase significantly local to sulfide mineralization. This suggests that if the sulfide minerals were magmatic, they remained mobile and did not precipitate until the melt was almost completely crystallized. Alternatively, the incompatible elements may have been transported by a later hydrothermal event. This may negate the requirment of the hypothesis that an injection of a more primitive melt to trigger sulfide saturation .

Other models for the formation of the PGE-enriched sulfide horizons are divided into late-stage magmatic and hydrothermal-fluid theories. It seems the difference in nomenclature is less important, because these models, as with all models of formation, are synchronous with magmatic crystallization, sulfide formation, and PGE-enrichment, and ultimately involve a magmatic origin. To minimize the confusing terminology, all models that involve late-stage magmatic fluids will be called such, whereas the term hydrothermal fluids is here reserved for post-magmatic fluids (Fig.41).
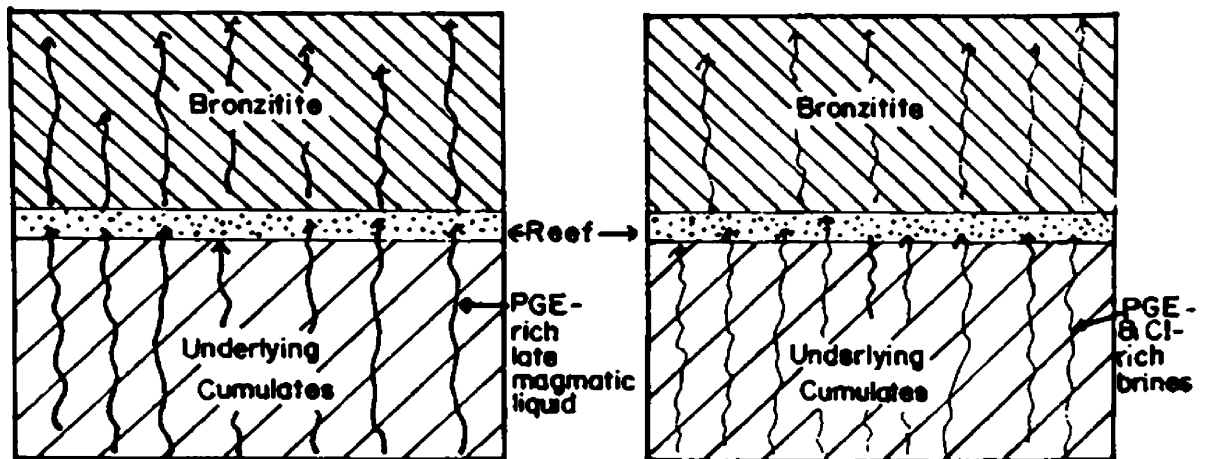
(A) Enrichment of existing sulfides by ascending late magmatic liquid

Bronzitite

←Reef→

PGE-rich late magmatic liquid

Underlying Cumulates

(B) Enrichment of existing sulfides by ascending hydrothermal fluids

Bronzitite

PGE-& Cl-rich brines

Underlying Cumulates
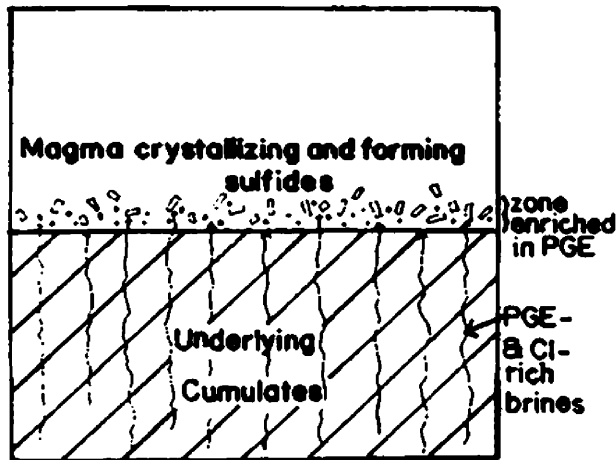
(C) Enrichment of zone of crystallization and sulfide liquid segregation by ascending hydrothermal fluids

Magma crystallizing and forming sulfides

zone enriched in PGE

PGE-& Cl-rich brines

Underlying Cumulates
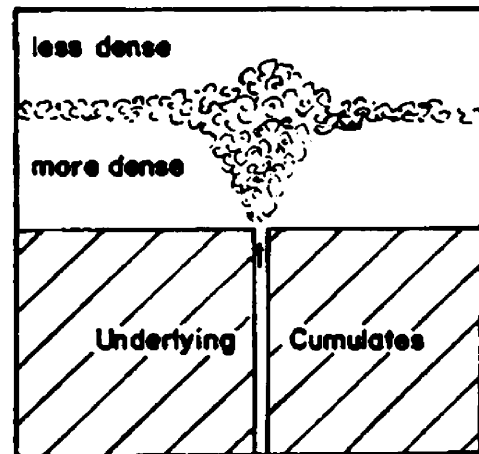
(D) Segregation of PGE-rich sulfides in turbulent plume in which they achieve a high 'R' factor

less dense

more dense

Underlying

Cumulates

Figure 41. Cartoon illustrating four hypothesized origins for reef-type PGE-enriched sulfide layers. (A) model after von Gruenewaldt, 1979; (B) model after Ballhaus and Stumpfl, 1985 and Johan and Watkinson, 1985; (C) model after Boudreau, 1988; (D) model after Campbell et al., 1983 and Naldrett et al., 1986. From Naldrett, 1989.

78

II. Late-Stage Magmatic Origin of PGEs

Models proposed by Vermaak (1976), von Gruenewaldt (1979), Ballhaus and Stumpfl (1985), and Boudreau (1988) all involve late-stage fluids rich in Cl migrating upwards to scavenge and deposit the PGEs at sulfide horizons. The models differ in where the fluid was derived. The early models suggest that the Cl-enriched fluids were derived from the intercumulate melt. Alternatively Boudreau (1988) suggests that the PGE-enriched sulfide minerals were derived from migrating fluids moving upwards through the cumulate pile. All of these models are synchronous with magmatic crystallization and sulfide precipitation.

The model suggested by Ballhaus and Stumpfl (1985), is summarized as a progression of melt-fluid evolution leading to the formation of reef-type PGE deposits as follows: 1) Mantle melting +/- contamination by C and S, 2) Differentiation of silicate melt, 3) Melt/fluid segregation, formation of pegmatites, strongly reducing conditions with the formation of graphite, sulfide minerals, and PGEs, 4) Injection of a new pulse of magma, 5) Mingling of the reduced fluids and oxidizing new magma, 6) Precipitation of sulfide minerals and PGEs at redox interface, 7) Low temperature (200°C) alteration, local remobilization and deposition of PGEs (Ballhaus et al., 1985).

The model favored by Boudreau (1988) can be summarized as follows: at some point in the crystallization of the cumulus pile, a lithologic change acted as a trap for the upwardly migrating, volatile-rich fluids. Partial re-melting occurred after some amount of volatile-rich fluid was trapped. The cumulus plagioclase dissolved to produce reversely zoned, and embayed grains. This fluid also led to the destruction of pyroxene which produced olivine,

chromite, and local ilmenite/magnetite by the incomplete equation:

$$(Mg,Fe)_2Si_2O_6 + H_2O \rightarrow (Mg,Fe)_2 SiO_4 + SiO_2.$$
orthopyroxene   fluid   olivine   quartz

This equation suggests a transfer of mafic components toward the fluid-rich regions and the plagioclase components outward. This transfer is suggested to create the characteristic olivine-rich rock/anorthosite association. The thickness of this zone increases with the increase of fluids. The result is suggested to have formed a stratigraphic horizon of pegmatitic rocks enriched in sulfide minerals and chromite.

However, the mafic components did not migrate to the fluid-rich zones, nor the plagioclase away from the fluid-rich zones as implied by this model. The opposite is found to be true in the current study. The mafic components are not spatially related to the fluid-rich (Na, K, REE, and PGE enriched zone), whereas the plagioclase-rich zones are. The Cr content is highest within the hydrothermally altered zones which include the altered pyroxene zones. If the Cr were derived from the alteration of the pyroxenes and migrated into the sulfide-bearing zones as suggested by Boudreau, then the altered pyroxene zones would be expected to have the lowest concentration of Cr, which they do not. No textural or geochemical evidence supports the sequence of pyroxene altered to form olivine. The pyroxene-rich zones that contain olivine, display no signs of alteration. As mentioned above, the pyroxenes are clearly altered to albite and chlorite. They are enriched in incompatible elements and Cr. Further, the pyroxenes are clearly being replaced by PGE-bearing sulfide minerals (see also Fig.14).

II. Remobilization Origin of PGE's

Although the remobilization hypothesis begs the question: Remobilized from where?, significant isotopic and textural evidence indicates that the PGE-bearing sulfide minerals have been remobilized (McCallum et al., 1999, Zientek and Ripley, 1990). It has been suggested that sulfur in the sulfide minerals within the Stillwater Complex is dominantly crustally derived. Certainly the emplacement of the Stillwater Complex involved considerable incorporation of crustal material into the melt. McCallum et al., (1999) show that the sulfide minerals contain a radiogenic Pb isotopic signature whereas the silicate minerals contain a primitive Pb isotopic signature. Therefore, the sulfide minerals are not in Pb isotopic equilibrium with the coexisting plagioclase that crystallized from the parental Stillwater magmas. Moreover, the textural evidence that the sulfide grains contain inclusions of hydrous minerals is similar to the textural evidence found in this study. This strongly suggests sulfide recrystallization after formation of the hydrous minerals. I conclude that the sulfide minerals are partly or totally precipitated or recrystallized by hydrothermal fluids after emplacement of the Stillwater Complex.

IV. Interpretation

Mineralogical and textural evidence presented here suggest three main events for the formation of the Picket Pin PGE deposit. These three events in chronological order these are: 1) the formation of the large, framework plagioclase grains, 2) crystallization of the intercumulate pyroxenes and plagioclase grains, 3) infiltration of hydrothermal fluids, alteration, and subsequent precipitation of the PGE-bearing sulfide minerals.

Origin of the large, framework plagioclase

The coarse grain size of the plagioclase suggests one or more conditions: 1) slow cooling, 2) the presence of volatile to slow nucleation, 3) an increase in pressure, and 4) a mixing of a more primitive melt which may result in reversely zoned adcumulate growth to the plagioclase grains. Slow cooling may have significant effect on the grain size. Considering the location of An II, roughly interpreted as located in the middle of the complex, heat loss would be at a minimum. The melt would cross the solidus curve at a very slow rate. Further, the melt would spend extended time in the melt+crystals field which may slow crystallization. The expected compositional zoning pattern may be broad and diffuse, which is a commonly observed feature of these grains. This assumes that no other melt was being injected above the position of An II to increase the pressure. Combining slow cooling and a gradual increase in pressure would increase the residence time within the melt+crystals field and further slow crystallization. If the overlying pressure increased drastically, such as by thrusting, any grain that had formed could be partially or totally resorbed into the melt. The zoning pattern would be expected to show single or multiple resorption textures within a single grain. Excluding the prominent resorption textures on the grain boundaries, unusual textures do exist within the grains and may record such an event. These large, framework plagioclase grains make up approximately 50 percent of the rocks throughout An II.

Alternatively, resorption textures and reverse zoning in the large plagioclase grains that may indicate a mixing and mingling with a more primitive melt. Microprobe evidence presented in the present study suggests that the reversely zoned rims of the large plagioclase compositionally match the composition of the small, intercumulate plagioclase grain cores. Both the large and small plagioclase grains have distinct compositional trends implying they were derived from two separate melts. The large plagioclase grains may have formed

elsewhere in the chamber (along the walls or the roof) and may have been emplaced along the floor of the chamber by a physical mechanism. The Stillwater Complex exhibits numerous sedimentary features suggestive of turbulent flows, cross-bedding, slump structures, and cut and fill structures. The large plagioclase grains of AN II may have been deposited in a fashion similar to that proposed by Haskin and Salpas (1992) and Loforski and Arcturus (1990). With this turbulent emplacement of the large plagioclase grains, the intercumulate melt was displaced by a more-primitive melt. The obvious lineation of the overlying medium-grained anorthosite may have formed from a similar process.

Crystallization of the intercumulate minerals

The intercumulate plagioclase grains exhibit a compositional trend from more-primitive in the high-pyroxene group (15-20%) to strongly fractionated in the low-pyroxene group (0-5%). This trend may suggest that the intercumulate melt fractionated outward from the high-pyroxene zones toward the low-pyroxene and sulfide-bearing zones. The pyroxene compositional trend further supports this fractionation trend. In the most-altered zones the pyroxene is altered to Fe-rich chlorite and albite. The high-Fe content of the chlorite may sugget that the original pyroxene was extremely enriched in Fe. Such an enrichment would reflect a compositional change within the melt. If this were strictly due to compositional change in the melt, then this would support the hypothesis that the melt was trapped within the plagioclase framework and did not communicate with the main body of melt within the Stillwater Complex chamber.

Perhaps more likely, this Fe-enrichment may be caused by Fe-rich hydrothermal fluids that altered the clinopyroxenes. Further support of this hypothesis is the high whole-rock Fe content within the clinozoisite patches (up to 2 wt % Fe), which are hydroxide

minerals of unquestionably hydrothermal origin. Clinozoisite contains very little Fe, therefore the hydrothermal fluid that formed the clinozoisite was significantly enriched in Fe (2 wt % Fe for the clinozoisite samples compared to a background value of > 1 wt % Fe). This data have strong implications on the origin of the sulfide-bearing horizons. The data support either a remobilization of the sulfide minerals or that the sulfide minerals are strictly hydrothermal. This data in conjunction with the microprobe data for the plagioclase grains suggest that the sulfide-bearing zones were the last to crystallize and were enriched in volatiles. Alternatively, a hydrothermal fluid influx would enrich the earlier sulfide-bearing zones with Na, K, incompatible trace elements, and volatiles. Microprobe data on the apparently magmatic intercumulate plagioclase grains (An >74) within the sulfide-bearing zones supports that at least some of the incompatible-element enrichment may have been derived from the melt as opposed to complete enrichment by a hydrothermal fluid.

Primary and Secondary Sulfide Emplacement

No direct evidence of primary (magmatic) sulfide emplacement exists in the study area. The PGE-bearing sulfide minerals are associated with the incompatible major and trace elements, and occur in the most-fractionated area of the melt, i.e., both K and Na increase significantly local to sulfide mineralization. This suggests that if the sulfide minerals were magmatic (primary), they remained fluid or mobile and did not precipitate until the melt was almost completely crystallized. This appears to conflict with the hypothesis that an injection of a more primitive melt triggered sulfide saturation which would place the sulfide minerals and PGE's in a zone of more primitive composition. Alternatively, the incompatible elements may have been transported by a later hydrothermal event. In contrast, the

intercumulate plagioclase grain cores from the 0-5% pyroxene group are relatively sodic suggesting they precipitated from a fractionated melt. This relationship between the sulfide minerals, PGEs and incompatible elements supports a late-stage fluid or hydrothermal hypothesis. Alternatively, the PGE-bearing sulfide minerals may have been remobilized hydrothermally to be reprecipitated in their present location.

The lack of a good spatial correlation between the PGEs and the sulfide phases supports the hypothesis that the PGEs may have migrated in a hydrothermal event. Thus, the sulfide minerals and the PGEs may represent two different events. If the fluids responsible for the sulfide phases migrated with the PGEs, then better correlations between these elements would be expected. The lack of correlations also argues against the aspect of the magmatic emplacement hypothesis that proposes that the PGEs were scavenged by sulfide droplets migrating through the melt.

V. Proposed Model

New data collected for the present study leads to the following interpretations of the timing of mineralization and ore-forming conditions of the Picket Pin deposit (Fig. 42). Sulfide mineralization in it's present form appears to have been post-magmatic as suggested by the pyroxene alteration halo. Mineralization preferentially occurred where the pyroxene content was below 5 percent and where the large- to small-plagioclase grain size ratio was greatest and more coarsely grained. This may be attributed to more numerous grain-to-grain contacts creating greater surface area for alteration-fluid contact. Grains of apatite and baddeleyite, and the oikocrystic nature of the intercumulate mafic minerals may suggest volatiles including H_2O were an important part of sulfide formation. The relationship between Pt, Pd and pyroxene mode confirm the preference of the PGEs to occur within the

pyroxene-poor regions of AN II. Therefore, the PGEs are also associated with the incompatible major and trace elements.

As mentioned above, this evidence is in contrast to the magmatic model which should place the sulfide minerals and PGEs in a zone of more primitive composition.

Sulfide mineralization is also accompanied by chlorite, zoisite, clinozoisite, and epidote, which can be used to constrain the temperature and oxidation state of the ore-bearing fluid. The intimate relationship between clinozoisite and the sulfide minerals may suggest a precipitation temperature for the sulfide minerals between 500-550°C using the quartz-clinozoisite system of Holloway (1964). The relationship of clinozoisite with the sulfide minerals, and epidote with the oxides, suggests precipitation of the PGE-sulfide minerals requires a change in oxidation state. It is likely that the PGEs, Fe, and Cu migrated in an oxidized hydrothermal fluid. This interpretation is supported by the experimental results of Sassani and Shock (1990). The lack of a clear spatial association between the PGEs and the sulfide phases supports the hypothesis that the PGEs migrated in a hydrothermal event. When this fluid came into contact with a primary sulfide horizon, the fluid became reduced and precipitated the PGE-bearing sulfide minerals. This is further supported by the close relationship between PGE-sulfide minerals and chalcopyrite, which occur texturally on grain boundaries of pyrrhotite and as isolated grains within the alteration mineralogy.

Information presented here suggests that the PGEs can be transported in a oxidized saline hydrothermal fluid with a temperature range of 500-550°C. They precipitated by reduction on coming into contact with the primary sulfide minerals.
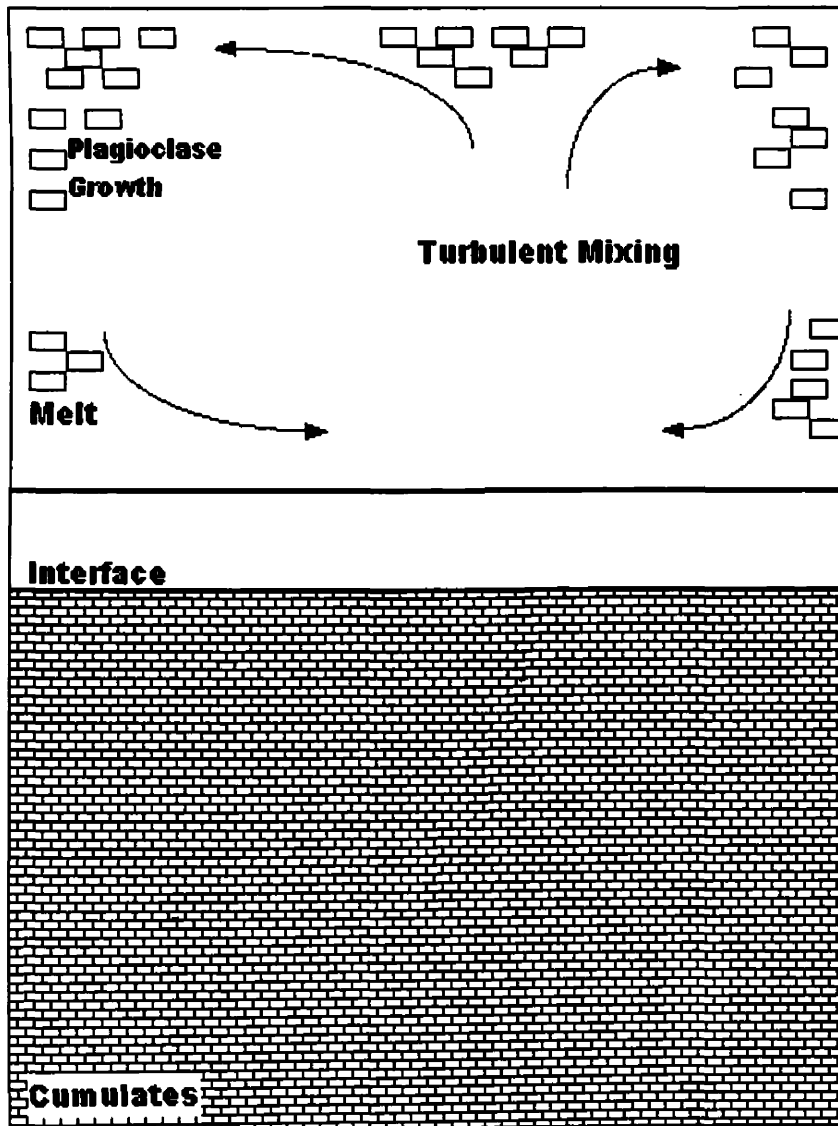
Figure 42. Proposed model. **Part 1.** Accumulation of plagioclase grains on chamber sides and roof.
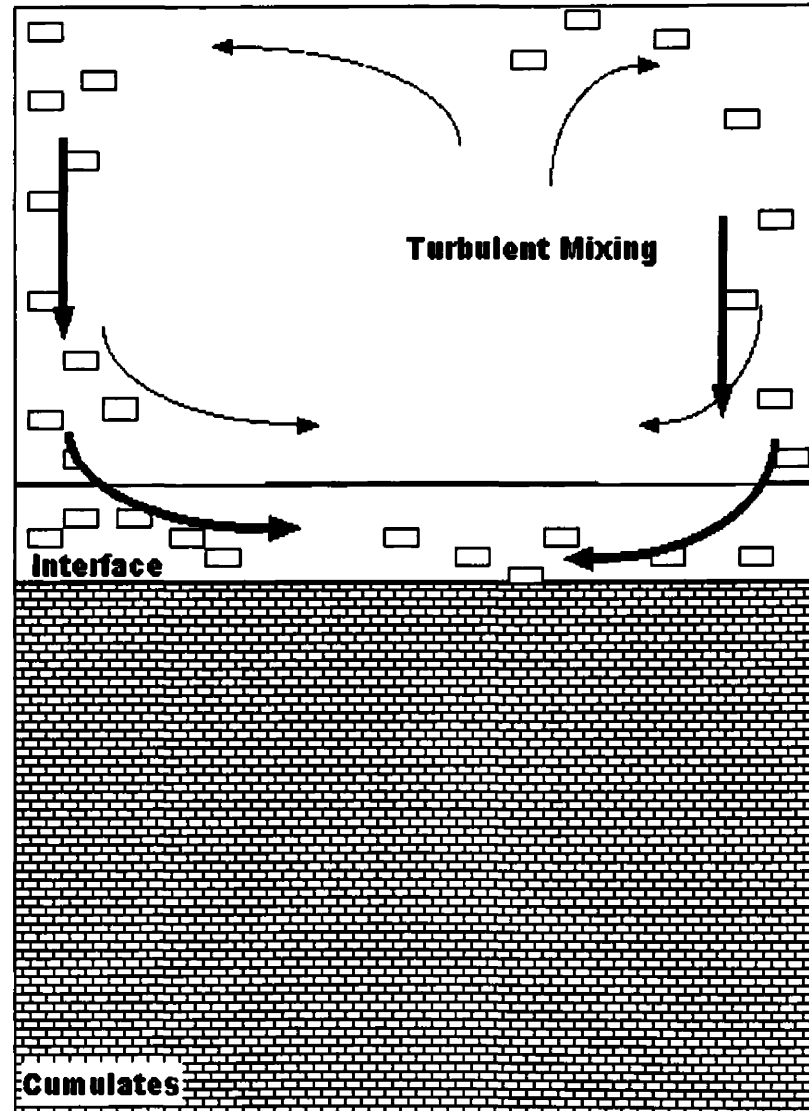
Part 2. Physical emplacement of plagioclase grains (Turbitity Flow?).

Turbulent Mixing

Melt

Interface

Trapped Melt
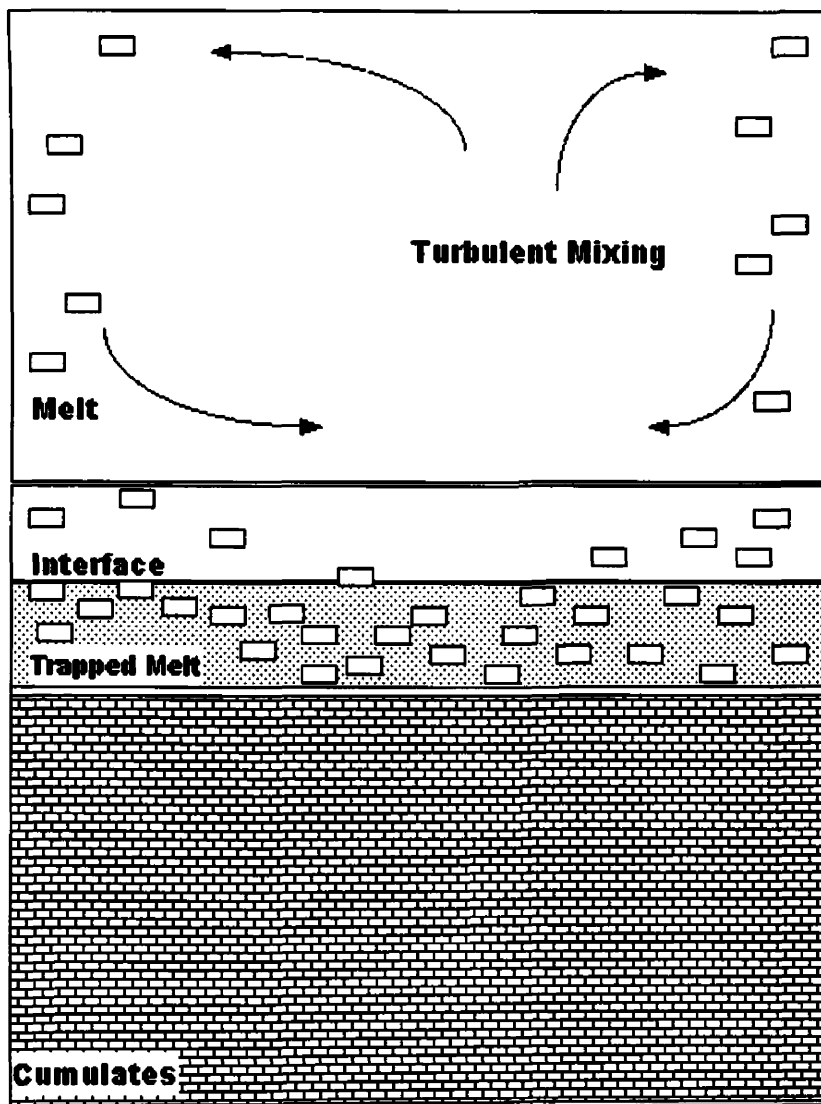
Cumulates

Part 3. Physical emplacement of plagioclase traps a more-primitive melt in the intercumulate spaces.
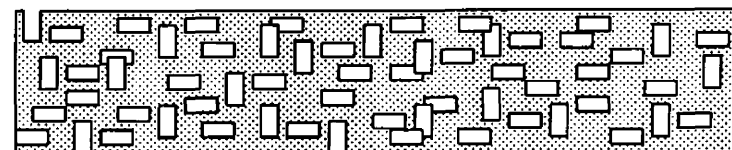
A. Large, 'Framework' plagioclase (An 78) mixing with a more primative trapped melt (An ~84).
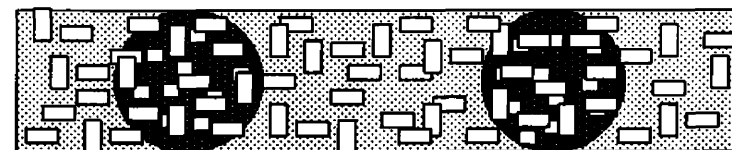
B. Crystallization of intercumulate olivine (Mg# 70) + plagioclase (An ~83). Adcumulate growth on 'Framework' plagioclase creating reversely zoned grains.

Migration of incompatible elements
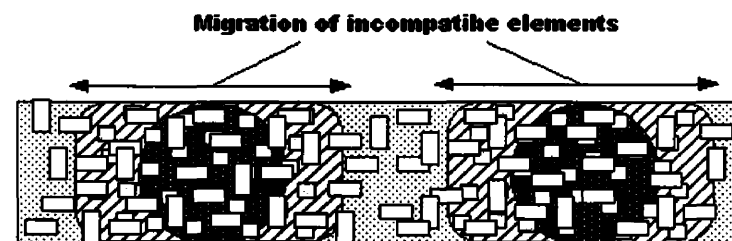
C. Trapped intercumulate melt moves into the bronzite + plagioclase field. The bronzite display a modest Mg enrichment (Mg#75), whereas the An content of the plagioclase decreases (An ~80). 'Framework' plagioclase grains continue to be reversely zoned.

Part 3A-G. Crystallization sequence of trapped intercumulate melt (see above). Cumulate plagioclase no longer in equilibrium, resulting in resorption and reverse-zoned adcumulate growth. Release of volatiles from trapped melt and resorbed plagioclase.

Migration of incompatible elements
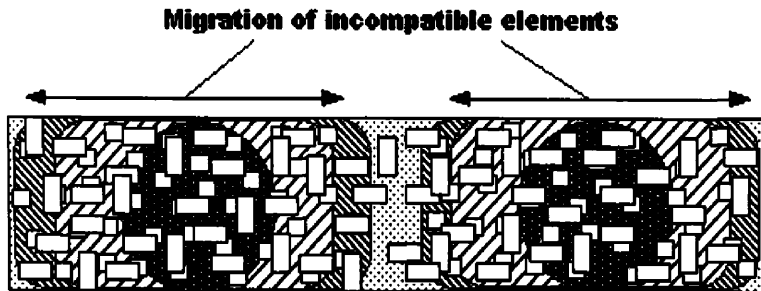
D. Intercumulate melt moves into the augite + plagioclase field. The composition of the augite grains is masked by later Fe-rich alteration. The intercumulate plagioclase grains have a composition of An 76, while the 'Framework' plagioclase grains continue to be resorbed.

Concentration of the incompatible elements
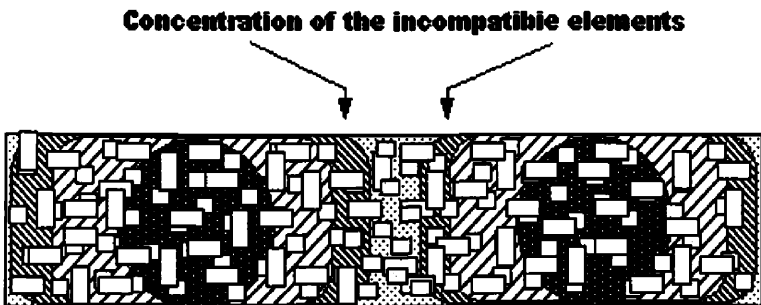
E. The remainder of the intercumulate melt moves into the plagioclase + augite field. The intercumulate plagioclase grains have a composition of An 75, and are enriched in the incompatible elements: Na, K, P, Cr, and H_2O.
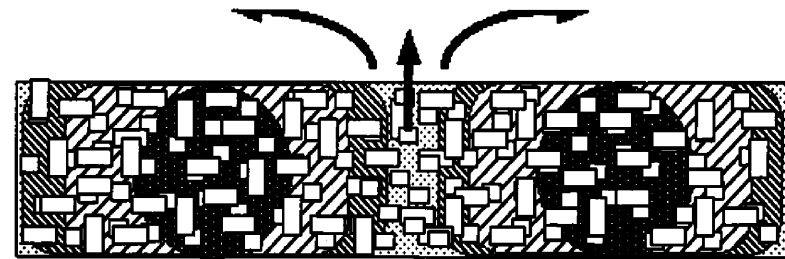
F.

Post-crystallization hydrothermal fluid enriched in Na, Cl, P, Fe, Cu, PGEs, and H_2O migrates through region with the least amount of intercumulate pyroxene (0-5% group).

Pyroxene Group:

| 15-20% | 10-15% | 5-10% | 0-5% | 5-10% | 10-15% | 15-20% |

Mg ◄──► Fe

High An content | **Concentration of incompatable element**
Resorbed Plagioclase | **Low An content**
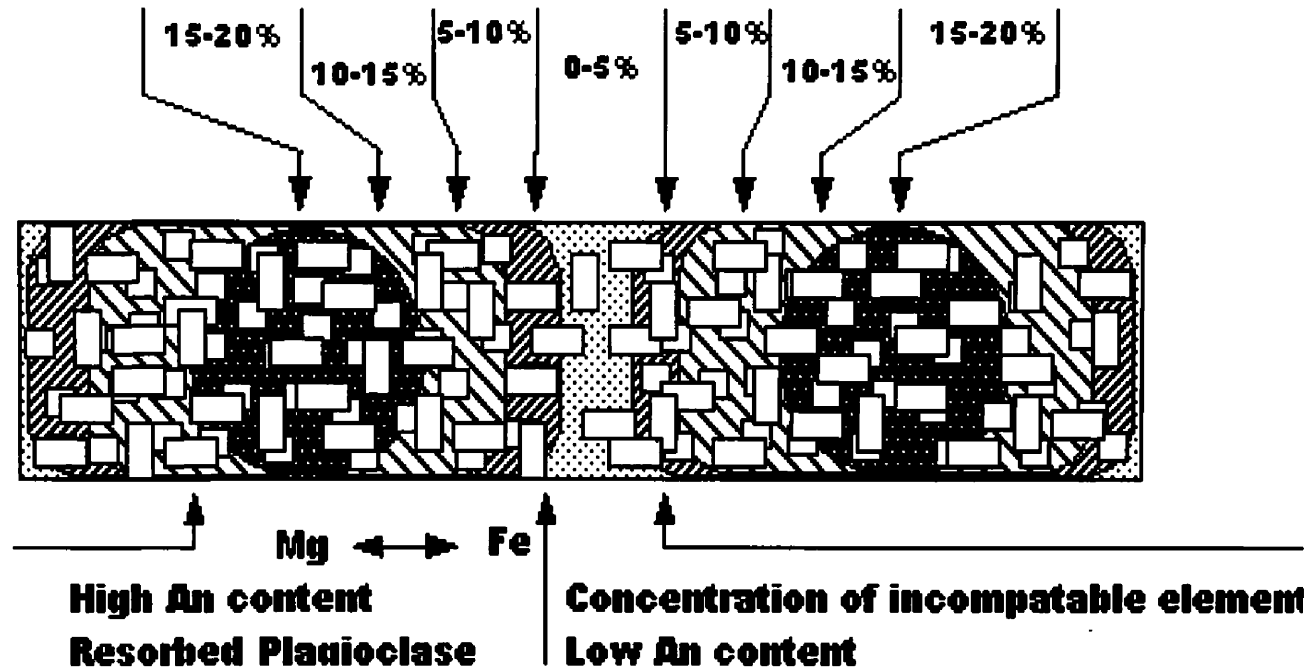
Proposed origin of variable pyroxene content (pyroxene groups).
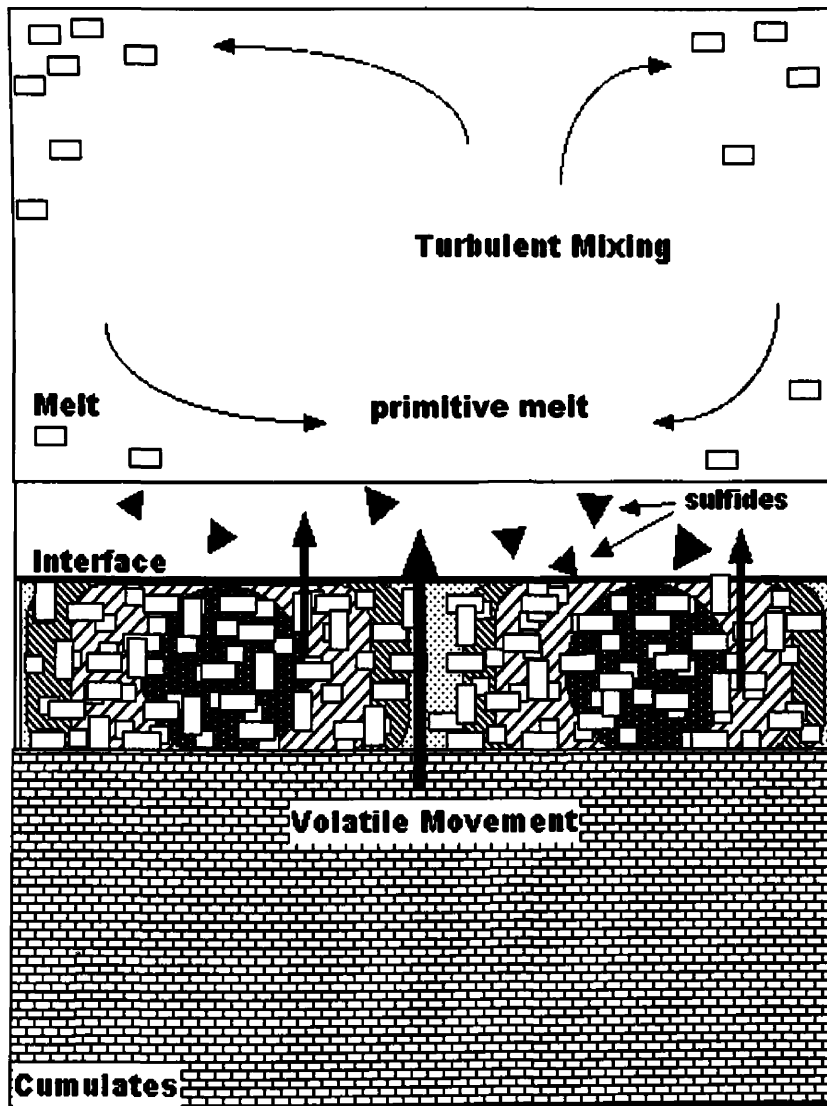
Part 4. Volatiles migrate upwards and react with primitive melt resulting in sulfur saturation, and subsequent precipitation of pyrrhotite and pentlandite.
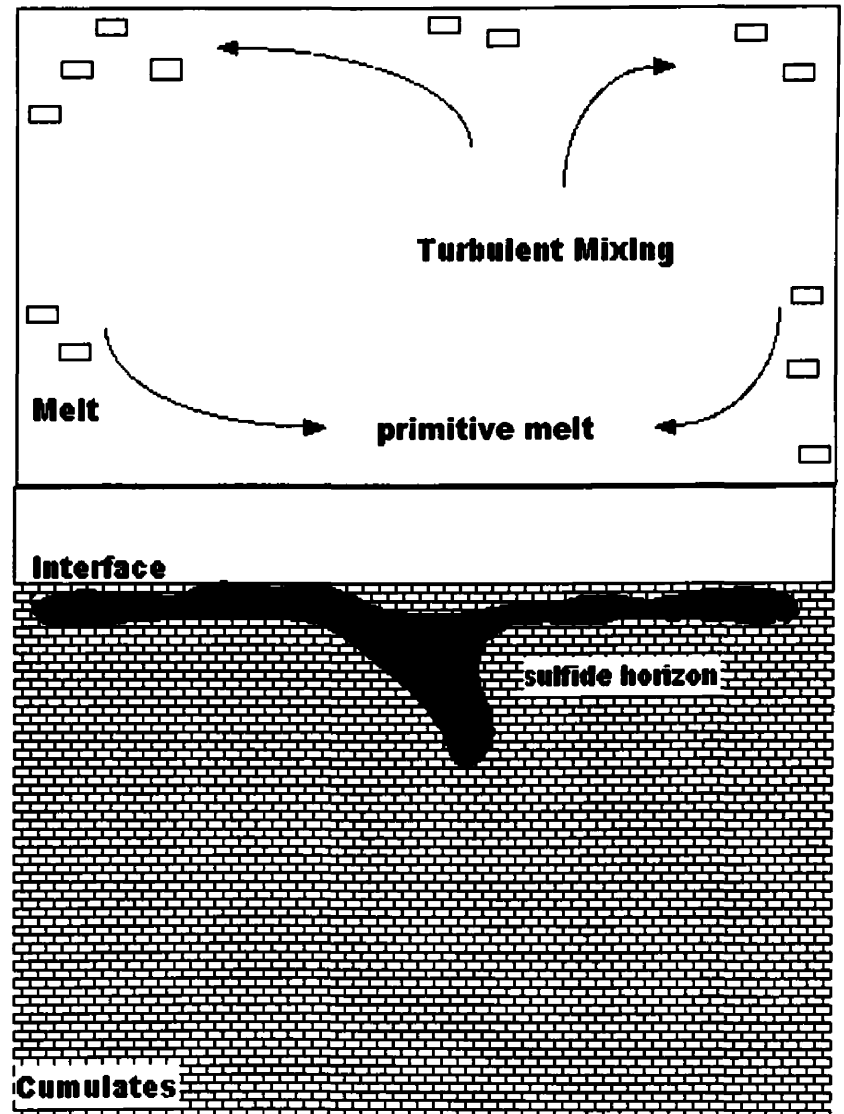
Part 5. Formation of sulfide horizon. Sulfides may sink into lower cumulates to seek neutral density.
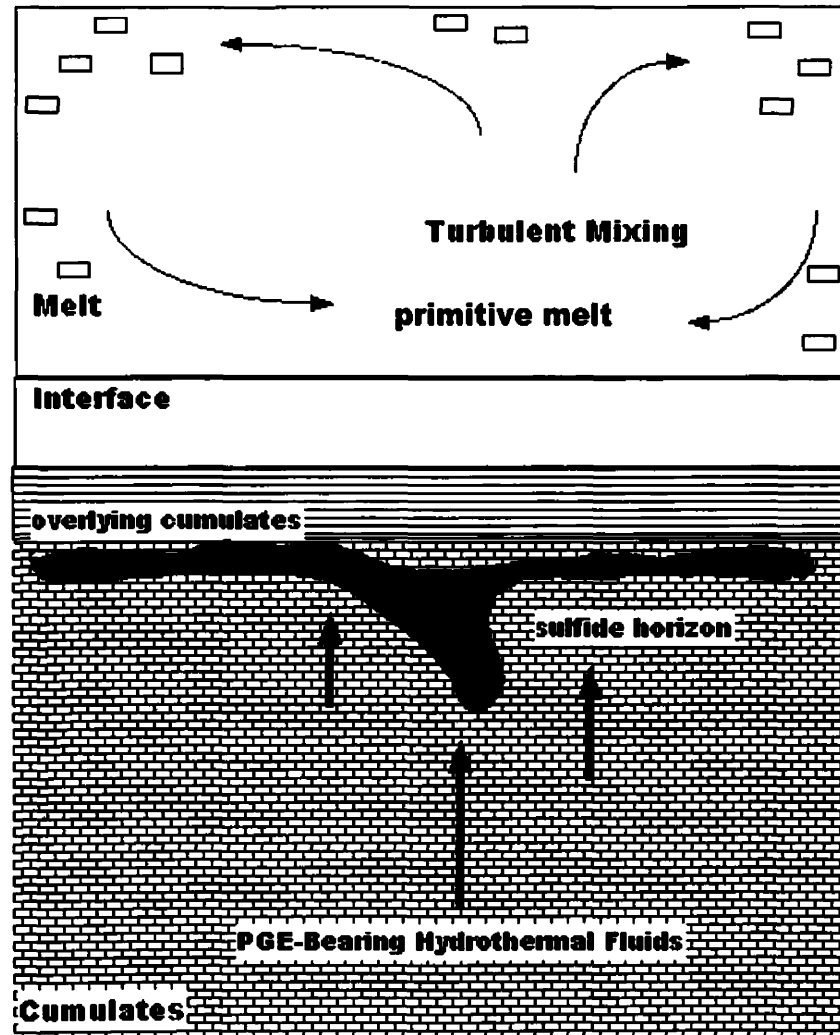
Part 6. Post-crystallization migration of oxidized hydrothermal fluids. These fluids scavenge and transport Au, Ag, and PGEs. The PGE's were then deposited and concentrated when the fluids encountered the reduced environment of the sulfide horizon.

REFERENCES

Alvarez, L.W., Alvarez, W., Asaro, F., Michel, H.W., 1980. Extraterrestrial cause for the Cretateous-Tertiary extinction. Science, 208: 1095.

Ballhaus, C., Stumpfl, E.F., 1986. Fluid inclusions in Merensky and bastard reefs, Western Bushveld complex. Economic Geology, 4th international platinum symposium.

Ballhaus, C., Stumpfl, E.F.,1985. Occurrence and petrological significance of graphite in the Upper Critical Zone, western Bushveld Complex, South Africa. Earth and Planetary Science Letters, 74: 58-68.

Barnes, S.J., Naldrett, A.J., 1985. Geochemistry of the J-M reef of the Stillwater Complex, Minneapolis Adit. Economic Geology, 80: 627-645.

Barrie, C.T., 1996, Magmatic Platinum-Group elements; in Geology of Canadian Mineral Deposit Types (Eckstrand, O.R., Sinclair, W.D., and Thorpe, R.I., eds); Geologic survey of Canada, no. 8, p. 605-614.

Blackerby, B.A., 1968, Convolute zoning of plagioclase phenocrysts in Miocene volcanics from the western Santa Monica Mountains, California, The American Mineralogist, v. 53, p. 954-962.

Boudreau, A.E., Stewart, M.A., and Spivack, A.J., 1997, Stable Cl isotopes and origin of high-Cl magmas of the Stillwater Complex, Montana, Geology, v. 9, p. 791-794.

Boudreau, A.E., and McCallum, S., 1992, Concentration of Platinum-group elements by magmatic fluids in layered intrusions, Economic Geology, v. 87, p. 1830-1848.

Boudreau, A.E., 1988, Investigations of the Stillwater Complex. IV. The role of volatiles in the petrogenesis of the JM Reef, Minneapolis Adit section, Canadian Mineralogist, v. 26, p. 193-208.

Boudreau, A.E., 1986, Platinum-Group metals in the Stillwater Complex, Montna, Ph.D. dissertation, University of Washington.

Boudreau, A.E., McCallum, I.S., 1985. Evidence for mineral reactions and metasomatism by silica-undersaturated Cl-rich fluids in the main pt-pd zone, Stillwater Complex, Montana. Canadian Mineralogist, 23: 296.

Boudreau, A.E., McCallum, I.S., 1985. Evidence for mineral reactions and metasomatism by silica-undersaturated Cl-rich fluids in the main pt-pd zone, Stillwater Complex, Montana. Canadian Mineralogist, 23: 296.

Boudreau, A.E., McCallum, I.S., 1985. The Picket Pin deposit, Stillwater Complex, Montana. Canadian Mineralogist, 23: 295.

Boudreau, A.E., and McCallum, S., 1985, Features of the Picket Pin Pt-Pd deposit: The Stillwater Complex, Montana: Geology and Guide (G.K. Czamanske and M. L. Zientek, eds.), Montana Bureau of Mines and Geology Special Publication 92, p. 346-357.

Bow, C., Wolfgram, D., Turner, A., Barnes, S., Evans, J., Zdepski, M., and Boudreau, A., 1982, Investigations of the Howland Reef of the Stillwater Complex, Minneapolis adit area: stratigraphy, structure, and mineralization, Economic Geology, v. 77, p. 1481-1492.

Cameron, E.N., 1982, The Upper Critical Zone of the eastern Bushveld Complex - precursor of the Merensky Reef, Economic Geology, v. 77, p. 1307-1327.

Cabri, L.J., 1981. PGEs: mineralogy, geology, recovery. CMI Special Volume 23, 267 pp.

Conn, K.H., 1979, The Johns-Manville platinum-palladium prospect, Stillwater Complex, Montana, U.S.A., Canadian Mineralogist, v. 17, p. 463-468.

Corkery, J.T., 2002, Mineralogy, petrography, and geochemistry of the Picet Pin PGE deposit, Stillwater Complex, Montana, Economic Geology annual meeting program with abstracts.

Corkery, J.T., 2001, Petrograpgy and Mineralogical Investigations of the Picket Pin PGE deposit, Stillwater Complex, Mt: Preliminary Results. Northwest Geology, v. 30, pp. 21-31.

Crocket, J.H., Fleet, M.E., and Stone, W.E., 1997, Implications of composition for experimental partitioning of platinum-group elements and gold between sulfide liquid and basalt melt: the significance of nickel content, Geochimica et Cosmochimica Acta, v. 61, p. 4139-4149.

Czamanske, G.K., and Loferski, P.J., 1996, Cryptic trace-element alteration of anorthosite, Stillwater Complex, Montana, Canadian Mineralogist, v. 34, p. 559-576.

Czamanske, G.K., Zientek, M.L., and Manning, C.E., 1991, Low-K granophyres of the Stillwater Complex, Montana, American Mineralogist, v. 76, p. 1646-1661.

Czamanske, G.K., and Scheidle, D.L., 1985, Characteristics of the Banded-series anorthosites, The Stillwater Complex, Montana: Geology and Guide (G.K. Czamanske and M. L. Zientek, eds.), Montana Bureau of Mines and Geology Special Publication 92, p. 334-346.

DePaolo, D.J., Wasserburg, G.J., 1979. Sm-Nd age of the Stillwater Complex and the mantle evolution curve for neodymium. Geochemica et Cosmochemica Acta, v. 43, pp. 999-1008.

Dressler, B.O., and Sharpton, V.L., 1998, Comment on 'Isotopic evidence for distinct crustal sources of the North and South Range ores, Sudbury Igneous Complex', Geochimica et Cosmochimica Acta, v. 62, p. 315-317.

Faure, G., 1986. Principles of isotope geology. Wiley and sons, New York, 587p.

Fleet, M.E., Crocket, J.H., Liu, M., and Stone, W.E., 1999, Laboratory partitioning of platinum-group elements and gold with application to magmatic sulfide-PGE deposits, Lithos, v. 47, p. 127-142.

Gammons, C.H., and Bloom, M.S., 1992, Experimental investigation of the hydrothermal geochemistry of platinum and palladium: I. solubility of platinum and palladium sulfide minerals in NaCl/H2SO4 solutions at 300C, Geochimica et Cosmochimica Acta, v. 56, p. 3881-3894.

Gammons, C.H., and Bloom, M.S., 1993, Experimental investigation of the hydrothermal geochemistry of platinum and palladium: II. The solubility of PtS and PdS in aqueous sulfide solutions at 300C, Geochimica et Cosmochimica Acta, v. 57, p. 2451-2467.

Geraghty, E.P., 1999. Drillhole test of Beartooth Uplift frontal fault; offset estimates and continuation at depth of the J-M Pd-Pt zone, Stillwater Complex, Montana. AAPG Bulletin, v. 83, #7, p. 1182-1183.

Graham, C., 1983, The epidote jigsaw, Nature, v. 305, p. 279.

Handler, M.R. and Bennett, V.C., 1999, Behaviour of Platinum-group elements in the subcontinental mantle of eastern Australia during variable metasomatism and melt depletion, Geochimica et Cosmochimica Acta, v. 63, p. 3597-3618.

Haskin, L.A., and Salpas, P.A., 1992, Genesis of compositional characteristics of Stillwater AN-I and AN II thick anorthosite units, Geochimica et Cosmochimica Acta, v. 56, p. 1187-1212.

Haughton, D.R., Roeder, P.L., and Skinner, B.J., 1974, Solubility of sulfur in mafic magmas, Economic Geology, v. 69, p. 451-467.

Higgins, M.D., 1998, Origin of anorthosite by textural coarsening: Quantitative measurements of a natural sequence of textural development, Journal of Petrology, v. 39, p. 1307-1323.

Helz, R.T., 1995, The Stillwater Complex, Montana: a subvolcanic magma chamber?, American Mineralogist, v. 80, p. 1343-1346.

Hess, H.H., 1960, Stillwater igneous complex, Montana – a quantitative mineralogical study: Geol. Soc. Am., Mem. 80.

Hodge, V.F., Stallard, M., Koide, M., Goldberg, E.D., 1985. Platinum and the platinum anomaly in the marine environment. Earth and Planetary Science Letters, 72: 158-162.

Holdaway, M.J., 1966, Hydrothermal stability of clinozoisite plus quartz, American Journal of Science, v.
.   264, p. 643-667.

Howland, A.L., Peoples, J.W., Sampson, E., 1936, The Stillwater igneous complex and associated occurrences of nickel and platinum metals: Mont. Bur. Mines and Geol. Misc. Contrib. 7.

Irvine, T.N., Keith, D.W., Todd, S.G., 1983. The J-M reef of the Stillwater Complex, Montana II. Economic Geology, 78: 1287-1334.

Irvine, T.N., 1980. Magmatic density currents and cumulus processes. American Journal of Science, v. 280-a, pp. 1-58.

Jenkins, D.M., Newton, R.C., and Goldsmith, J.R., 1983, Fe-free clinozoisite stability relative to zoisite, Nature, v. 304, p. 622-623.

Kucha, H., 1981. PGEs in the Zechstien Copper deposits, Poland. Economic Geology, 77:1587-1591.

Labotka, T. C., and Kath, R.L., 2001, petrogenesis of the contact-metamorphic rocks beneath the Stillwater Complex, Montana, GSA Bulletin, v. 113, no. 10, p. 1312-1323.

Lambert, D.D., Morgan, R.J., Walker, R.J., Shirley, S.B., Carlson, R.W., Zientek, M.L., Koski, M.S., 1989. Rhenium-osmium and samarium-neodymium isotopic systematics of the Stillwater Complex, Science, v. 244, pp. 1169-1174.

Lambert, D.D., Foster, J.G., Frick, L.R., Ripley, E.M., and Zientek, M.L., 1998, Geodynamics of magmatic Cu-Ni-PGE sulfide deposits: New insights from the Re-Os isotope system, Economic Geology, v. 93, p. 121-136

Lambert, D.D., Unruh, D.M., Simmons, E.C., 1985. Isotopic investigations of the Stillwater Complex: A review. Montana Bureau of Mines and Geology Special Publication #92, p. 46-53.

Leroy, L.W., 1985. Troctolite-Anorthosite Zone I and the JM Reef: Frog Pond Adit to Graham Creek area. Montana Bureau of Mines and Geology Special Publication 92, p.325-333.

Loferski, P.J., and Arculus, R.J., 1993, Multiphase inclusions in plagioclase from anorthosites in the Stillwater Complex, Montana: implications for the origin of the anorthosites, Contrib. Mineral Petrol, v. 114, p. 63-78.

Maier, W.D., and Barnes, S-J, 1999, PGE in the western Bushveld Complex, Journal of Petrology, v. 10, p. 1650-1671.

Manhes, G., Allegre, C. J., Dupre, B, Hamelin, B., 1980. Pb Isotope study of basic-ultrabasic layered complexes. Earth and Planetary Science Letters, v. 47, p. 370-382.

Markl, G., Frost, B.R., and Bucher, K., 1998, The origin of anorthosites and related rocks form the Lofoten Islands, Northern Norway: I. Field relations and estimations of intrinsic variables, Journal of Petrology, v. 39, p. 1425-1452.

Marshall, D.M., 1994, Geology and mineralization of the Picket Pin platinum-palladium horizon, Stillwater Complex, South-Central Montana, Northwest Geology, v. , p. 63-64.

Mathez, E.A., and Peach, C.L., 1989, The geochemistry of the Platinum-group elements in mafic and ultramafic rocks, (Naldrett, A.J. ed.) Economic Geology Special Publication: Magmatic Ore Deposits, p. 33-41.

McBirney, A.R., and Nicolas, A., 1997, The Skaergaard Layered Series. Part II. Magmatic flow and dynamic layering, Journal of Petrology, v. 38, p. 569-580.

McCallum I.S., Thurber, M.W., O'Brian, H.E., Nelson, B.K., 1999. Lead isotopes in sulfides from the Stillwater Complex, Montana, Contrib. Mineral Petrol, v. 137, pp. 206-219.

McCallum, I.S., Raedeke, L.D., and Mathez, E.A., 1980, Investigations of the Stillwater Complex: part I. Stratigraphy and structure of the Banded zone, American Journal of Science, v. 280-A, p. 59-87.

McKibben, M.A., Williams, A.E., and Hall, G.E., 1990, Solubility and transport of Platinum-group elements and Au in saline hydrothermal fluids: constraints from geothermal brine data, Economic Geology, v. 85, p. 1926-1934.

Meurer, W.P., Willmore, C.C., and Boudreau, A.E., 1999, Metal redistributionduring fluid exsolution and migration in the Middle Banded Series of the Stillwater Complex, Montana, Lithos, v. 47, p. 143-156.

Meurer W.P. and Boudreau, A.E., 1998, Compaction of igneous cumulates Part I: Geochemical consequences for cumulates and liquid fractionation trends, Journal of Geology, v. 106, p. 281-292.

Meurer W.P. and Boudreau, A.E., 1998, Compaction of igneous cumulates Part II: Compaction and the development of igneous foliations, Journal of Geology, v. 106, p. 293-304.

Moody, J.B., Jenkins, J.E., and Meyer, D., 1985, An experimental investigation of the albitization of plagioclase, Canadian Mineralogist, v. 23, p. 583-596.

Mountain, B.W., and Wood, S.A., 1988, Chemical controls on the solubility, transport, and deposition od platinum and palladium in hydrothermal solutions: A thermodynamic approach, Economic Geology, v. 83. p. 492-510.

Naldrett, A.J., 1989, Sulfide melts- Crystallization temperatures, solubilities in silicate melts, and Fe, Ni, and Cu partitioning between basaltic magmas and olivine, (Naldrett, A.J. ed.) Economic Geology Special Publication: Magmatic Ore Deposits, p. 5-19.

Naldrett, A.J., 1969, A portion of the system Fe-S-O between 900 and 1080 C and its applications to sulfide ore magmas, Journal of Petrology, v. 10, p. 171-201.

Nunes, P.D.,1981. The age of the Stillwater Complex-a comparison of U-Pb zircon and Sm-Nd isochron systematics. Geochemica et Cosmochemica Acta, v. 45, pp. 1961-1963.

Nunes,P.D., Tilton , G.R.,1971. U-Pb ages of minerals from the Stillwater Complex and associated rocks, Montana, GSA Bulletin, v. 82, pp. 2231-2250.

Nyman, M.W., Sheets, R.W., and Bodnar, R.J., 1990, Fluid-inclusion evidence for the physical and chemical conditions associated with intermediate-temperature PGE mineralization at the New Rambler deposit, Southeastern Wyoming, Canadian Mineralogist, v. 28, p. 629-638.

Page, N.J. and Moring, B.C., 1990, Petrology of the noritic and gabbronoritic rocks below the JM Reef in the Mountain View area, Stillwater Complex, Montana, USGS Open File report, Bulletin no. 1674.

Page, N.J., Prichard, H.M., 1985. Platinum group minerals. Metallogeny of Basic and ultrabasic rocks, 375-469.

Page, N.J., 1977. Stillwater Complex, Montana: Rock successions, metamorphism and structure of the complex and adjacent rocks. U.S.G.S. Professional paper, 999: 79.

Pass, K., 1993, Isotopic investigations of the Stillwater Complex, Masters Thesis, Auburn University, Auburn, Alabama

Poli, S., and Schmidt, M.W., 1998, The high-pressure stability of zoisite and phase relationships of zoisite-bearing assenblages, Contrib Mineral Petrol, v. 130, p. 162-175.

Premo, W.R., Helz, R.T., Zientek, M.L., Langston, R.B.,1990. U-Pb and Sm-Nd ages for the Stillwater Complex and its associated sills and dikes, Beartooth Mountains, Montana: Identification of a parental magma? Geology, v. 18, pp. 1065-1068.

Raedeke, L.D., McCallum, I.S., 1984. Investigations of the Stillwater Complex: Part II. Petrology and petrogenesis of the Ultramafic series. Journal of Petrology, v. 25, p. 395-420.

Raedeke, L.D., McCallum, I.S., 1980. A comparison of fractionation trends in the lunar crust and the Stillwater Complex. Proc. Conf. Lunar Highlands Crust., Pergamon, New York: pp. 133-153.

Rehkamper, M., Halliday, A.N., Alt, J., Fitton, J.G., Zipfel, J. and Takazawa, E., 1999, Non-chondritic platinum-group element ratios in ocean mantle lithosphere: petrogenetic signature of melt percolation?, Eart and Planetary Science Letters, v. 172, p. 65-81.

Sassani, D.C., and Shock, E.L., 1998, Solubility and transport of platinum-group elements in supercritical fluids: Summary and estimates of thermodynamic properties for ruthenium, rhodium, palladium, and platinumsolids, aqueous ions, and complexes to 1000C and 5 kbar, Geochimica et Cosmochimica Acta, v. 62, p. 2643-2671.

Sassani, D.C., and Shock, E.L., 1990, Speciation and solubility of palladium in aqueous magmatic-hydrothermal solutions, Geology, v.10, p. 925-928.

Schmidt, G., Palme, H. Kratz, K.L., and Kurat, G., 2000, Are highly siderophile elements (PGE, Re, and Au) frationated in the upper mantle of the Earth? New results on peridotites from Zabargad, Chemical Geology, v. 163, p. 167-188.

Schoenberg, R., Kruger, F.J., Nagler, T.F., Meisel, T., and Kramers, J., 1999, PGE enrichment in chromitite layers and the Merensky Reef of the western Bushveld Complex: a Re-Os and Rb-Sr isotope study, Earth and Planetary Science Letters, v. 172, p. 49-64.

Seitz, H-M, and Keays, R.R., 1997, Platinum-group element segregation and mineralization in a noritic ring complex formed from Proterozoic siliceous high-magnesium basalt magmas in the Vestfold Hills, Antarctica, Journal of Petrology, v. 38, p. 703-725.

Sharpe, M.R., 1982, Noble metals in the marginal rocks od the Bushveld Complex, Economic Geology, v. 77, p. 1286-1295.

Simmons, E.C., Lambert, D.D., 1982. Magma evolution in the Stillwater Complex, Montana. Montana Bureau of Mines and Geology Special Publication # 84, p. 91-106.

Stumpfl, E.F., 1985. Distribution, transport and concentration of platinum group elements. Metallogeny of Basic and ultrabasic rocks, 379-394.

Talkington, R.W., and Lipin, B.R., 1986, Platinum-group minerals in chromite seams of the Stillwater Complex, Montana, Economic Geology, v. 81, p. 1179-1186.

Todd, S.G., Keith, D.W., Le Roy, L.W., Schissel, D.J., Mann, E.L., and Irvine, T.N., 1982, The JM platinum-palladium Reef of the Stillwater Complex, Montana: I. Stratigraphy and petrology, Economic Geology, v. 77, p. 1454-1480.

Vance, J.A., 1964, Zoning in igneous plagioclase: patchy zoning, American Journal of Science, v. 270, p. 746-760.

Vance, J.A., 1962, Zoning in igneous plagioclase: normal and oscillatory zoning, American Journal of Science, v. 260, p. 746-760.

Vaniman, D.T., Labotka, T.C., Papike, J.J., 1980, Contact-metamorphic effects of the Stillwater Complex, Montana: Eos, v. 60, p.422.

Volborth, A., Tarkian, M, Stumpfl, E.F., and Housley, R.M., 1986, A survey of the Pt-Pd mineralization along the 35 km strike of the JM Reef, Stillwater Complex, Montana, Canadian Mineralogist, v. 24, p. 329-346.

Watkinson, D.H. and Melling, D.R., 1992, Hydrothermal origin of Platinum-Group Mineralization in low-temperature copper sulfide-rich assemeblages, Salt Chuck Intrusion, Alaska, Economic Geology, v. 87, p. 175-184.

Watkinson, D.H., and Dunning, G., 1979, Geology and platinum-group mineralization, Lac des Iles, Northwest Ontario, Canadian Mineralogist, v. 17, p. 453-462.

Wood, S.A, Mountain, B.W., and Fenlon, B.J., 1989, Thermodynamic constraints on the solubility of platinum and palladium in hydrothermal solutions: reassassment of hydroxide, bisulfide, and ammonia complexing, Economic Geology, v. 84, p. 2020-2028.

Zientek, M.L. 1993, Mineral resource appraisal for locatable minerals: the Stillwater Complex: U.S. Geol. Surv., Open-File Rep. 93-207, F1-F83.

Zientek, M.L., Czamanske, G.K., Irvine, T.N., 1985. Stratigraphy and nomenclature of the Stillwater Complex, Montana Bureau of Mines and Geology Special Publication #92, p. 21-32.

Zientek, M.L., 1983. Petrogenesis of the Basal zone of the Stillwater Complex, Montana. Ph.D. Thesis, Stanford University, Stanford, California: 246 pp.

Zoller, W.H., Parrington, J.R., 1983. Iridium enrichment in airborne particles from Kilauea volcano. Science, 222: 1118-1121.

Appendix I
Whole-rock Geochemisrty

Pyroxene %	TiO2 in percent	Al2O3	Fe2O3	MnO	MgO	CaO	Na2O	K2O
0-5%	0.1	25.25	3.47	0.018	0.54	9.56	2.9	0.182
0-5%	0.1	22.92	4.17	0.018	0.42	8.72	2.55	0.121
0-5%	0.1	23.55	4.06	0.019	0.46	8.84	2.58	0.121
0-5%	0.1	28.5	2.41	0.026	0.96	12.02	3.18	0.121
0-5%	0.1	12.3	1.87	0.012	0.94	9	3.12	0.06
0-5%	0.1	18.33	2.57	0.02	1.44	6.16	2.06	0.121
0-5%	0.1	18.88	3.6	0.014	0.56	6.72	2.24	0.121
0-5%	0.1	19.4	3.12	0.026	0.76	9.4	2.3	0.182
0-5%	0.1	27.75	2.88	0.016	0.68	11.82	3.36	0.182
0-5%	0.1	16.45	3.42	0.022	0.8	13.52	1.87	0.182
0-5%	0.1	28.63	3.53	0.021	0.46	12.36	2.45	0.182
0-5%	0.3	20.5	2.95	0.012	0.62	15.28	1.03	0.121
0-5%	0.4	21.15	3	0.019	1.08	9.88	2.39	0.03
0-5%	0.3	19.25	2.72	0.05	0.68	9.08	2.21	0.212
0-5%	0.1	24.1	2.78	0.026	2.58	13.68	3.72	0.151
Average	**0.1467**	**21.8**	**3.103**	**0.021**	**0.865**	**10.4**	**2.531**	**0.139**
5-10%	0.1	26.63	3.41	0.082	3.42	11.68	3.15	0.121
5-10%	0.1	26.5	1.97	0.034	1.84	10.38	2.7	0.09
5-10%	0.1	27.75	3.05	0.04	1.64	12.1	3.93	0.181
5-10%	0.4	20.83	3.64	0.02	0.25	9.98	3.3	0.121
5-10%	0.1	28.88	3.75	0.04	1.27	12.42	2.48	0.091
5-10%	0.1	27.5	3.72	0.044	1.81	12.08	0.03	0.121
5-10%	0.1	27.25	2.84	0.03	1.24	10.52	2.54	0.152
5-10%	0.5	27.13	3.28	0.04	0.72	12.1	1.63	0.125
5-10%	0.1	27.75	3.5	0.09	1.96	11.66	3.57	0.212
5-10%	0.4	28.63	2.73	0.044	0.92	12.12	3.06	0.122
5-10%	0.1	31	2.77	0.032	0.98	12.84	3.36	0.09
5-10%	0.3	22.2	3.1	0.028	1.24	12.88	3.24	0.121
5-10%	0.1	31	3.05	0.044	0.34	11.85	2.9	0.181
Average	**0.1923**	**27.16**	**3.139**	**0.044**	**1.356**	**11.74**	**2.761**	**0.133**
10-15%	0.15	28.66	2.81	0.034	1.37	15.23	2.4	0.086
10-15%	0.135	28.21	2.92	0.039	1.56	15.28	2.35	0.091
10-15%	0.238	28.89	2.71	0.033	1.18	15.35	2.37	0.087
10-15%	0.23	27.7	3.28	0.042	1.86	15.41	2.27	0.074
10-15%	0.138	27.27	3.57	0.047	2.15	14.68	2.26	0.077
10-15%	0.133	26.67	3.87	0.057	2.71	14.69	2.12	0.061
10-15%	0.155	28.75	2.74	0.04	1.28	14.87	2.48	0.111
10-15%	0.183	29.05	2.33	0.031	0.87	14.99	2.48	0.138
10-15%	0.13	27.28	3.43	0.049	2.46	15.04	2.17	0.073
Average	**0.1658**	**28.05**	**3.073**	**0.041**	**1.716**	**15.06**	**2.322**	**0.089**
15-20%	0.15	27.69	3.42	0.049	2.22	14.78	2.21	0.075
15-20%	0.155	26.33	3.86	0.056	2.74	15.05	2.11	0.079
15-20%	0.143	28.16	3.08	0.04	1.95	15.25	2.37	0.079
15-20%	0.133	26.09	3.73	0.059	2.96	14.98	2.12	0.064
Average	**0.1453**	**27.07**	**3.523**	**0.051**	**2.468**	**15.02**	**2.203**	**0.074**
Med. Grained An.	0.1	4.55	2.67	240	1.22	1.18	0.151	0.03
Med. Grained An.	0.1	19.05	1.4	240	1.62	7.2	2.03	0.121
Med. Grained An.	0.1	26.88	1.88	180	1.02	10.7	2.96	0.121
Med. Grained An.	0.1	28.5	3.85	200	1.02	9	2.18	0.09
Average	**0.1**	**19.75**	**2.45**	**215**	**1.22**	**7.02**	**1.83**	**0.091**
Clinozoisite	0.2	7.68	1.84	200	0.46	3.2	0.67	0.09
Clinozoisite	0.1	12.2	1.55	200	0.52	4.86	1.34	0.212
Average	**0.15**	**9.94**	**1.695**	**200**	**0.49**	**4.03**	**1.005**	**0.151**

Appendix I
Whole-rock Geochemistry

Pt	Pd	Au	Ag	Cu	Ni	Cr	Co	Sr	Ba	Sc	La
in ppb				in ppm							
2470	1840	240	1800	5160	2390	29	74	105	10	<1	<10
1095	1350	280	1800	5840	3320	17	106	91	10	<1	<10
1030	1350	310	2000	6050	3190	17	102	93	10	<1	<10
768	896	96	800	3060	1015	18	36	122	20	<1	<10
1664	960	128	1000	2200	1215	39	46	43	10	2	<10
1024	1024	192	1400	4080	1315	47	44	72	10	<1	<10
640	2176	160	1600	5180	1715	23	62	76	10	<1	<10
2560	1984	128	800	4150	1985	35	72	80	10	<1	<10
576	1600	160	800	3130	797	23	36	109	10	2	<10
384	1024	132	1000	4140	1680	24	62	63	10	<1	<10
1984	1020	210	2800	3160	1975	48	67	134	20	<1	<10
960	2304	192	1200	3480	1465	49	95	98	10	<1	<10
1216	1088	160	1200	663	718	41	56	87	20	<1	<10
576	448	220	100	1290	1715	58	52	71	20	<1	<10
1024	1088	192	600	5690	185	27	11	25	10	<1	<10
1198	**1343**	**186.67**	**1260**	**3818**	**1645**	**33**	**61.4**	**85**	**12.7**	**<1**	**<10**
64	64			56	313	26	42	122	30	<1	<10
171.5	440	1	200	1450	590	23	31	108	10	<10	<10
32	64	1	300	180	109	30	52	122	40	<1	<10
280	260	1	<200	4820	3250	68	86	152	30	<1	<10
75	64	1	<200	3070	1435	27	58	92	20	<1	<10
50	35	1	350	3060	1015	34	48	131	30	<1	<10
0.5	2	<1	200	2320	939	31	39	127	20	<1	<10
0.5	2	<1	200	923	721	45	45	124	30	<1	<10
3	1	<1	<200	191	49.7	31	27	124	10	<1	<10
2	1	<1	<200	539	1130	19	9	163	10	<1	<10
0.5	1	<1	200	80	29.3	31	10	133	30	<1	<10
54	50	<1	200	23.5	27	23	39	84	20	<1	<10
0.5	1	<1	200	328	2350	45	27	125	30	<1	<10
56.42	**75.77**	**1**	**231.25**	**1311**	**919.8**	**33**	**39**	**114**	**22.2**	**<1**	**<10**
0.5	<1	<1	<200	NA	10	8.34	9	159	42	7.43	
0.5	<1	<1	<200	NA	26	9.47	10.16	189	41	8.2	
<.5	<1	<1	<200	NA	18	7.75	8.08	199	43	6.78	
<.5	<1	<1	<200	NA	27	16.3	11.88	188	41	10.3	
<.5	<1	<1	<200	NA	26	8.93	14.38	198	41	8.86	
<.5	<1	<1	<200	NA	43	14.8	17.05	160	30	9.73	
<.5	<1	<1	<200	NA	19	3.96	8.32	184	52	5.3	
<.5	<1	<1	<200	NA	8	3.42	6.07	176	64	4.64	
<.5	<1	<1	<200	NA	47	18	14.63	163	36	10.1	
<.5	**<1**	**<1**	**<200**	**NA**	**24.89**	**10**	**11.1**	**180**	**43.3**	**7.9**	
<.5	<1	<1	<200	NA	34	13.7	13.66	181	36	7.53	
<.5	<1	<1	<200	NA	55	22.4	16.71	152	33	11.9	
<.5	<1	<1	<200	NA	24	12.6	11.28	209	47	8.16	
<.5	<1	<1	<200	NA	58	29.5	17.01	155	28	12.5	
<.5	**<1**	**<1**	**<200**	**NA**	**42.75**	**20**	**14.7**	**174**	**36**	**10**	
352	860	18	1000	704	87	48	3	10	10	10	
1	0.02	1	200	19	34	27	5	85	10	10	
4	4	18	200	964	517	31	17	112	10	10	
896	768	96	800	2000	960	60	23	97	10	10	
313.3	**408**	**33.25**	**550**	**922**	**399.5**	**42**	**12**	**76**	**10**	**10**	
320	320	41	200	490	237	44	8	32	10	10	
141.5	120	18	200	427	304	39	12	51	20	10	
230.8	**220**	**29.5**	**200**	**459**	**270.5**	**42**	**10**	**42**	**15**	**10**	

Microprobe Analyses

Line Numbers	SiO2 Oxide Percents	Al2O3 Oxide Percents	FeO Oxide Percents	Na2O Oxide Percents
STDS:	1	4	62	1
Un 4 808109 feldspar				
472	48.81	31.30	0.40	3.17
Un 5 8819lp				
473	49.95	32.83	0.37	3.03
474	49.41	33.66	0.39	2.48
475	54.84	32.80	0.43	4.79
476	48.77	34.03	0.56	2.21
477	48.42	34.24	0.37	2.25
478	47.65	27.57	2.02	4.91
479	48.32	33.40	0.48	2.16
480	49.67	33.12	0.40	2.73
Un 7 8819lp2				
481	48.44	33.91	0.49	2.33
482	47.78	32.96	0.40	2.23
483	48.06	32.70	0.37	2.63
484	48.58	32.29	0.34	2.78
485	48.13	32.53	0.44	2.50
486	47.98	32.42	0.48	2.40
487	48.63	31.83	0.46	2.78
488	49.02	31.90	0.36	2.89
489	48.48	31.96	0.46	2.84
490	47.69	32.56	0.51	2.43
Un 8 8819lp3				
491	49.61	33.42	0.37	2.55
492	48.77	33.83	6.59	2.27
493	49.89	33.43	0.40	2.74
494	48.84	34.04	0.43	2.19
495	48.97	33.80	0.52	2.26
496	104.77	0.22	0.09	0.03
497	49.07	33.68	0.39	2.40
498	48.13	32.95	0.45	2.47
499	48.31	32.47	0.44	2.68
Un 9 8819sp1				
500	48.71	32.46	0.26	2.73
501	49.35	32.02	0.36	3.09
502	49.04	31.93	0.37	2.97
503	48.90	31.98	0.40	2.92
504	53.79	33.09	0.32	4.25
Un 10 8819sp2				
505	49.44	32.88	0.38	3.08
506	48.94	32.92	0.39	2.77
507	49.14	33.58	0.39	2.46
508	49.39	33.54	0.43	2.60
509	49.63	33.70	0.36	2.40
Un 11 8819sp3				
510	81.07	4.49	2.95	2.11
511	49.74	32.11	0.43	3.03
512	48.93	32.56	0.39	3.05
513	49.19	32.72	0.44	2.87
Un 12 8819sprim				
514	42.87	35.56	2.11	0.00
Un 13 8819clno				
515	42.85	35.67	13.19	0.02
516	37.63	29.61	4.81	0.03
517	38.64	32.09	2.16	0.13
518	32.81	20.78	6.11	0.37
519	38.21	28.87	6.81	0.02

Un 14 8812lp1				
520	45.18	34.35	0.33	1.48
Un 15 8812lp1				
521	48.64	33.03	0.51	2.65
522	48.13	32.72	1.18	2.76
523	48.63	32.39	0.48	2.87
524	47.97	32.85	0.59	2.64
525	47.17	32.68	0.49	2.49
526	45.71	31.75	0.49	2.45
527	46.71	32.70	0.42	2.36
528	46.68	32.36	0.48	2.49
529	47.00	31.91	0.49	2.57
530	36.08	20.85	21.33	1.09
531	46.93	33.08	0.50	2.28
532	47.09	32.17	0.57	2.51
533	46.58	32.66	0.52	2.28
534	46.32	32.43	0.60	2.28
Un 16 8812lp2				
535	47.71	33.25	0.40	2.38
536	47.90	33.79	0.45	2.33
537	48.77	33.10	0.45	2.50
538	34.41	9.94	17.06	0.08
Un 17 8812lp2				
539	45.83	32.87	0.42	2.72
540	46.78	32.86	0.36	2.37
541	46.47	30.36	1.26	2.50
542	47.66	33.08	0.37	2.54
543	47.27	33.81	0.41	2.20
544	35.02	25.90	15.02	1.02
545	48.02	32.32	0.52	2.47
546	46.62	32.86	0.54	2.08
547	47.29	33.06	0.49	2.13
548	47.46	33.00	1.64	2.38
549	47.88	33.12	0.47	2.32
550	49.33	32.84	0.41	2.71
Un 18 8812lp3				
551	45.26	30.26	0.42	2.73
552	44.17	30.95	0.50	2.24
553	48.77	33.26	0.50	2.51
554	50.36	32.24	0.46	3.23
555	49.17	33.26	0.51	2.61
556	48.63	32.93	0.48	2.60
557	48.93	32.62	0.41	2.75
558	48.62	33.71	0.59	2.19
559	46.85	33.14	0.49	2.04
560	48.41	32.30	0.33	2.83
Un 19 8812sp1				
561	46.45	0.83	18.59	0.00
562	46.67	31.59	0.40	2.60
563	47.96	32.41	0.48	2.48
564	47.38	33.17	0.51	2.11
Un 20 8812sp2				
565	42.66	2.52	15.88	0.13
566	48.64	32.51	0.33	2.85
567	48.20	31.77	0.44	2.85
568	47.37	32.56	0.42	2.37
Un 21 8812sp3				
569	52.77	1.98	18.34	0.10
570	48.79	31.63	0.39	2.64
571	49.07	32.74	0.48	2.79
572	48.51	32.56	0.40	2.65
573	47.94	32.24	0.51	2.72
574	47.97	32.81	0.47	2.45
Un 22 8812sp4				
575	48.23	33.18	0.41	2.47

576	47.69	33.69	0.41	2.29
577	48.48	33.84	0.41	2.38
578	48.73	33.18	0.41	2.55
579	48.55	32.94	0.43	2.54
580	46.47	31.23	1.95	2.12
Un 28 8812plg				
627	48.82	30.02	0.30	0.94
Un 32 8812rimplg1				
646	45.62	34.31	0.46	1.71
Un 34 8812rimplg2				
647	47.02	32.22	0.39	2.68
Un 35 8812rimplg3				
648	46.32	32.39	0.46	2.57
Un 36 8812rimplg4				
649	46.91	34.55	0.53	1.84
Un 37 8812rimplg5				
650	48.12	34.01	0.33	2.18
Un 38 8812rimplg6				
651	28.94	17.24	20.82	0.41
Un 39 8812rimplg7				
652	46.89	33.44	0.53	2.27
Un 40 8812rimplg8				
653	47.60	33.16	0.38	2.53
Un 41 8812rimplg9				
654	47.92	32.86	0.35	2.58
Un 42 8812rimplg10				
655	46.57	31.87	0.44	2.68
Un 43 898lp1				
656	47.56	33.43	0.44	2.36
657	47.88	33.84	0.33	2.28
658	47.98	33.53	0.49	2.37
659	49.24	33.22	0.42	2.75
660	48.84	33.67	0.43	2.49
661	50.02	32.76	0.36	2.96
662	49.39	33.60	0.51	2.35
663	49.68	33.78	0.45	2.62
664	34.85	26.73	7.28	2.33
665	51.20	32.28	0.38	3.37
Un 44 898lp2				
666	48.49	32.07	0.52	2.85
667	47.95	32.16	0.41	2.76
668	48.12	32.68	0.46	2.57
669	49.02	29.76	4.32	3.05
670	51.96	21.72	0.08	5.58
671	48.21	32.46	0.41	2.63
Un 45 898lp2				
672	49.64	31.92	0.34	3.39
673	48.85	32.46	0.39	2.85
674	48.31	32.70	0.46	2.54
Un 46 898lp3				
675	48.48	33.09	0.41	2.58
676	47.22	33.37	0.33	2.08
677	48.16	30.26	0.65	3.71
678	45.84	31.32	7.13	1.71
679	49.58	33.12	0.78	4.16
680	48.54	32.03	0.52	2.94
681	63.12	24.19	0.22	9.65
682	67.66	21.82	0.06	10.43
683	49.67	31.67	0.53	2.85

684	48.20	32.55	0.48	2.60
685	51.65	30.99	1.18	3.54
686	49.80	32.00	0.30	3.14
687	47.64	32.89	0.48	2.32
688	48.50	32.72	0.68	2.68
689	48.14	33.08	0.44	2.59
690	48.57	32.70	0.40	2.77
691	48.73	32.22	0.24	3.03
692	47.37	32.56	0.39	2.50
693	48.69	32.65	0.42	2.76
694	48.74	32.44	0.31	2.98
Un 47 898lp3a				
695	59.58	23.92	0.04	7.48
696	47.93	32.80	0.46	2.45
697	47.46	32.78	0.48	2.44
698	48.30	32.96	1.57	0.85
699	48.16	31.53	0.49	3.08
Un 48 898lp4				
700	46.78	34.09	0.33	2.16
701	47.25	33.85	0.39	2.13
702	48.20	33.24	0.39	2.47
703	49.44	33.51	0.39	2.78
704	48.93	32.24	0.69	2.96
705	49.51	33.44	0.41	2.78
706	49.32	33.63	0.45	2.82
707	47.56	33.43	0.59	2.32
708	48.28	32.00	0.39	2.94
709	47.74	32.71	0.38	2.51
Un 49 898sp1				
710	101.30	0.45	0.24	0.02
711	102.08	0.00	0.00	0.00
712	68.76	20.26	0.21	11.53
Un 50 898sp2				
713	48.70	33.39	0.43	2.86
714	49.00	32.17	0.37	3.19
715	47.45	33.36	0.42	2.40
716	47.66	33.52	0.40	2.53
Un 51 898sp3				
717	61.95	28.51	0.25	9.13
718	47.98	33.60	0.48	2.29
719	48.39	33.08	0.47	2.64
720	49.87	32.68	0.35	3.11
Un 52 898sp4				
721	47.62	32.74	0.52	2.74
722	47.66	31.31	0.66	4.29
723	48.59	33.36	0.54	3.49
724	49.53	32.17	0.36	2.95
Un 53 898sp5				
725	48.53	33.36	0.47	2.51
726	48.04	32.80	0.35	2.89
727	47.68	32.88	0.41	2.62
728	48.80	32.58	0.32	2.88
Un 55 898rmplg1				
737	64.14	17.43	0.17	9.92
Un 56 898rmplg2				
738	66.44	20.75	0.06	10.35
Un 57 898rmplg3				
739	67.01	20.88	0.11	10.68
Un 58 898rmplg4				
740	38.61	31.62	3.44	0.00
Un 60 883lp1				
742	46.54	36.51	0.42	1.30
743	49.88	34.46	0.46	2.66

	CaO Oxide	K2O Oxide	Oxide	Si Formula
744	47.14	32.94	0.52	2.58
745	48.29	32.73	0.59	2.53
746	49.25	32.52	0.47	2.83
747	54.04	29.51	0.68	5.13
748	47.80	32.82	0.53	2.29
749	47.69	33.54	0.61	2.28
750	41.88	30.30	0.53	1.94
751	48.09	32.94	0.61	2.36
752	48.05	33.01	0.55	2.30
753	46.79	32.98	0.62	2.28
754	47.75	32.56	0.59	2.30
755	47.52	33.25	0.55	2.27
756	47.36	32.96	0.46	2.30
757	46.83	32.95	0.67	2.11
758	47.71	33.41	0.52	2.18
759	47.10	32.94	0.42	2.21
760	48.73	32.28	0.44	2.80
761	46.25	33.12	0.50	2.01
Un 61 883lp2				
762	45.90	31.51	0.39	2.71
763	47.66	34.12	0.58	2.02
764	49.51	33.07	0.50	2.72
765	47.14	35.65	0.77	1.55
766	47.95	33.97	0.48	2.08
767	48.64	34.33	0.55	2.23
768	47.87	33.74	0.56	2.11
769	47.87	34.00	0.57	2.12
770	47.65	33.12	0.44	2.62
771	45.42	34.31	0.40	1.54
Un 62 883lp3				
772	48.08	32.85	0.51	2.61
773	47.00	31.82	1.70	2.60
774	49.02	32.98	0.79	2.77
775	46.98	33.75	0.61	2.26
776	47.50	1.49	9.32	0.31
777	46.48	32.23	1.46	2.50
778	46.99	33.12	0.54	2.50
779	45.29	33.43	0.56	2.03
780	42.86	31.33	0.54	2.04
781	46.65	32.17	0.47	2.57
Un 63 883sp1				
782	46.76	32.06	0.62	2.78
783	45.42	33.06	0.49	2.23
784	45.66	32.88	0.43	2.32
785	45.67	32.92	0.52	2.15
786	46.28	32.30	0.51	2.50
Un 64 883sp2				
787	45.16	31.12	0.35	2.44
Un 65 883sp2				
788	45.21	32.68	0.48	2.25
789	44.65	32.23	0.48	2.19
790	44.71	32.37	0.61	2.17
791	42.81	34.12	0.47	1.28
Un 66 883sp3				
792	47.11	1.15	17.62	0.02
793	46.63	32.16	0.44	2.65
794	46.01	32.42	0.50	2.35
795	46.67	32.01	0.52	2.59
Un 67 883sp4				
796	48.38	33.06	0.39	2.64
797	49.48	34.22	0.69	2.65
798	47.40	33.48	0.48	2.54
799	47.88	33.36	0.50	2.36
800	46.90	33.26	0.85	2.20

CaO Oxide   K2O Oxide   Oxide   Si Formula

Percents	Percents 4	Percents 6	Totals		Atoms	
	14.20	0.11	98.01	472		2.275
				Un 5		
				8819lp		
	14.85	0.12	101.17	473		2.255
	15.81	0.10	101.87	474		2.220
	12.03	0.11	105.02	475		2.363
	16.10	0.10	101.79	476		2.196
	16.20	0.07	101.56	477		2.185
	8.89	0.24	91.30	478		2.379
	16.18	0.09	100.65	479		2.201
	15.27	0.07	101.27	480		2.241
				Un 7		
				8819lp2		
	15.75	0.08	101.01	481		2.196
	15.90	0.08	99.37	482		2.204
	15.47	0.13	99.35	483		2.217
	15.42	0.10	99.53	484		2.236
	15.69	0.09	99.43	485		2.219
	15.63	0.09	99.03	486		2.221
	14.99	0.11	98.83	487		2.252
	14.65	0.13	98.95	488		2.263
	15.21	0.12	99.08	489		2.242
	15.77	0.10	99.10	490		2.209
				Un 8		
				8819lp3		
	15.58	0.10	101.66	491		2.231
	8.04	0.13	99.64	492		2.245
	15.30	0.08	101.85	493		2.238
	16.30	0.07	101.89	494		2.197
	16.00	0.09	101.67	495		2.206
	0.08	0.01	105.20	496		3.989
	15.89	0.10	101.57	497		2.212
	15.92	0.09	100.03	498		2.207
	15.50	0.09	99.50	499		2.225
				Un 9		
				8819sp1		
	15.09	0.12	99.36	500		2.241
	14.70	0.14	99.68	501		2.263
	14.68	0.13	99.11	502		2.261
	14.91	0.13	99.26	503		2.254
	12.98	0.21	104.64	504		2.332
				Un 10		
				8819sp2		
	14.91	0.10	100.82	505		2.242
	15.36	0.12	100.50	506		2.229
	15.64	0.10	101.35	507		2.218
	15.64	0.09	101.73	508		2.222
	15.32	0.10	101.51	509		2.231
				Un 11		
				8819sp3		
	0.19	0.02	90.83	510		3.710
	14.43	0.15	99.95	511		2.272
	14.90	0.12	99.95	512		2.240
	15.12	0.12	100.48	513		2.240
				Un 12		
				8819sprim		
	23.81	0.01	104.40	514		1.949
				Un 13		
				8819clno		
	22.73	0.01	114.49	515		1.861

24.22	0.02	96.38	516	1.909
23.13	0.00	96.18	517	1.923
18.59	0.21	78.90	518	2.052
23.51	0.01	97.48	519	1.929
			Un 14 8812lp1	
17.28	0.04	98.66	520	2.109
			Un 15 8812lp1	
15.20	0.12	100.19	521	2.223
15.18	0.12	100.31	522	2.207
14.88	0.14	99.41	523	2.239
15.41	0.10	99.60	524	2.209
15.55	0.09	98.50	525	2.198
16.01	0.20	96.65	526	2.181
15.88	0.07	98.17	527	2.186
15.67	0.10	97.78	528	2.193
14.93	0.10	97.03	529	2.219
5.26	0.02	84.64	530	2.161
16.03	0.09	98.94	531	2.180
15.18	0.10	97.64	532	2.212
15.94	0.10	98.11	533	2.183
15.85	0.09	97.59	534	2.183
			Un 16 8812lp2	
15.28	0.10	99.15	535	2.202
15.59	0.08	100.17	536	2.190
15.16	0.09	100.10	537	2.227
0.30	0.07	61.87	538	2.723
			Un 17 8812lp2	
15.21	0.09	97.18	539	2.167
14.60	0.09	97.09	540	2.201
12.93	0.11	93.67	541	2.266
14.64	0.09	98.44	542	2.212
15.55	0.08	99.35	543	2.179
4.77	0.05	81.81	544	2.082
15.46	0.09	98.93	545	2.225
16.18	0.07	98.42	546	2.178
16.24	0.08	99.31	547	2.187
15.11	0.52	100.19	548	2.187
15.97	0.09	99.88	549	2.199
15.44	0.11	100.87	550	2.238
			Un 18 8812lp3	
14.45	0.10	93.23	551	2.227
15.15	0.08	93.12	552	2.182
15.76	0.09	100.89	553	2.215
14.56	0.13	101.02	554	2.277
15.53	0.12	101.24	555	2.224
15.49	0.10	100.29	556	2.221
15.35	0.12	100.20	557	2.236
16.16	0.08	101.38	558	2.199
16.39	0.09	99.03	559	2.175
15.24	0.09	99.20	560	2.235
			Un 19 8812sp1	
0.93	0.01	67.10	561	3.337
15.06	0.08	96.43	562	2.219
15.53	0.10	99.01	563	2.220
16.49	0.05	99.72	564	2.184
			Un 20 8812sp2	

1.31	0.07	62.74		565	3.254
15.31	0.11	99.77		566	2.233
15.07	0.10	98.49		567	2.242
15.68	0.08	98.49		568	2.205
			Un 21 8812sp3		
0.80	0.03	74.22		569	3.360
15.33	0.10	98.94		570	2.257
15.25	0.12	100.48		571	2.236
15.38	0.11	99.65		572	2.229
15.15	0.23	98.83		573	2.225
15.49	0.08	99.30		574	2.213
			Un 22 8812sp4		
15.73	0.09	100.13		575	2.207
16.25	0.09	100.44		576	2.180
16.15	0.08	101.37		577	2.193
15.54	0.09	100.54		578	2.219
15.54	0.09	100.11		579	2.221
13.79	0.12	95.69		580	2.230
			Un 28 8812plg		
21.90	0.03	102.04		627	2.227
			Un 32 8812rimplg1		
16.97	0.04	99.14		646	2.120
			Un 34 8812rimplg2		
15.11	0.06	97.47		647	2.211
			Un 35 8812rimplg3		
15.51	0.08	97.35		648	2.187
			Un 36 8812rimplg4		
16.64	0.05	100.54		649	2.144
			Un 37 8812rimplg5		
16.34	0.08	101.06		650	2.184
			Un 38 8812rimplg6		
1.06	0.12	68.59		651	2.156
			Un 39 8812rimplg7		
16.38	0.07	99.60		652	2.166
			Un 40 8812rimplg8		
15.75	0.10	99.53		653	2.194
			Un 41 8812rimplg9		
15.61	0.08	99.40		654	2.209
			Un 42 8812rimplg10		
15.35	0.09	97.01		655	2.205
			Un 43 898lp1		
14.39	0.08	98.26		656	2.208
16.32	0.09	100.76		657	2.181
15.97	0.06	100.41		658	2.192
15.38	0.10	101.14		659	2.228
15.96	0.10	101.50		660	2.206
14.38	0.10	100.58		661	2.266
15.95	0.08	101.89		662	2.219

15.35	0.09	102.00		663	2.226
0.55	0.26	72.02		664	2.211
14.17	0.11	101.54		665	2.297
			Un 44 898lp2		
15.08	0.12	99.18		666	2.240
15.36	0.09	98.74		667	2.226
15.70	0.08	99.63		668	2.215
11.41	0.13	97.69		669	2.313
5.91	0.10	85.35		670	2.696
15.49	0.09	99.32		671	2.224
			Un 45 898lp2		
14.41	0.11	99.84		672	2.271
15.15	0.11	99.83		673	2.239
15.67	0.09	99.82		674	2.219
			Un 46 898lp3		
15.45	0.08	100.10		675	2.217
16.32	0.09	99.43		676	2.180
10.32	0.79	93.90		677	2.328
21.16	0.06	107.23		678	2.067
15.17	0.15	102.98		679	2.219
14.29	0.23	98.59		680	2.251
2.52	0.42	100.11		681	2.782
2.02	0.03	102.02		682	2.906
14.74	0.11	99.58		683	2.278
15.58	0.09	99.55		684	2.220
12.75	0.05	100.18		685	2.345
14.65	0.05	99.96		686	2.274
16.10	0.09	99.54		687	2.198
15.59	0.08	100.27		688	2.220
15.78	0.08	100.15		689	2.205
15.33	0.09	99.91		690	2.226
15.10	0.09	99.44		691	2.243
15.89	0.09	98.82		692	2.201
15.42	0.11	100.07		693	2.229
15.08	0.13	99.71		694	2.237
			Un 47 898lp3a		
5.67	0.03	96.73		695	2.726
15.71	0.09	99.47		696	2.209
15.97	0.09	99.25		697	2.196
5.30	9.19	98.20		698	2.292
14.84	0.10	98.22		699	2.247
			Un 48 898lp4		
15.36	0.07	98.80		700	2.167
15.47	0.07	99.19		701	2.180
15.06	0.09	99.48		702	2.215
14.96	0.10	101.21		703	2.231
10.54	0.92	96.30		704	2.300
15.14	0.09	101.39		705	2.232
15.06	0.10	101.41		706	2.224
16.15	0.08	100.14		707	2.182
14.93	0.10	98.67		708	2.240
15.58	0.10	99.02		709	2.210
			Un 49 898sp1		
0.01	0.02	102.03		710	3.980
0.01	0.01	102.11		711	3.999
0.19	0.02	100.96		712	2.975
			Un 50		

			898sp2		
14.35	0.08	99.82		713	2.226
14.60	0.13	99.49		714	2.252
15.76	0.09	99.51		715	2.187
15.70	0.10	99.93		716	2.188
			Un 51		
			898sp3		
5.61	0.19	105.64		717	2.615
15.97	0.08	100.41		718	2.191
15.07	0.47	100.15		719	2.216
14.04	0.15	100.21		720	2.267
			Un 52		
			898sp4		
15.64	0.11	99.41		721	2.201
2.69	0.29	86.91		722	2.406
15.53	0.15	101.68		723	2.199
14.58	0.13	99.73		724	2.267
			Un 53		
			898sp5		
15.75	0.09	100.70		725	2.209
15.61	0.09	99.78		726	2.209
15.36	0.10	99.09		727	2.205
15.20	0.10	99.88		728	2.236
			Un 55		
			898rmplg1		
0.92	0.02	92.61		737	3.021
			Un 56		
			898rmplg2		
1.17	0.02	98.81		738	2.938
			Un 57		
			898rmplg3		
1.21	0.03	99.93		739	2.934
			Un 58		
			898rmplg4		
24.39	0.01	98.08		740	1.905
			Un 60		
			883lp1		
17.77	0.03	102.59		742	2.088
15.65	0.08	103.20		743	2.211
15.60	0.10	98.92		744	2.189
15.66	0.12	99.96		745	2.216
15.27	0.08	100.46		746	2.244
11.28	0.12	100.79		747	2.429
15.85	0.11	99.41		748	2.206
16.18	0.09	100.40		749	2.183
15.77	0.09	90.55		750	2.138
15.96	0.10	100.07		751	2.206
15.86	0.08	99.88		752	2.206
16.01	0.09	98.81		753	2.178
15.90	0.10	99.22		754	2.209
15.97	0.10	99.68		755	2.189
16.13	0.10	99.36		756	2.190
16.05	0.08	98.72		757	2.181
16.32	0.10	100.25		758	2.186
16.36	0.08	99.15		759	2.184
15.29	0.12	99.69		760	2.239
16.47	0.07	98.45		761	2.162
			Un 61		
			883lp2		
15.23	0.10	95.87		762	2.200
16.45	0.07	100.93		763	2.169
15.19	0.11	101.14		764	2.238
17.34	0.05	102.50		765	2.118

111

			Sample	K Formula
16.18	0.09	100.78	766	2.182
16.30	0.08	102.13	767	2.185
16.48	0.09	100.84	768	2.181
16.23	0.09	100.89	769	2.178
15.50	0.11	99.48	770	2.197
17.26	0.03	98.96	771	2.114
			Un 62 883lp3	
15.68	0.07	99.83	772	2.210
14.34	0.14	97.64	773	2.215
15.12	0.10	100.81	774	2.228
16.02	0.11	99.74	775	2.165
22.12	0.01	81.23	776	2.920
14.07	0.63	97.40	777	2.199
15.84	0.09	99.11	778	2.179
16.76	0.08	98.18	779	2.129
16.28	0.08	93.17	780	2.129
15.51	0.10	97.49	781	2.198
			Un 63 883sp1	
15.47	0.11	97.83	782	2.199
16.14	0.09	97.46	783	2.147
15.92	0.07	97.30	784	2.159
16.19	0.09	97.56	785	2.156
15.70	0.10	97.40	786	2.185
			Un 64 883sp2	
14.55	0.12	93.76	787	2.207
			Un 65 883sp2	
16.20	0.09	96.94	788	2.150
16.33	0.08	95.98	789	2.147
15.99	0.08	95.97	790	2.148
17.51	0.03	96.23	791	2.059
			Un 66 883sp3	
1.11	0.01	67.35	792	3.344
15.45	0.11	97.46	793	2.198
15.65	0.10	97.07	794	2.179
15.34	0.07	97.23	795	2.204
			Un 67 883sp4	
15.39	0.11	100.01	796	2.215
15.66	0.11	102.86	797	2.205
16.00	0.10	100.05	798	2.178
15.98	0.09	100.21	799	2.193
16.18	0.02	99.42	800	2.171

Al Formula Atoms	Fe Formula Atoms	Na Formula Atoms	Ca Formula Atoms	K Formula Atoms	Formula Totals
1.719	0.015	0.287	0.709	0.006	13.012
1.747	0.014	0.265	0.718	0.007	13.007
1.782	0.015	0.216	0.761	0.006	13.000
1.666	0.015	0.401	0.556	0.006	13.007
1.806	0.021	0.193	0.777	0.006	13.000
1.821	0.014	0.197	0.783	0.004	13.005
1.623	0.084	0.476	0.476	0.015	13.054
1.793	0.018	0.191	0.790	0.005	12.999
1.761	0.015	0.239	0.738	0.004	12.999
1.812	0.019	0.205	0.765	0.005	13.002

1.792	0.016	0.200	0.786	0.005	13.002
1.778	0.014	0.235	0.764	0.007	13.015
1.752	0.013	0.248	0.760	0.006	13.015
1.768	0.017	0.224	0.775	0.006	13.010
1.769	0.019	0.216	0.775	0.005	13.005
1.737	0.018	0.249	0.743	0.007	13.007
1.735	0.014	0.258	0.724	0.008	13.002
1.742	0.018	0.255	0.753	0.007	13.018
1.777	0.020	0.218	0.783	0.006	13.013
1.771	0.014	0.223	0.751	0.006	12.997
1.835	0.254	0.203	0.396	0.008	12.942
1.767	0.015	0.238	0.735	0.004	12.999
1.804	0.016	0.191	0.785	0.004	12.999
1.795	0.019	0.197	0.772	0.005	12.996
0.010	0.003	0.002	0.003	0.000	12.007
1.789	0.015	0.210	0.768	0.006	13.000
1.781	0.017	0.219	0.782	0.005	13.014
1.763	0.017	0.239	0.765	0.005	13.015
1.760	0.010	0.243	0.744	0.007	13.004
1.730	0.014	0.275	0.722	0.008	13.013
1.735	0.014	0.266	0.725	0.007	13.008
1.737	0.015	0.261	0.736	0.008	13.012
1.691	0.012	0.357	0.603	0.012	13.006
1.757	0.015	0.271	0.724	0.006	13.016
1.767	0.015	0.245	0.750	0.007	13.013
1.786	0.015	0.215	0.756	0.006	12.998
1.778	0.016	0.227	0.754	0.005	13.004
1.786	0.013	0.209	0.738	0.006	12.983
0.242	0.113	0.187	0.009	0.001	12.263
1.728	0.016	0.268	0.706	0.009	13.001
1.757	0.015	0.271	0.731	0.007	13.020
1.756	0.017	0.253	0.738	0.007	13.011
1.906	0.080	0.000	1.160	0.001	13.097
1.826	0.479	0.002	1.057	0.001	13.227
1.770	0.204	0.003	1.316	0.001	13.206
1.882	0.090	0.012	1.233	0.000	13.141
1.532	0.320	0.045	1.246	0.016	13.212
1.718	0.287	0.002	1.272	0.001	13.211
1.890	0.013	0.134	0.864	0.003	13.014
1.779	0.020	0.235	0.744	0.007	13.008
1.768	0.045	0.246	0.746	0.007	13.027
1.757	0.018	0.257	0.734	0.008	13.014
1.783	0.023	0.236	0.761	0.006	13.019
1.795	0.019	0.225	0.776	0.005	13.019
1.785	0.019	0.226	0.818	0.012	13.044
1.803	0.016	0.214	0.796	0.004	13.021
1.792	0.019	0.226	0.789	0.006	13.026
1.776	0.019	0.236	0.755	0.006	13.012
1.472	1.068	0.126	0.337	0.002	13.167
1.811	0.019	0.206	0.798	0.005	13.020
1.781	0.023	0.229	0.764	0.006	13.014
1.804	0.020	0.207	0.800	0.006	13.021
1.801	0.024	0.208	0.800	0.005	13.022
1.809	0.016	0.213	0.756	0.006	13.002

1.821	0.017	0.206	0.764	0.005	13.004
1.781	0.017	0.221	0.742	0.005	12.995
0.927	1.129	0.012	0.025	0.007	12.823
1.832	0.017	0.249	0.771	0.006	13.043
1.822	0.014	0.217	0.736	0.005	12.997
1.745	0.051	0.237	0.676	0.007	12.982
1.809	0.015	0.229	0.728	0.006	12.999
1.837	0.016	0.197	0.768	0.005	13.002
1.815	0.747	0.118	0.304	0.004	13.071
1.765	0.020	0.222	0.767	0.005	13.006
1.809	0.021	0.189	0.810	0.004	13.012
1.802	0.019	0.191	0.805	0.005	13.009
1.792	0.063	0.212	0.746	0.031	13.035
1.793	0.018	0.207	0.786	0.005	13.009
1.756	0.016	0.239	0.751	0.006	13.006
1.755	0.017	0.260	0.762	0.006	13.028
1.801	0.021	0.214	0.802	0.005	13.026
1.781	0.019	0.221	0.767	0.005	13.008
1.718	0.017	0.283	0.705	0.007	13.008
1.773	0.019	0.229	0.753	0.007	13.006
1.773	0.018	0.231	0.758	0.006	13.009
1.756	0.016	0.244	0.751	0.007	13.011
1.797	0.022	0.192	0.783	0.004	13.000
1.813	0.019	0.184	0.815	0.005	13.012
1.757	0.013	0.253	0.754	0.005	13.016
0.070	1.117	0.000	0.071	0.001	12.613
1.770	0.016	0.240	0.767	0.005	13.018
1.768	0.019	0.223	0.770	0.006	13.008
1.802	0.020	0.188	0.814	0.003	13.011
0.227	1.013	0.019	0.107	0.007	12.636
1.758	0.013	0.253	0.753	0.007	13.017
1.742	0.017	0.257	0.751	0.006	13.017
1.787	0.016	0.214	0.782	0.005	13.010
0.149	0.976	0.013	0.054	0.003	12.564
1.724	0.015	0.237	0.760	0.006	13.001
1.758	0.018	0.247	0.744	0.007	13.011
1.763	0.015	0.236	0.757	0.007	13.009
1.763	0.020	0.245	0.753	0.014	13.022
1.784	0.018	0.219	0.766	0.005	13.006
1.790	0.016	0.219	0.771	0.005	13.009
1.815	0.015	0.203	0.796	0.005	13.015
1.805	0.015	0.209	0.783	0.005	13.011
1.781	0.016	0.225	0.758	0.005	13.005
1.776	0.017	0.225	0.761	0.005	13.006
1.766	0.078	0.197	0.709	0.008	12.989
1.614	0.011	0.083	1.070	0.002	13.008
1.879	0.018	0.154	0.845	0.002	13.019
1.785	0.015	0.244	0.761	0.003	13.020
1.802	0.018	0.235	0.785	0.005	13.031
1.861	0.020	0.163	0.815	0.003	13.008
1.818	0.013	0.192	0.795	0.004	13.005

1.513	1.297	0.059	0.085	0.012	13.122
1.821	0.020	0.203	0.811	0.004	13.026
1.801	0.015	0.226	0.778	0.006	13.020
1.786	0.013	0.230	0.771	0.005	13.015
1.778	0.017	0.246	0.779	0.005	13.031
1.829	0.017	0.212	0.716	0.005	12.986
1.817	0.012	0.201	0.797	0.005	13.013
1.805	0.019	0.210	0.782	0.004	13.012
1.772	0.016	0.241	0.746	0.006	13.009
1.792	0.016	0.218	0.772	0.006	13.010
1.749	0.014	0.260	0.698	0.006	12.992
1.780	0.019	0.205	0.768	0.005	12.996
1.784	0.017	0.228	0.737	0.005	12.998
1.999	0.386	0.287	0.037	0.021	12.943
1.707	0.014	0.293	0.681	0.006	12.999
1.746	0.020	0.256	0.746	0.007	13.017
1.760	0.016	0.248	0.764	0.005	13.020
1.773	0.018	0.229	0.774	0.005	13.014
1.655	0.170	0.279	0.577	0.008	13.003
1.328	0.003	0.561	0.329	0.006	12.924
1.765	0.016	0.235	0.766	0.005	13.012
1.721	0.013	0.300	0.707	0.007	13.020
1.754	0.015	0.253	0.744	0.006	13.013
1.770	0.018	0.227	0.771	0.005	13.011
1.784	0.016	0.229	0.757	0.005	13.007
1.816	0.013	0.186	0.807	0.005	13.008
1.724	0.026	0.348	0.534	0.048	13.008
1.665	0.269	0.149	1.022	0.003	13.176
1.747	0.029	0.361	0.727	0.009	13.092
1.750	0.020	0.265	0.710	0.013	13.011
1.256	0.008	0.825	0.119	0.024	13.014
1.104	0.002	0.869	0.093	0.001	12.976
1.712	0.020	0.253	0.724	0.006	12.995
1.767	0.019	0.233	0.769	0.006	13.014
1.658	0.045	0.312	0.620	0.003	12.983
1.722	0.011	0.278	0.717	0.003	13.006
1.788	0.018	0.207	0.796	0.005	13.014
1.765	0.026	0.237	0.764	0.005	13.018
1.786	0.017	0.230	0.774	0.005	13.018
1.767	0.015	0.246	0.753	0.005	13.015
1.748	0.009	0.271	0.745	0.005	13.021
1.783	0.015	0.225	0.791	0.005	13.022
1.762	0.016	0.245	0.756	0.006	13.015
1.755	0.012	0.265	0.742	0.008	13.020
1.290	0.002	0.664	0.278	0.002	12.961
1.782	0.018	0.219	0.776	0.005	13.010
1.788	0.019	0.219	0.792	0.005	13.021
1.843	0.062	0.078	0.270	0.556	13.102
1.734	0.019	0.279	0.742	0.006	13.027
1.861	0.013	0.194	0.762	0.004	13.001
1.840	0.015	0.190	0.765	0.004	12.996
1.800	0.015	0.220	0.741	0.005	12.997

1.782	0.015	0.243	0.723	0.005	13.001
1.786	0.027	0.269	0.531	0.055	12.969
1.776	0.015	0.243	0.731	0.005	13.004
1.787	0.017	0.246	0.728	0.006	13.008
1.808	0.023	0.206	0.794	0.004	13.019
1.750	0.015	0.265	0.742	0.006	13.019
1.784	0.015	0.225	0.773	0.006	13.013
0.021	0.008	0.002	0.000	0.001	12.011
0.000	0.000	0.000	0.000	0.000	12.000
1.033	0.007	0.967	0.009	0.001	12.993
1.799	0.017	0.253	0.703	0.005	13.003
1.743	0.014	0.284	0.719	0.008	13.021
1.812	0.016	0.215	0.779	0.005	13.015
1.814	0.015	0.225	0.772	0.006	13.021
1.418	0.009	0.747	0.254	0.010	13.054
1.809	0.018	0.203	0.781	0.005	13.008
1.785	0.018	0.235	0.739	0.027	13.022
1.751	0.013	0.274	0.684	0.009	12.998
1.783	0.020	0.246	0.774	0.006	13.032
1.863	0.028	0.420	0.145	0.019	12.881
1.779	0.020	0.306	0.753	0.009	13.068
1.735	0.014	0.262	0.715	0.007	13.000
1.789	0.018	0.221	0.768	0.005	13.010
1.778	0.013	0.258	0.769	0.006	13.033
1.793	0.016	0.235	0.761	0.006	13.017
1.759	0.012	0.256	0.746	0.006	13.015
0.968	0.007	0.906	0.046	0.001	12.949
1.081	0.002	0.888	0.055	0.001	12.966
1.077	0.004	0.907	0.057	0.001	12.981
1.839	0.142	0.000	1.289	0.001	13.176
1.931	0.016	0.113	0.854	0.002	13.004
1.800	0.017	0.228	0.743	0.005	13.005
1.803	0.020	0.233	0.776	0.006	13.028
1.770	0.023	0.225	0.770	0.007	13.013
1.746	0.018	0.250	0.745	0.005	13.009
1.563	0.025	0.447	0.543	0.007	13.016
1.785	0.021	0.205	0.783	0.006	13.007
1.809	0.023	0.202	0.793	0.005	13.016
1.823	0.022	0.193	0.863	0.006	13.047
1.781	0.023	0.210	0.785	0.006	13.011
1.786	0.021	0.205	0.780	0.005	13.004
1.809	0.024	0.206	0.799	0.005	13.022
1.776	0.023	0.206	0.788	0.006	13.008
1.805	0.021	0.203	0.788	0.006	13.012
1.796	0.018	0.206	0.799	0.006	13.017
1.809	0.026	0.191	0.801	0.005	13.012
1.804	0.020	0.194	0.801	0.006	13.011
1.800	0.016	0.198	0.813	0.005	13.017
1.748	0.017	0.249	0.753	0.007	13.014
1.825	0.020	0.183	0.825	0.004	13.019
1.780	0.016	0.252	0.782	0.006	13.037
1.830	0.022	0.178	0.802	0.004	13.006

1.762	0.019	0.238	0.736	0.007	13.002
1.888	0.029	0.135	0.835	0.003	13.007
1.822	0.018	0.183	0.789	0.005	13.000
1.817	0.021	0.194	0.784	0.005	13.006
1.811	0.021	0.186	0.804	0.005	13.009
1.823	0.022	0.187	0.791	0.005	13.007
1.800	0.017	0.234	0.766	0.007	13.022
1.883	0.015	0.139	0.861	0.002	13.015
1.779	0.020	0.233	0.772	0.004	13.018
1.768	0.067	0.238	0.724	0.008	13.022
1.767	0.030	0.244	0.736	0.006	13.013
1.833	0.023	0.202	0.791	0.006	13.022
0.108	0.479	0.037	1.457	0.001	13.023
1.797	0.058	0.229	0.713	0.038	13.035
1.810	0.021	0.225	0.787	0.005	13.030
1.852	0.022	0.185	0.844	0.005	13.039
1.834	0.022	0.197	0.866	0.005	13.054
1.786	0.019	0.235	0.783	0.006	13.028
1.777	0.025	0.253	0.780	0.006	13.041
1.842	0.019	0.204	0.817	0.005	13.036
1.832	0.017	0.212	0.807	0.004	13.032
1.831	0.020	0.197	0.819	0.005	13.029
1.797	0.020	0.229	0.794	0.006	13.033
1.793	0.014	0.231	0.762	0.007	13.015
1.831	0.019	0.208	0.825	0.006	13.040
1.827	0.019	0.204	0.841	0.005	13.043
1.833	0.024	0.202	0.823	0.005	13.037
1.934	0.019	0.120	0.902	0.002	13.035
0.097	1.046	0.003	0.085	0.001	12.592
1.787	0.017	0.242	0.780	0.006	13.032
1.810	0.020	0.216	0.794	0.006	13.025
1.782	0.020	0.237	0.776	0.004	13.025
1.784	0.015	0.235	0.755	0.006	13.012
1.797	0.026	0.229	0.748	0.006	13.013
1.813	0.018	0.226	0.788	0.006	13.031
1.801	0.019	0.209	0.784	0.005	13.013
1.815	0.033	0.197	0.802	0.001	13.020